

Isospin Properties of (K^-, N) Reactions for the Formation of Deeply-bound Antikaonic Nuclei

TAKAHISA KOIKE*

*Advanced Meson Science Laboratory, RIKEN Nishina Center,
Wako-shi, Saitama 351-0198, Japan*

TORU HARADA†

*Research Center for Physics and Mathematics,
Osaka Electro-Communication University,
Neyagawa, Osaka, 572-8530, Japan*

(Dated: November 2, 2018)

Abstract

The formation of deeply-bound antikaonic K^-/\bar{K}^0 nuclear states by nuclear (K^-, N) reactions is investigated theoretically within a distorted-wave impulse approximation (DWIA), considering the isospin properties of the Fermi-averaged $K^- + N \rightarrow N + \bar{K}$ elementary amplitudes. We calculate the formation cross sections of the deeply-bound \bar{K} states by the (K^-, N) reactions on the nuclear targets, ^{12}C and ^{28}Si , at incident K^- lab momentum $p_{K^-} = 1.0 \text{ GeV}/c$ and $\theta_{\text{lab}} = 0^\circ$, introducing a complex effective nucleon number N_{eff} for unstable bound states in the DWIA. The results show that the deeply-bound \bar{K} states can be populated dominantly by the (K^-, n) reaction via the total isoscalar $\Delta T = 0$ transition owing to the isospin nature of the $K^- + N \rightarrow N + \bar{K}$ amplitudes, and that the cross sections described by $\text{Re}N_{\text{eff}}$ and $\text{Arg}N_{\text{eff}}$ enable to deduce the structure of the \bar{K} nuclear states; the calculated inclusive nucleon spectra for a deep \bar{K} -nucleus potential do not show distinct peak structure in the bound region. The few-body $\bar{K} \otimes [NN]$ and $\bar{K} \otimes [N NN]$ states formed in (K^-, N) reactions on s -shell nuclear targets, ^3He , ^3H and ^4He , are also discussed.

PACS numbers: 25.80.Nv, 13.75.Jz, 36.10.Gv, 21.45.+v

Keywords: (K^-, N) reaction, K^- nuclear states, Formation cross section, Isospin dependence, DWIA

* E-mail:tkoike@riken.jp

† E-mail:harada@isc.osakac.ac.jp

I. INTRODUCTION

The antikaon-nucleon ($\bar{K}N$) interaction in nuclei is very important to elucidate the nature of high dense nuclear matter [1, 2, 3]. The attractive $\bar{K}N$ interaction in the isospin $I = 0$ channel is sufficiently strong to produce a quasibound state $\Lambda(1405)$ at about 27 MeV below the K^-p threshold. This state is often described as a $\bar{K}N$ bound state decaying into the main $\pi\Sigma$ -channels with a width of about 50 MeV [4]. Such a $\bar{K}N$ interaction, together with the moderately attractive $\bar{K}N$ $I = 1$ channel, would give a strong attractive potential for the \bar{K} in nuclei, leading naively to the existence of deeply-bound \bar{K} nuclear states [5]. Indeed, comprehensive analysis of the shifts and widths of K^- atomic X-ray data suggests strongly attractive \bar{K} optical potentials, of the depth between 150-200 MeV at the nuclear center [6, 7, 8]. Since the K^- atomic state is sensitive only to behavior of the K^- wave function at the nuclear surface, it is ambiguous to extrapolate smoothly to nuclear matter density, and it would be inconclusive [9]; see however [10]. Enhancement in K^- production by heavy ion reactions suggests a strongly attractive interaction [11] although the recent analysis of details of the reaction mechanism leads to attraction of only -80 MeV [12]. The existence of the deeply-bound \bar{K} nuclear states would provide constraints on kaon condensation in compact stars and neutron stars [13]; the equation of state (EOS) of nuclear matter is softened due to the appearance of the kaon condensation.

Recent theoretical calculations have found that the \bar{K} -nucleus attraction amounts to 110 MeV at normal nuclear density ρ_0 , being constructed by the chiral SU(3) effective Lagrangian involving $\bar{K}N$ - πY coupled channels [14], whereas the \bar{K} potential calculated self consistently has a relatively shallow depth of 40-60 MeV with a broad width of about 100 MeV [14, 15, 16, 17]. We believe that more theoretical developments are needed in order to describe a quasibound state having a broad width in the complicated nuclear medium.

On the other hand, the production of the deeply-bound \bar{K} nuclear states has been investigated theoretically and experimentally for the forward (K^- , N) reaction, in order to search directly for signals of \bar{K} nuclear bound states, as proposed by Kishimoto [18]. Ikuta et al. [19] attempted to calculate the inclusive (K^- , p) spectra by the Green's function technique [20], using (energy-dependent) K^- -nucleus potentials by fits to the K^- atomic data [6, 7, 8]. Kishimoto and his collaborators [21] performed experimentally the measurements for searching deeply-bound \bar{K} nuclei by (in-flight K^- , N) reactions on ^{12}C and ^{16}O targets

in the PS-E548 experiment at KEK, but there was no clear evidence in both (K^-, n) and (K^-, p) spectra. Yamagata et al. [22, 23] also calculated the corresponding cross sections by (K^-, p) reactions on ^{12}C and ^{16}O targets, using K^- optical potentials based on Chiral unitary and phenomenological approaches, and showed the difficulties to find clear signals for \bar{K} nuclear states due to their broad width, even if the bound states exist, within Green's function technique [23].

Akaishi and Yamazaki [24, 25] predicted that the light \bar{K} nuclear K^-ppn/\bar{K}^0pnn system with total isospin $T = 0$ has a deeply bound state with a relatively narrow width, by over $B_{\bar{K}} = 108$ MeV for which the main decay channel $\bar{K}N \rightarrow \pi\Sigma$ would be kinematically closed. Thus its width becomes relatively narrow, about 20 MeV due to the isospin selection. Surprisingly, Suzuki et al. [26] reported experimentally evidence of the tribaryon $S^0(3115)$ by the $^4\text{He}(\text{stopped } K^-, p)$ reaction, and the signal was interpreted as such a state. Although it was withdrawn [27], the data analysis from the improved-statistics experiment E549 is in progress [28]. Is there such a narrow deeply-bound \bar{K} state ?

Recently, FINUDA collaboration at DAΦNE [29] reported experimentally the evidence of a deeply-bound K^-pp state in invariant mass spectroscopy by $K^-pp \rightarrow \Lambda + p$ decay processes from K^- absorption on ^6Li , ^7Li and ^{12}C at rest, where the measured energy and width are $B_{\bar{K}} = 115$ MeV and $\Gamma_{\bar{K}} = 67$ MeV, respectively. The three-body \bar{K} bound state with a configuration of $[\bar{K} \otimes \{NN\}_{I=1}]_{T=1/2}$ [30] is expected to play a fundamental role in constructing the various \bar{K} nuclear bound states. This state is often called “ K^-pp ” symbolically. Several theoretical works [31, 32, 33, 34, 35, 36, 37, 38] supported the existence of the K^-pp bound state: Yamazaki and Akaishi [31] predicted the binding energy of $B_{\bar{K}} = 48$ MeV and the width of $\Gamma_{\bar{K}} = 61$ MeV for the K^-pp bound state by a few-body calculation using ATMS method. Shevchenko et al. [32, 33] obtained $B_{\bar{K}} = 55\text{-}70$ MeV and $\Gamma_{\bar{K}} = 95\text{-}110$ MeV for the K^-pp bound state by a $\bar{K}NN\text{-}\pi\Sigma N$ coupled-channel Faddeev calculation. We believe that the search for a deeply-bound K^-pp state is one of the most important subjects to verify the reliable evidence of the deeply-bound \bar{K} nuclei, and that this state might be a doorway for access to kaon condensation in neutron stars [39]. More experimental data are required in order to confirm clearly whether deeply-bound states exist or not.

Very recently, Iwasaki et al. [40] proposed a new experiment searching the deeply-bound K^-pp state at J-PARC, by the missing-mass spectrum of the $^3\text{He}(\text{in-flight } K^-, n)$ reaction, together with the invariant-mass spectra detecting all particles via decay processes (J-PARC

E15). In a previous paper [41], we demonstrated the inclusive and semi-exclusive spectra of the ${}^3\text{He}(\text{in-flight } K^-, n)$ reaction at $p_{K^-} = 1.0 \text{ GeV}/c$ and $\theta_{\text{lab}} = 0^\circ$ within the distorted wave impulse approximation (DWIA), in order to see theoretically the expected spectra of the ${}^3\text{He}(\text{in-flight } K^-, n)$ reaction for preparing the forthcoming J-PARC E15 experiment [40]. Yamazaki and Akaishi [42] also proposed the K^-pp formation via $p + p \rightarrow K^+ + \Lambda(1405)p \rightarrow K^+ + K^-pp$, assuming a $\Lambda(1405)p$ doorway. Such a K^-pp experiment with a $\sim 4 \text{ GeV}$ proton beam on a proton target is planned by FOPI collaboration at GSI [43].

In this paper, we investigate theoretically the (in-flight K^- , N) reaction for the formation of the deeply-bound \bar{K} states on nuclei, within a distorted-wave impulse approximation (DWIA). One of our main purpose is to understand the formation mechanism for the deeply-bound \bar{K} states by the nuclear (K^-, n) and (K^-, p) reactions, which would provide the selectivity of the isospin excitation in the \bar{K} nuclear bound states. We discuss in some detail the isospin properties of the cross section by the nuclear (K^-, n) or (K^-, p) reaction on a ${}^{12}\text{C}$ target, together with the isospin-dependence of the \bar{K} -nucleus potentials which are suggested from the recent analyses of K^-/K^+ production in heavy ion reactions at KaoS [11, 12], and of ${}^{12}\text{C}(\text{in-flight } K^-, N)$ reaction experiments (PS-E548) at KEK [21].

The outline of this paper is as follows. In Section II, we present the amplitudes and the cross sections of the forward $K^- + N \rightarrow N + \bar{K}$ reaction, on the basis of the K^-N elastic scattering amplitudes analyzed by Gopal et al. [44]. The isospin properties of the forward $K^- + N \rightarrow N + \bar{K}$ reactions are shown, together with Fermi-averaged $K^- + N \rightarrow N + \bar{K}$ amplitudes which take into account the Fermi motion of a nucleon in the nucleus. In Section III, we discuss the formation of the deeply-bound \bar{K} nuclear state by nuclear (K^-, N) reactions within the DWIA, introducing a *complex* effective nucleon number for the *unstable* bound states. We stress the importance of the kinematical effects in terms of the momentum transfer to a residual \bar{K} nucleus for the (K^-, N) reaction, which differs considerably from hypernuclear production reactions by the nuclear (π^+, K^+) and (K^-, K^+) ones. We discuss the properties of the formation cross sections of the deeply-bound K^- states by the nuclear (K^-, N) reactions on the closed-shells ${}^{12}\text{C}$ and ${}^{28}\text{Si}$ targets at the incident K^- lab momentum $p_{K^-} = 1.0 \text{ GeV}/c$, and the isospin selection by the (K^-, n) and (K^-, p) reactions. In Section IV, we concentrate on isospin dependence of the relative cross sections for the deeply-bound three-body $\bar{K} \otimes [NN]$ and four-body $\bar{K} \otimes [NNN]$ states in order to study the formation of light deeply-bound \bar{K} states. Summary and conclusion are given in Section V. A derivation

of kinematical factors in the DWIA is given in in Appendices A and B, together with the relation between the integrated cross section and the inclusive spectrum. Spin-isospin states for s -shell \bar{K} -nuclear systems are given in Appendix C.

II. THE (K^-, N) REACTIONS

A. The elementary reactions $K^- + N \rightarrow \bar{K} + N$ and $K^- + N \rightarrow N + \bar{K}$

Kishimoto [18] suggested that the forward (K^-, N) reaction on a nuclear target could result in a discovery of \bar{K} nuclear states. This has triggered experimental and theoretical studies of the (K^-, N) reaction for searching deeply-bound \bar{K} nuclear states. Because the forward $K^- + N \rightarrow N + K^-$ scattering amplitudes ($\theta_{\text{c.m.}} = 0^\circ$) in the c.m. frame are equivalent to the backward $K^- + N \rightarrow K^- + N$ scattering ones ($\theta_{\text{c.m.}} = 180^\circ$), we considered the $K^- + N \rightarrow \bar{K} + N$ elastic and charge-exchange reactions, in order to understand the nature of the $K^- + N \rightarrow N + \bar{K}$ reaction which is needed to calculate the production cross section by the nuclear (K^-, N) reaction within the DWIA.

The c.m. backward $K^- + N \rightarrow \bar{K} + N$ scattering amplitudes are equivalent to the c.m. forward $K^- + N \rightarrow N + \bar{K}$ ones in free space [18]. Thus, the c.m. $K^- + N \rightarrow N + \bar{K}$ amplitudes are given as

$$\begin{aligned} f_{K^-n \rightarrow nK^-}(\theta_{\text{c.m.}}) &= f_{K^-n \rightarrow K^-n}(\pi - \theta_{\text{c.m.}}), \\ f_{K^-p \rightarrow n\bar{K}^0}(\theta_{\text{c.m.}}) &= f_{K^-p \rightarrow \bar{K}^0n}(\pi - \theta_{\text{c.m.}}), \\ f_{K^-p \rightarrow pK^-}(\theta_{\text{c.m.}}) &= f_{K^-p \rightarrow K^-p}(\pi - \theta_{\text{c.m.}}), \end{aligned} \quad (1)$$

where the labels by $K^-n \rightarrow nK^-$, $K^-p \rightarrow n\bar{K}^0$ and $K^-p \rightarrow pK^-$ denote the c.m. backward cross sections for $K^- + n \rightarrow K^- + n$, $K^- + p \rightarrow \bar{K}^0 + n$ and $K^- + p \rightarrow K^- + p$ reactions, respectively; $\theta_{\text{c.m.}}$ is the nucleon angle relative to K^- beam direction in the c.m. frame. The c.m. differential cross sections for the $K^- + N \rightarrow N + \bar{K}$ reactions can be obtained by

$$\left(\frac{d\sigma}{d\Omega}(\theta_{\text{c.m.}}) \right)_{\text{c.m.}}^{K^-N \rightarrow N\bar{K}} = |f_{K^-N \rightarrow N\bar{K}}(\theta_{\text{c.m.}})|^2, \quad (2)$$

for these channels. In Fig. 1, we show the c.m. differential cross sections for the $K^- + N \rightarrow N + \bar{K}$ reactions at the incident K^- lab momentum $p_{K^-} = 1.0$ GeV/c, as a function of the scattering angle θ , together with the lab differential cross sections. The dashed and solid

curves are the angular distributions of $(d\sigma/d\Omega)_{c.m.}^{K^-N \rightarrow N\bar{K}}$ and $(d\sigma/d\Omega)_{lab}^{K^-N \rightarrow N\bar{K}}$, respectively, which are obtained by Gopal et al. [44]. The experimental data are taken from Conforto et al. [45]. These values are connected by the relation [46]

$$\frac{(d\sigma/d\Omega)_{lab}^{K^-N \rightarrow N\bar{K}}}{(d\sigma/d\Omega)_{c.m.}^{K^-N \rightarrow N\bar{K}}} = \frac{m_N p_{K^-} p_N}{p_{K^-c.m.} p_{Nc.m.}} \left(E_{K^-} + m_N - E_N \frac{p_{K^-}}{p_N} \cos \theta_{lab} \right)^{-1}, \quad (3)$$

where $\{p_{K^-}, E_{K^-}\}$ and $\{p_N, E_N\}$ are lab momenta and total energies for the incoming K^- and the outgoing nucleon, respectively, and the quantities labeled by c.m. subscript are in the c.m. frame. m_N is the mass of a nucleon. The lab scattering angle θ_{lab} satisfies

$$\cos \theta_{lab} = \frac{E_{K^-} E_N - E_{K^-c.m.} E_{Nc.m.} + p_{K^-c.m.} p_{Nc.m.} \cos \theta_{c.m.}}{p_{K^-} p_N}, \quad (4)$$

where there is a kinematical focussing [46] of the lab cross section to a cone for the maximum angle $\theta_{lab}^{max} = \pi/2$, because $m_{\bar{K}}/m_N < 1$ in the $K^- + N \rightarrow N + \bar{K}$ reactions.

————— **FIG. 1** —————

In Fig. 2, we show the lab differential cross sections for $K^- + n \rightarrow n + K^-$, $K^- + p \rightarrow n + \bar{K}^0$ and $K^- + p \rightarrow p + K^-$ reactions at $\theta_{lab} = 0^\circ$, as a function of the incident K^- lab momentum. These values are maximum near $p_{K^-} = 1.0$ GeV/c because of the existence of several Σ^* and Λ^* resonances in the 0.9-1.2 GeV/c region, e.g., $S_{11}(1750)$, $D_{15}(1775)$, $S_{01}(1800)$, $F_{05}(1820)$, etc. At $p_{K^-} = 1.0$ GeV/c, thus,

$$\begin{aligned} \left(\frac{d\sigma}{d\Omega}(0^\circ) \right)_{lab}^{K^-N \rightarrow N\bar{K}} &= 24.5 \text{ mb/sr,} & \text{for } K^- + n \rightarrow n + K^-, \\ &= 13.1 \text{ mb/sr,} & \text{for } K^- + p \rightarrow n + \bar{K}^0, \\ &= 9.4 \text{ mb/sr,} & \text{for } K^- + p \rightarrow p + K^-. \end{aligned} \quad (5)$$

————— **FIG. 2** —————

B. Isospin properties for the $K^- + N \rightarrow N + \bar{K}$ reaction

Now we introduce the s -channel isospin transition amplitudes f_I for the (K^-, N) reactions, in order to clarify the isospin properties of these reactions. The amplitudes for $K^- + n \rightarrow n + K^-$, $K^- + p \rightarrow n + \bar{K}^0$ and $K^- + p \rightarrow p + K^-$ processes have the relations

$$f_{K^-n \rightarrow nK^-} = f_1, \quad (6)$$

$$f_{K^-p \rightarrow n\bar{K}^0} = (f_1 + f_0)/2, \quad (7)$$

$$f_{K^-p \rightarrow pK^-} = (f_1 - f_0)/2, \quad (8)$$

where f_0 and f_1 denote the s -channel isospin 0 and 1 amplitudes for the (K^-, N) reactions, respectively. One has to notice that the definitions of Eqs. (7) and (8) are interchanged for the (K^-, \bar{K}) reactions, as given by Eqs. (9) and (10) of Ref. [18].

Considering the isospins $\mathbf{i}_1 + \mathbf{i}_2 \rightarrow \mathbf{i}'_1 + \mathbf{i}'_2$ for the $K^- + N \rightarrow N + \bar{K}$ reactions in the isospin algebra [46], we can represent the t -channel forward two-body reaction amplitude $f^{(t)} = \langle (i_2 i'_2) t | f | (i_1 i'_1) t \rangle$ by expanding the s -channel amplitude $f_I = \langle (i'_1 i'_2) I | f | (i_1 i_2) I \rangle$, so as to derive the isospin decomposition of the nuclear reactions:

$$f^{(t)} = \sum_I (-)^{i_1+i_2+I} (2I+1) \begin{Bmatrix} i'_1 & i'_2 & I \\ i_2 & i_1 & t \end{Bmatrix} f_I. \quad (9)$$

For the (K^-, N) reactions, thus, we obtain

$$f^{(0)} = (f_0 + 3f_1)/2 = f_{K^-n \rightarrow nK^-} + f_{K^-p \rightarrow n\bar{K}^0}, \quad (10)$$

$$f^{(1)} = (f_1 - f_0)/2 = f_{K^-n \rightarrow nK^-} - f_{K^-p \rightarrow n\bar{K}^0} = f_{K^-p \rightarrow pK^-}, \quad (11)$$

where $f^{(0)}$ and $f^{(1)}$ denote (unnormalized) t -channel isospin 0 and 1 amplitudes for the $K^- + N \rightarrow N + \bar{K}$ reactions, respectively. Note that these amplitudes correspond to u -channel isospin 0 and 1 amplitudes for the $K^- + N \rightarrow \bar{K} + N$ reactions. The amplitudes in Eq. (11) are related by isospin to the amplitudes of the neutron and proton reactions,

$$f_{K^-n \rightarrow nK^-} = f_{K^-p \rightarrow n\bar{K}^0} + f_{K^-p \rightarrow pK^-}, \quad (12)$$

which is easily verified by a combination of Eqs. (6)-(8). The isospin relation between the amplitudes for (K^-, N) reactions is summarized in Table I.

————— **TABLE I** —————

C. Fermi-averaging in nuclear medium

When we calculate the nuclear (K^-, N) cross sections with the elementary $K^- + N \rightarrow N + \bar{K}$ amplitudes $f_{K^-N \rightarrow N\bar{K}}$, it is important to take into account the Fermi motion of a struck nucleon moving with a Fermi-momentum $p_F \simeq 270$ MeV/ c in nuclear medium [47, 48], because a momentum transfer $|q| \simeq 200$ MeV/ c in the forward $K^- + N \rightarrow N + \bar{K}$ reaction at $p_{K^-} = 1.0$ GeV/ c is scarcely smaller than the Fermi-momentum. Dover and Walker [49] have pointed out that Fermi-averaging for $K^- + N \rightarrow \bar{K} + N$ reaction acts

considerably on the (K^- , \bar{K}) inelastic cross sections; particularly, the effect appears near a narrow resonance, e.g., $\Lambda(1520)$ at $p_{K^-} \sim 390$ MeV/c, because its width is smaller than the Fermi-motion energy of a struck nucleon. In the case of the nuclear (K^- , N) reaction, let us obtain the Fermi-averaged amplitudes which play an important role of calculating the cross section with the DWIA.

According to the procedure by Rosental and Tabakin [47], we perform the Fermi-averaging of the $K^- + N \rightarrow N + \bar{K}$ scattering T -matrix in the lab frame. Using the K^-N amplitudes by Gopal et al. [44], we obtain the Fermi-averaged T -matrix for the lab momenta of 0.3-2.0 GeV/c at $\theta_{\text{lab}} = 0^\circ$, which is given by

$$\bar{t}_{K^-N \rightarrow N\bar{K}}(0^\circ) = \frac{1}{2} \int_{-1}^1 dx \int_0^\infty p^2 dp \rho(p) t_{K^-N \rightarrow N\bar{K}}(E_{K^-N}), \quad (13)$$

as a function of the effective lab energy $E_{K^-N} = \sqrt{\mathbf{p}_{K^-}^2 + m_{K^-}^2} + \sqrt{\mathbf{p}^2 + m_N^2}$, where \mathbf{p} and m_N are the momentum and the mass of a struck nucleon in the nucleus, respectively, and $x = \hat{\mathbf{p}}_{K^-} \cdot \hat{\mathbf{p}}$. Here we use a lab momentum distribution $\rho(p)$ of the struck nucleon with a sum of squares of harmonic oscillator wave functions [49]

$$\rho(p) = \rho_0 \left(N_s + \frac{2}{3} N_p (bp)^2 \right) \exp(-(bp)^2), \quad (14)$$

where N_s and N_p are the numbers of s - and p -shell nucleon, respectively, and $\rho_0 = (b/\sqrt{\pi})^3$ with the size parameter $b = 1.64$ fm for ^{12}C . The resultant T -matrix is not so sensitive to a choice of the form of $\rho(p)$ constrained by a comparable value of $\langle p^2 \rangle^{1/2}$, as shown in Ref. [49]. Thus, the Fermi-averaged forward amplitude in nuclear medium is given as

$$\bar{f}_{K^-N \rightarrow N\bar{K}}(0^\circ) = -\frac{1}{2\pi} \left(\frac{p_N}{p_{K^-}} \right) \left[\frac{E_{K^-} E_N E_{\bar{K}}}{E_{K^-} + m_N - E_N (p_{K^-}/p_N)} \right]^{\frac{1}{2}} \bar{t}_{K^-N \rightarrow N\bar{K}}(0^\circ), \quad (15)$$

where a participant nucleon involving a Fermi-averaged T -matrix is considered approximately to be at rest in the target. In Fig. 3, we show the Fermi-averaged forward cross section for ^{12}C in the lab frame,

$$\left\langle \frac{d\sigma}{d\Omega}(0^\circ) \right\rangle_{\text{lab}}^{K^-N \rightarrow N\bar{K}} = |\bar{f}_{K^-N \rightarrow N\bar{K}}(0^\circ)|^2 \quad (16)$$

for $K^- + n \rightarrow n + K^-$, $K^- + p \rightarrow n + \bar{K}^0$ and $K^- + p \rightarrow p + K^-$ channels. The nucleon Fermi-motion appreciably moderates the effects of resonances. The shape of the cross sections near 1.0 GeV/c becomes sizably broader, and a narrow $\Lambda(1520)$ resonance affects more strongly

the cross sections near 0.4 GeV/c. Even after the Fermi-averaging, there remains rather strongly energy-dependence for the $K^- + N \rightarrow N + \bar{K}$ reactions, and also their charge (isospin) state-dependence, as suggested by Rosental and Tabakin [47]. The absolute values of the Fermi-averaged forward cross sections at $p_{K^-} = 1.0$ GeV/c are calculated by

$$\begin{aligned} \left\langle \frac{d\sigma}{d\Omega}(0^\circ) \right\rangle_{\text{lab}}^{K^-N \rightarrow N\bar{K}} &= 13.9 \text{ mb/sr}, & \text{for } K^- + n \rightarrow n + K^-, \\ &= 7.5 \text{ mb/sr}, & \text{for } K^- + p \rightarrow n + \bar{K}^0, \\ &= 3.5 \text{ mb/sr}, & \text{for } K^- + p \rightarrow p + K^-. \end{aligned} \quad (17)$$

We find that these values for $K^- + n \rightarrow n + K^-$, $K^- + p \rightarrow n + \bar{K}^0$ and $K^- + p \rightarrow p + K^-$ are reduced by about 0.57, 0.57 and 0.37, respectively, in comparison with those for free space, Eq. (5). If we replace the T -matrix $t_{K^-N \rightarrow N\bar{K}}$ in Eq. (13) by $|t_{K^-N \rightarrow N\bar{K}}|$ neglecting its phase, we find the values of 18.3 mb/sr, 11.3 mb/sr and 4.8 mb/sr for the corresponding Fermi-averaged cross sections at $p_{K^-} = 1.0$ GeV/c, which would be equivalent to the Fermi-averaging for the differential cross sections instead of the T -matrices. This means that the resultant cross sections are further more reduced by the phase at this momentum region. When we do the Fermi-averaging for ^4He (^3He) in the s -shell nuclei, we use $b = 1.21$ fm (1.38 fm) with $N_p = 0$ in the momentum distribution $\rho(p)$ in Eq. (14). We confirm that the calculated cross sections are not so changed by choosing the targets, e.g., ^{12}C or ^4He , as discussed by Dover et al. [50].

———— **FIG. 3** ————

In Figs. 4 and 5, we show the Fermi-averaged lab amplitudes for s -channel isospin \bar{f}_I and for t -channel isospin $\bar{f}^{(t)}$, respectively. We shall employ these Fermi-averaged amplitudes $\bar{f}_{K^-N \rightarrow N\bar{K}}$ in the following calculations.

———— **FIG. 4** ————

———— **FIG. 5** ————

III. FORMATION OF THE DEEPLY-BOUND ANTIKAONIC NUCLEI

A. Distorted-wave impulse approximation (DWIA)

The formation of the deeply-bound \bar{K} nuclear states for the nuclear (\bar{K}, N) reaction has been investigated experimentally [21, 26, 29] and theoretically [9, 18, 19, 22, 23, 25, 41]. Iwasaki et al., [27] have proposed the experiment searching the deeply-bound K^-pp states by ${}^3\text{He}(\text{in-flight } K^-, N)$ reaction at $p_{K^-} = 1.0 \text{ GeV}/c$ and $\theta_{\text{lab}} = 0^\circ$. In order to clarify these reaction mechanism, let us consider the nuclear (K^-, N) reaction for the formation of deeply-bound \bar{K} nuclear states within the distorted-wave impulse approximation (DWIA) [46, 51, 52, 53]. In Fig. 6, we illustrate a diagram of the nuclear $A(K^-, N)_{\bar{K}}B$ reaction with the impulse approximation; the final states in ${}_{\bar{K}}B$ will be unstable due to the strong-interaction decay processes by the one-body \bar{K} absorption $K^-/\bar{K}^0 + \text{“}N\text{”} \rightarrow \pi + \Sigma/\Lambda$ and the multi-nucleonic \bar{K} absorption, e.g., $K^-/\bar{K}^0 + \text{“}NN\text{”} \rightarrow \Sigma/\Lambda + N$, in the nucleus. In this paper, we focus on the formation stage of the deeply-bound \bar{K} nuclear states via $K^- + N \rightarrow N + \bar{K}$ processes on the nuclear targets. In a previous paper [41], we studied the inclusive and semi-exclusive spectra of the ${}^3\text{He}(\text{in-flight } K^-, n)$ reaction at $p_{K^-} = 1.0 \text{ GeV}/c$ and $\theta_{\text{lab}} = 0^\circ$ for searching the deeply-bound K^-pp states, and discussed briefly a kinematical factor for the K^-pp states and the isospin excitation of their cross sections in the DWIA. Such formation reactions have an unique kinematics similar to the formation of π , ρ and ω -nuclear bound states [54], rather than hypernuclear production by (K^-, π) [51, 52, 53, 55], (π, K^+) [56, 57, 58, 59] and (K^-, K^+) [46, 60] reactions, as we will mention below.

————— **FIG. 6** —————

The double-differential cross section for the formation of deeply-bound \bar{K} nuclear states by the (K^-, N) reaction at a nucleon direction angle θ_{lab} is given within the DWIA [20, 41, 46, 53, 55], assuming a zero-range interaction for elementary $K^- + N \rightarrow N + \bar{K}$ reactions, as

$$\left(\frac{d^2\sigma}{d\Omega_N dE_N} \right)_{\text{lab}} = \beta \frac{1}{2J_A + 1} \sum_{M_A} \sum_{m_s, B} |\langle \Psi_B | \hat{F} | \Psi_A \rangle|^2 \delta(\omega + E_B - E_A) \quad (18)$$

with

$$\hat{F} = \int d\mathbf{r} \chi_{N,m_s}^{(-)*}(\mathbf{p}_N, \mathbf{r}, \sigma) \chi_{K^-}^{(+)}(\mathbf{p}_{K^-}, \mathbf{r}) \sum_{j=1}^A \bar{f}_{K^-N \rightarrow N\bar{K}} \hat{O}_{N_j} \delta(\mathbf{r} - \mathbf{r}_j), \quad (19)$$

where $|\Psi_B\rangle$ and $|\Psi_A\rangle$ are final states of the \bar{K} nuclear states with total spin J_B and initial states of the target nucleus with total spin J_A , respectively. $\chi_{N,m_s}^{(-)}(\mathbf{p}_N, \mathbf{r}, \sigma)$ and $\chi_{K^-}^{(+)}(\mathbf{p}_{K^-}, \mathbf{r})$ denote distorted waves for an outgoing spin- $(\frac{1}{2}, m_s)$ nucleon with the detected lab momentum \mathbf{p}_N and for an incoming K^- with the incident lab momentum \mathbf{p}_{K^-} , respectively. The operator \hat{O}_{N_j} changes a j -th nucleon into the \bar{K} in the nucleus; $\bar{f}_{K^-N \rightarrow N\bar{K}}$ is the Fermi-averaged lab amplitude for the $K^- + N \rightarrow N + \bar{K}$ reaction in nuclear medium, and β is a kinematical factor, as mentioned in Appendix A. Here we consider only the non-spin-flip processes, because we are interested in the cross section at the forward direction. In our previous paper [41], the formation cross sections for K^-pp bound states were evaluated by the Green's function technique [20]. This technique can describe unstable hadron nuclear systems such as the Σ and Ξ nuclear bound states very well, so as to compare theoretical spectra with experimental ones [55, 59, 60]. In \bar{K} nuclear physics, the spectral calculations have been performed by several authors [19, 21, 23, 41]. Using Green's function $G(\omega)$ for the \bar{K} -nucleus system, a sum of the final states of Eq. (18) is written as

$$\sum_B |\Psi_B\rangle \delta(\omega + E_B - E_A) \langle \Psi_B | = (-) \frac{1}{\pi} \text{Im} G(\omega), \quad (20)$$

where ω is the energy transfer to the residual B nucleus. Then the inclusive spectrum of the double-differential cross section in Eq. (18) is rewritten as

$$\left(\frac{d^2\sigma}{d\Omega_N dE_N} \right)_{\text{lab}} = \beta(-) \frac{1}{\pi} \text{Im} \left[\sum_{\alpha'\alpha} \int d\mathbf{r}' d\mathbf{r} F_{\alpha'}^\dagger(\mathbf{r}') G_{\alpha'\alpha}(\omega; \mathbf{r}', \mathbf{r}) F_\alpha(\mathbf{r}) \right], \quad (21)$$

where \mathbf{r} is the relative coordinate between the \bar{K} and the core-nucleus. $F_\alpha(\mathbf{r})$ presents the \bar{K} -nucleus doorway states excited initially as

$$F_\alpha(\mathbf{r}) = \chi_{N,m_s}^{(-)*}(\mathbf{p}_N, \frac{M_C}{M_B} \mathbf{r}, \sigma) \chi_{K^-}^{(+)}(\mathbf{p}_{K^-}, \frac{M_C}{M_A} \mathbf{r}) \bar{f}_{K^-N \rightarrow N\bar{K}} \langle \alpha | \hat{\psi}_N(\mathbf{r}) | \Psi_A \rangle, \quad (22)$$

where $\langle \alpha | \hat{\psi}_N(\mathbf{r}) | \Psi_A \rangle$ is a hole-state wave function for a struck nucleon in the target, and α denotes the complete set of eigenstates for the system. The factors of M_C/M_B and M_C/M_A take into account the recoil effects, where M_A , M_B and M_C are masses of the target, the \bar{K} -nucleus and the core-nucleus, respectively.

B. Kinematics

Now let us consider the kinematics for the (K^-, N) reaction on a nuclear target. The momentum-energy transfers to the \bar{K} nuclear bound states are given by

$$\mathbf{q} = \mathbf{p}_{K^-} - \mathbf{p}_N, \quad (23)$$

$$\omega = E_{K^-} - E_N = E_B - E_A \simeq m_{\bar{K}} - m_N - B_{\bar{K}} - \varepsilon_N + T_{\text{recoil}}, \quad (24)$$

where $m_{\bar{K}}$ and m_N are masses of an \bar{K} and a nucleon, respectively, and $B_{\bar{K}}$ is an \bar{K} binding energy measured from the K^- +core-nucleus threshold. ε_N is a single-particle energy of a nucleon-hole state in the target, and T_{recoil} is a recoil energy to the \bar{K} nuclear bound state. The momentum transfer \mathbf{q} into the residual nucleus B in the lab frame is very important for characterizing a nuclear reaction

$$a + A \rightarrow b + B, \quad (25)$$

where a , b , A and B are the incident, the detected, the target and the residual particles, respectively. Dalitz and Gal [61] discussed the kinematics of the exothermic reaction ($m_a + M_A > m_b + M_B$) such as $K^- + N \rightarrow \pi + \Lambda$ for Λ -hypernuclear production with “substitutional” states due to the recoilless condition with $q \simeq 0$ MeV/c. Dover and his collaborators [46, 56] studied for the endothermic reaction ($m_a + M_A < m_b + M_B$) such as $\pi + N \rightarrow K^+ + \Lambda$ for Λ -hypernuclear production and $K^- + N \rightarrow K^+ + \Xi^-$ for Ξ -hypernuclear production, leading to “spin-stretched” states due to a high momentum transfer $q \simeq 400$ -500 MeV/c. In the case of the (K^-, N) reaction, the momentum transfer at $p_{K^-} = 1.0$ GeV/c and $\theta_{\text{lab}} = 0^\circ$ becomes $q \simeq 200$ -400 MeV/c, depending on $B_{\bar{K}}$ in the \bar{K} nuclear bound state [9, 18, 22]. This situation seems to be similar to hypernuclear production by (π, K^+) reactions [9], but $M_A > M_B$ is different from $M_A < M_B$ occurred in hypernuclear production. Such a kinematical condition is often found in the (γ, p) or (π, p) reaction for searching the π , ω , ρ -nuclear bound states [54]. The kinematics for the (K^-, N) reaction differs completely from that for any hypernuclear production reactions, as we will discuss below; the momentum transfer $q(0^\circ)$ is negative, $q(0^\circ) = p_{K^-} - p_N < 0$, because the detected nucleon momentum p_N becomes 1.2-1.4 GeV/c at the incident K^- momentum $p_{K^-} = 1.0$ GeV/c [41]. The negative value of $q(0^\circ)$ means that the residual \bar{K} recoils backward relative to the incident particle K^- in the lab frame, as illustrated in Fig. 6.

Now we study the (K^-, N) reactions on the ^{12}C target, following the helpful arguments by Dalitz and Gal [61]. In Fig. 7, we show the momentum transfer of $q(0^\circ) = p_{K^-} - p_N$ in the (K^-, N) reaction on ^{12}C at $\theta_{\text{lab}} = 0^\circ$, as a function of the incident K^- lab momentum p_{K^-} . Similar figures drawing the momentum transfer would be found in several papers [18, 22], but Fig. 7 represents explicitly a sign of $q(0^\circ)$; the solid curve denotes $q(0^\circ)$ for \bar{K} binding energies with $B_{\bar{K}} = 0, 50$ and 100 MeV in the nucleus. The dashed curve corresponds to the recoil $q(0^\circ)$ in the case of $B_{\bar{K}} = -\varepsilon_N = 16.0$ MeV, which gives a “nonthermic” condition as $m_{K^-} + M_A = m_N + M_B$.

In the endothermic case of $m_{K^-} + M_A < m_N + M_B$, there is a threshold lab momentum p_{th} , which is 129.4 MeV/ c when we choose $B_{\bar{K}} = 0$ MeV. The dotted line in Fig. 7 denotes the relation $q_{\text{th}} = (M_B - m_N)/(M_B + m_N)p_{\text{th}}$ at the threshold in the endothermic condition. Moreover, the magic momentum p_0 can be found at 188.1 MeV/ c , fulfilling the recoilless condition $\sqrt{p_0^2 + m_{K^-}^2} + M_A = \sqrt{p_0^2 + m_N^2} + M_B$; its value is obtained by the relation

$$p_0 = \sqrt{\prod (M_B - M_A \pm m_{K^-} \pm m_N)} / 2(M_A - M_B), \quad (26)$$

where $\prod(a \pm b \pm c) = (a + b + c)(a + b - c)(a - b + c)(a - b - c)$, as given in Ref. [61]. In the exothermic case of $m_{K^-} + M_A > m_N + M_B$, the recoil momentum q_0 at $p_{K^-} = 0$ GeV/ c is given by

$$q_0 = \sqrt{\prod (m_{K^-} + M_A \pm m_N \pm M_B)} / 2(m_{K^-} + M_A), \quad (27)$$

under the condition $m_{K^-} + M_A = \sqrt{q_0^2 + m_N^2} + \sqrt{q_0^2 + M_B^2}$. Thus, the values of q_0 are -244.2 and -387.8 MeV/ c for $B_{\bar{K}} = 50$ and 100 MeV, respectively. Moreover, there is a point of inflection in $q(0^\circ)$, which is given by the condition $\partial q(0^\circ)/\partial p_{K^-} = 0$. This point gives a minimum of $|q(0^\circ)|$, q_{min} , of which values are -173.4 MeV/ c at $p_{K^-} = 192.6$ MeV/ c and -279.2 MeV/ c at $p_{K^-} = 310.0$ MeV/ c for $B_{\bar{K}} = 50$ and 100 MeV, respectively. When we consider $p_{K^-} \rightarrow +\infty$, we confirm that $q(0^\circ)$ goes into the limit $q_\infty = (M_B^2 - M_A^2)/2M_A$, leading to $-420.4, -468.4$ and -516.1 MeV/ c for $B_{\bar{K}} = 0, 50$ and 100 MeV, respectively.

———— **FIG. 7** ————

The kinematical factor β [60] used in Eq. (18) expresses the translation from the two-body \bar{K} -nucleon lab system to the many-body \bar{K} -nucleus lab system [46]. It is defined by

$$\beta = \left(1 + \frac{E_N^{(0)} p_N^{(0)} - p_{K^-} \cos \theta_{\text{lab}}}{E_{\bar{K}}^{(0)} p_N^{(0)}} \right) \frac{p_N E_N}{p_N^{(0)} E_N^{(0)}}, \quad (28)$$

where p_{K^-} and p_N ($E_{\bar{K}}$ and E_N) are momenta of the incident K^- and the detected N (energies of \bar{K} and N) in the many-body $K^- + A \rightarrow N + \bar{K}B$ reaction, respectively, and the quantities bearing an (0) superscript are in the two-body $K^- + N \rightarrow N + \bar{K}$ reaction. For the forward direction ($\theta = 0^\circ$), the kinematical factor β in Eq. (28) is reduced to

$$\beta(0^\circ) = \left(1 - \frac{v_{\bar{K}}^{(0)}}{v_N^{(0)}}\right) \frac{p_N E_N}{p_N^{(0)} E_N^{(0)}}, \quad (29)$$

where $v_N^{(0)} = p_N^{(0)}/E_N^{(0)}$ is a velocity of the detected nucleon, and $v_{\bar{K}}^{(0)} = q(0^\circ)/E_{\bar{K}}^{(0)}$ that of the residual \bar{K} . The recoilless reaction under $q(0^\circ) \simeq 0$ MeV/c appears in the case of $B_{\bar{K}} = 0$ MeV and $p_{K^-} \simeq 0.18$ GeV/c, leading to $\beta(0^\circ) \simeq 1$. We stress that when we choose $p_{K^-} \geq \sim 0.5$ GeV/c, the value of $\beta(0^\circ)$ is larger than 1, because the momentum transfer $q(0^\circ) < 0$ and also $v_{\bar{K}}^{(0)} < 0$. On the other hand, the hypernuclear production by (π^+, K^+) and (K^-, K^+) reactions shows that the value of $\beta(0^\circ)$ is smaller than 1, because $q(0^\circ) = p_{\pi^+} - p_{K^+} > 0$ for the Λ -hypernuclei [56] and $q(0^\circ) = p_{K^-} - p_{K^+} > 0$ for the Ξ -hypernuclei [46]. One should recognize the different nature of the nuclear (K^-, N) reaction from the well-known (π^+, K^+) and (K^-, K^+) reactions.

In Fig. 8, we show a kinematical factor $\beta(0^\circ)$ in the (K^-, N) reaction on the ^{12}C target at $\theta_{\text{lab}} = 0^\circ$, as a function of the incident K^- lab momentum, together with a kinematical factor $\alpha(0^\circ)$ given by Eq. (B11) in Appendix B, which is often used in DWIA calculations [9, 46]. The calculated values also depend on the \bar{K} binding energies of $B_{\bar{K}}$; we find $\beta(0^\circ) = 1.52, 1.62$ and 1.75 for $B_{\bar{K}} = 0, 50$ and 100 MeV at $p_{K^-} = 1.0$ GeV/c, respectively, and these effects are not negligible. Cieplý et al. [9] calculated the integrated cross section for the \bar{K} nuclear $(1s)_{\bar{K}}$ bound state by (K^-, p) reactions on ^{12}C within the DWIA. When we assume $B_{K^-} = 122$ MeV, which corresponds to the same binding energy given in Ref. [9], for the $(1s)_{\bar{K}}$ bound state in the K^- - ^{11}B nucleus, we find $\alpha(0^\circ) = 1.76$, rather than 0.69 obtained in Ref. [9] which seems to arise as an error by the opposite sign of $q(0^\circ)$. Obviously, the kinematical factor is needed to reproduce the absolute value of the cross section of the (K^-, N) reaction.

————— **FIG. 8** —————

C. Eikonal distortion

Full distorted-waves of the nucleon- and K^- -nucleus are important to reproduce absolute values of the production cross sections. Since the (K^- , N) reaction requires a large momentum transfer and a high angular-momentum, we simplify the computational procedure by using the eikonal approximation to the distorted waves of the nucleon- and K^- -nucleus states [51, 52, 56, 57, 58]:

$$\begin{aligned}\chi_{N,m_s}^{(-)*}(\mathbf{p}_N, \mathbf{r}, \sigma) &= \exp\left(-i\mathbf{p}_N \cdot \mathbf{r} - \frac{i}{v_n} \int_z^{+\infty} U_N(\mathbf{b}, z') dz'\right) \chi_{\frac{1}{2},m_s}^\dagger(\sigma), \\ \chi_{K^-}^{(+)}(\mathbf{p}_{K^-}, \mathbf{r}) &= \exp\left(+i\mathbf{p}_{K^-} \cdot \mathbf{r} - \frac{i}{v_{K^-}} \int_{-\infty}^z U_{K^-}(\mathbf{b}, z') dz'\right)\end{aligned}\quad (30)$$

with an impact parameter coordinate \mathbf{b} and the optical potential for $\lambda = N$ or K^- ,

$$U_\lambda(r) = -i \frac{v_\lambda}{2} \bar{\sigma}_{\lambda N}^{\text{tot}} (1 - i\alpha_{\lambda N}) \rho(r), \quad (31)$$

where $\rho(r)$ is a nuclear density distribution, and $\bar{\sigma}_{\lambda N}^{\text{tot}}$ and $\alpha_{\lambda N}$ are an isospin-averaged total cross section and a ratio of the real to imaginary parts of the forward amplitude for the $\lambda + N$ scattering, respectively. $\chi_{\frac{1}{2},m_s}^\dagger(\sigma)$ is a spin- $(\frac{1}{2}, m_s)$ state of the nucleon. Reducing the r.h.s. in Eq. (30) by partial waves expansion, the distorted-waves at θ_{lab} in Eq. (19) can be expressed as

$$\begin{aligned}&\chi_{N,m_s}^{(-)*}(\mathbf{p}_N, \mathbf{r}, \sigma) \chi_{K^-}^{(+)}(\mathbf{p}_{K^-}, \mathbf{r}) \\ &= \sum_{J=L\pm\frac{1}{2}, M'} \sqrt{4\pi(2L+1)} i^L \tilde{j}_{LM}(p_N, p_{K^-}, \theta_{\text{lab}}; r) [Y_{LM}(\hat{\mathbf{r}}) \otimes \chi_{\frac{1}{2},m_s}^\dagger(\sigma)]_{JM'},\end{aligned}\quad (32)$$

where $\tilde{j}_{LM}(p_N, p_{K^-}, \theta_{\text{lab}}; r)$ is a radial part of the distorted-wave for angular-momentum transfer L , depending on the momentum transfer q . If the distortion is switched off, i.e., $\bar{\sigma}_{NN}^{\text{tot}} = \bar{\sigma}_{K^-N}^{\text{tot}} = 0$, it becomes $j_L(qr)\delta_{M0}$ for the plane-wave approximation, where $j_L(x)$ is the spherical Bessel function.

D. Isospin states

Now we discuss isospin properties of the residual \bar{K} -nuclear bound states in the forward (K^- , p) and (K^- , n) reactions on a nuclear target. Dover and his collaborators examined that the isospin properties in (K^- , π^\mp) and (π^\pm , K^+) reactions for Σ -hypernuclear production [50], and also (K^- , K^+) reactions for Ξ -hypernuclear production [46]. We attempt to

apply their treatment into the \bar{K} nuclear bound states, and to discuss the (K^-, n) and (K^-, p) reactions on the nuclear target. The isospin vectors relevant in the nuclear $A(K^-, N)B$ reaction, and their z -components, satisfy

$$\frac{\mathbf{1}}{2} + \mathbf{T}_A = \frac{\mathbf{1}}{2} + \mathbf{T}_B, \quad i_{K^-} + \tau_A = i_N + \tau_B, \quad (33)$$

respectively. For instance, we obtain the \bar{K} nuclear states by the (K^-, p) reaction on the ^{12}C target with $J_A^\pi = 0^+$ and $T_A = 0$ as

$$|\frac{11}{\bar{K}}\text{Be}\rangle_{T_B=1, \tau_B=-1} = |K^-\rangle|^{11}\text{B}\rangle \quad (34)$$

for $T_B = 1$ states, and by the (K^-, n) reactions,

$$\begin{aligned} |\frac{11}{\bar{K}}\text{B}\rangle_{T_B=1, \tau_B=0} &= \sqrt{\frac{1}{2}}|\bar{K}^0\rangle|^{11}\text{B}\rangle + \sqrt{\frac{1}{2}}|K^-\rangle|^{11}\text{C}\rangle, \\ |\frac{11}{\bar{K}}\text{B}\rangle_{T_B=0, \tau_B=0} &= \sqrt{\frac{1}{2}}|\bar{K}^0\rangle|^{11}\text{B}\rangle - \sqrt{\frac{1}{2}}|K^-\rangle|^{11}\text{C}\rangle, \end{aligned} \quad (35)$$

for both $T_B = 1$ and $T_B = 0$ states.

Using the Fermi-averaged elementary amplitudes $\bar{f}_{K^-N \rightarrow N\bar{K}}$ which give the isospin transition with $\Delta T = 1$ and $\Delta T = 0$, we obtain the explicit isospin dependence of the nuclear amplitudes for the nuclear (K^-, N) reactions involving an isospin transition $(T_A, \tau_A) \rightarrow (T_B, \tau_B)$ [46];

$$\begin{aligned} F^{(K^-, p)} &= \sqrt{3(2T_A + 1)(2T_B + 1)}(-)^{T_B - \tau_B} \begin{pmatrix} T_B & 1 & T_A \\ -\tau_B & -1 & \tau_A \end{pmatrix} \\ &\quad \times (-)^{T_B + T_C - \frac{1}{2}} \begin{Bmatrix} \frac{1}{2} & T_B & T_C \\ T_A & \frac{1}{2} & 1 \end{Bmatrix} \bar{f}^{(1)}, \end{aligned} \quad (36)$$

$$\begin{aligned} F^{(K^-, n)} &= \delta_{T_A, T_B} \frac{1}{2} \bar{f}^{(0)} - \sqrt{\frac{3(2T_A + 1)(2T_B + 1)}{2}}(-)^{T_B - \tau_B} \begin{pmatrix} T_B & 1 & T_A \\ -\tau_B & 0 & \tau_A \end{pmatrix} \\ &\quad \times (-)^{T_B + T_C - \frac{1}{2}} \begin{Bmatrix} \frac{1}{2} & T_B & T_C \\ T_A & \frac{1}{2} & 1 \end{Bmatrix} \bar{f}^{(1)}, \end{aligned} \quad (37)$$

where $\bar{f}^{(0)}$ and $\bar{f}^{(1)}$ are the Fermi-averaged t -channel 0 and 1 amplitudes, respectively, and T_C denotes the isospin of the core-nucleus. These expression indicates clearly that the nuclear (K^-, p) reaction has $\Delta T = 1$, while the nuclear (K^-, n) reaction $\Delta T = 1, 0$.

When we assume closed-shells targets with $J_A^\pi = 0^+$ and $T_A = 0$ such as ^4He , ^{12}C and ^{28}Si , we find that only $T_B = 1$ levels are excited by the (K^-, p) reaction due to the restriction to $T_A = 0$, as seen in Eq.(36). Thus, we obtain

$$F_{T_A=0, T_B=1}^{(K^-, p)} = -\frac{1}{\sqrt{2}}\bar{f}^{(1)}. \quad (38)$$

For the (K^-, n) reaction, both $T_B = 0, 1$ types of levels can be excited in the \bar{K} nuclear states;

$$F_{T_A=0, T_B=0}^{(K^-, n)} = \frac{1}{2}\bar{f}^{(0)}, \quad F_{T_A=0, T_B=1}^{(K^-, n)} = \frac{1}{2}\bar{f}^{(1)}. \quad (39)$$

In order to clarify the isospin properties of the lab cross section with the final T_B states in the \bar{K} nuclear bound states, therefore, we evaluate the ratios of the cross sections

$$\frac{\sigma(K^-, n)_{T_A=0, T_B=1}}{\sigma(K^-, p)_{T_A=0, T_B=1}} = \frac{1}{2}, \quad (40)$$

and for the summed cross section

$$\begin{aligned} \frac{\sum_B \sigma(K^-, n)_{T_A=0, T_B=0}}{\sum_B \sigma(K^-, p)_{T_A=0, T_B=1}} &= \frac{1}{2} \frac{|\bar{f}^{(0)}|^2}{|\bar{f}^{(1)}|^2} \\ &= \frac{1}{2} \frac{|f_{K^-n \rightarrow nK^-} + f_{K^-p \rightarrow n\bar{K}^0}|^2}{|f_{K^-p \rightarrow pK^-}|^2} = \frac{1}{2} \left| 2 \frac{f_{K^-n \rightarrow nK^-}}{f_{K^-p \rightarrow pK^-}} - 1 \right|^2. \end{aligned} \quad (41)$$

Here we used the last equality in Eq.(12). In the case that the forward $K^- + n \rightarrow n + K^-$ cross section is much larger than the forward $K^- + p \rightarrow p + K^-$ cross section at 1.0 GeV/c, the ratio (41) shows approximately

$$\frac{\sum_B \sigma(K^-, n)_{T_A=0, T_B=0}}{\sum_B \sigma(K^-, p)_{T_A=0, T_B=1}} \simeq 2 \frac{\langle d\sigma/d\Omega \rangle_{0^\circ}^{K^-n \rightarrow nK^-}}{\langle d\sigma/d\Omega \rangle_{0^\circ}^{K^-p \rightarrow pK^-}} = 2 \times \frac{13.9}{5.2} \simeq 5.3. \quad (42)$$

Comparing Eq.(40) with Eq.(42), we obtain roughly the ratio

$$\frac{\sum_B \sigma(K^-, n)_{T_A=0, T_B=0}}{\sum_B \sigma(K^-, n)_{T_A=0, T_B=1}} \simeq 10, \quad (43)$$

which shows a strong preference for the excitation of $T_B = 0$ states by the (K^-, n) reaction. This fact indicates that the (K^-, n) reaction on the closed-shells targets $J_A^\pi = 0^+$, $T_A = 0$ can populate dominantly isospin $T_B = 0$ states. We obtain the isoscalar $\Delta T = 0$ and isovector $\Delta T = 1$ transition cross sections in the lab frame,

$$\begin{aligned} \sigma(\Delta T = 0) &= \frac{1}{2} |\bar{f}^{(0)}|^2 = \left| \frac{1}{\sqrt{2}} \bar{f}_{K^-n \rightarrow nK^-} + \frac{1}{\sqrt{2}} \bar{f}_{K^-p \rightarrow n\bar{K}^0} \right|^2, \\ \sigma(\Delta T = 1) &= \frac{1}{2} |\bar{f}^{(1)}|^2 = \left| \frac{1}{\sqrt{2}} \bar{f}_{K^-n \rightarrow nK^-} - \frac{1}{\sqrt{2}} \bar{f}_{K^-p \rightarrow n\bar{K}^0} \right|^2, \end{aligned} \quad (44)$$

for the nuclear (K^-, n) reaction on the closed-shell targets. These transition cross sections in Eq. (44) are rewritten as

$$\begin{aligned}\sigma(\Delta T = 0) &= \frac{1}{2}\sigma(\bar{K}^0) + \frac{1}{2}\sigma(K^-) + \sqrt{\sigma(\bar{K}^0)\sigma(K^-)} \cos \varphi_R, \\ \sigma(\Delta T = 1) &= \frac{1}{2}\sigma(\bar{K}^0) + \frac{1}{2}\sigma(K^-) - \sqrt{\sigma(\bar{K}^0)\sigma(K^-)} \cos \varphi_R,\end{aligned}\quad (45)$$

where $\sigma(\bar{K}^0)$ and $\sigma(K^-)$ are the Fermi-averaged cross sections of the \bar{K}^0 and the K^- production, respectively, in the (K^-, n) reaction. φ_R denotes the relative phase between $\bar{f}_{K^-n \rightarrow nK^-}$ and $\bar{f}_{K^-p \rightarrow n\bar{K}^0}$.

In Fig. 9, we show the Fermi-averaged transition cross sections of $\sigma(\Delta T = 0)$ and $\sigma(\Delta T = 1)$, together with $\sigma(\bar{K}^0)$ and $\sigma(K^-)$, and also that for $K^- + p \rightarrow p + K^-$. We find that the magnitude of $\Delta T = 0$ is quite larger than that of $\Delta T = 1$ over a wide momentum range, since the interference terms between $K^- + n \rightarrow n + K^-$ and $K^- + p \rightarrow n + \bar{K}^0$ channels in the r.h.s. of Eq. (45) are positive in the momentum region of $p_{K^-} = 0.6\text{-}2.0$ GeV/c where the relative phase has $14.4^\circ \leq \varphi_R \leq 64.1^\circ$, leading to $\sigma(\Delta T = 0) > \sigma(\Delta T = 1)$. Indeed, the value of $\sigma(\Delta T = 0)$ at $p_{K^-} = 1.0$ GeV/c amounts to 19.6 mb/sr, while the value of $\sigma(\Delta T = 1)$ is 1.7 mb/sr, which corresponds to a half of the cross section of the $K^- + p \rightarrow p + K^-$ reaction. The interference effects are significant and have to be considered in calculations of cross sections for nuclear targets.

———— **FIG. 9** ————

In Fig. 10, we show the ratios of the Fermi-averaged cross sections $\sigma(\Delta T = 0)/\sigma(\Delta T = 1)$ in isospin base and $\sigma(K^-)/\sigma(\bar{K}^0)$ in charge base in the nuclear (K^-, n) reactions, as a function of p_{K^-} . We find that the excitation of the isospin states with $\Delta T = 0$ dominates the 0.6-1.6 momentum region. Particularly, the ratio of $\sigma(\Delta T = 0)/\sigma(\Delta T = 1)$ is quite large near 1.4 GeV/c, because the cross section of $\sigma(\Delta T = 1)$ is reduced, as seen in Fig. 9. On the other hand, the cross sections of charged K^- and \bar{K}^0 states in this region are not so different from each other; $\sigma(K^-)/\sigma(\bar{K}^0) \simeq 1\text{-}2$. We recognize that the contributions of both K^- and \bar{K}^0 are necessary to explain the cross section in the nuclear (K^-, n) reaction.

———— **FIG. 10** ————

E. \bar{K} -nucleus potentials and \bar{K} nuclear bound states

The \bar{K} -nucleus potentials have been obtained by analyzing strong-interaction shifts and widths of K^- atomic X-ray data of 65 data points [8]. However, it is known that it is difficult to clarify the geometry and strengths inside the nucleus from the K^- atomic data, because the calculated values of the shifts and widths are sensitive to almost only a tail part of the potential outside the nuclear surface [8]. Hence, several types of the \bar{K} -nucleus potential have been proposed to reproduce the K^- atomic data, taking theoretical constraints into consideration: (a) the $t_{\text{eff}}\rho$ -type potential [62] determined earlier by an effective $\bar{K}N$ scattering length, e.g., $\bar{a} = 0.62 + i0.92$ fm which corresponds to $U_{\bar{K}}(0) = -89 - i133$ MeV at the nuclear center in ^{11}B ; (b) the density-dependent (DD) potential [8] determined by fitting its phenomenological parameters based by the $\bar{K}N$ scattering length; (c) the Chiral-motivated potential [14, 63, 64] constrained microscopically by the $\bar{K}N$ - πY coupled-channels describing the $\Lambda(1405)$ in the nuclear medium, leading to a strongly attraction of $\text{Re}U_{\bar{K}} \simeq -110$ MeV. But a version of the potentials calculated *self consistently* in the in-medium propagator yields $\text{Re}U_{\bar{K}} \simeq -40$ - (-60) MeV [15, 16, 17, 65, 66]; (d) the relativistic mean-field (RMF) potential calculated for the L-SH or NL-SH model with the α_σ and α_ω parameters [67]. One of the current problems in \bar{K} -nuclear physics is whether the depth of the \bar{K} -nucleus potential is deep, $\text{Re}U_{\bar{K}} \simeq -100$ - (-200) MeV, or shallow, $\text{Re}U_{\bar{K}} \simeq -40$ - (-60) MeV.

In this paper, we employ the *deep* \bar{K} -nucleus DD potential [8] involving an isovector term, in order to see the isospin dependence of the deeply-bound \bar{K} -nuclear states which are expected to be observed as relative narrow signals if these bound states exist below the $\pi\Sigma$ -threshold. The \bar{K} -nucleus DD potential [8] is given as

$$2\mu U_{\bar{K}}(r) = -4\pi \left(1 + \frac{\mu}{m_N}\right) \left\{ \left[b_0 + B_0 \left(\frac{\rho(r)}{\rho(0)}\right)^\alpha \right] \rho(r) + \left[b_1 + B_1 \left(\frac{\rho(r)}{\rho(0)}\right)^\alpha \right] \delta\rho(r) \right\}, \quad (46)$$

where the point nucleon distribution $\rho(r) = \rho_p(r) + \rho_n(r)$ and the isovector one $\delta\rho(r) = \rho_n(r) - \rho_p(r)$, and phenomenological parameters $b_0 = -0.15 + i0.62$ fm, $b_1 = -0.20 + i0.15$ fm, $B_0 = 1.58 + i0.02$ fm, $B_1 = 0.0$ fm and $\alpha = 0.17$. It is also rewritten in a general form by

$$U_{\bar{K}}(r) = U_0^{\bar{K}}(r) + U_1^{\bar{K}}(r)(\mathbf{T}_C \cdot \mathbf{t}_{\bar{K}})/A_{\text{core}}, \quad (47)$$

where \mathbf{T}_C is the isospin operator of the core nucleus with its z -projection $\tau_C = (Z - N)/2$, and $\mathbf{t}_{\bar{K}}$ is the \bar{K} isospin operator with $\tau_{\bar{K}} = \pm 1/2$ for the (\bar{K}^0, K^-) isodoublet; $U_0^{\bar{K}}$ and $U_1^{\bar{K}}$

are isoscalar and isovector (Lane term) parts of the potential, respectively. This real parts of the potential has the attraction corresponding to $\text{Re}U_{\bar{K}} \simeq -150-(-200)$ MeV at nuclear matter density.

The study of the (K^-, n) reaction on the closed shells targets yields information concerning the potential properties of the isoscalar and isovector parts in the \bar{K} -nucleus potential, because the reaction can populate both isospin $T_B = 0$ and $T_B = 1$ states. The configurations of the potentials for isospin $T_B = 0, 1$ states represent

$$\begin{aligned} U_{\bar{K}}^{T_B=0} &= U_0^{\bar{K}} - U_1^{\bar{K}}/4A_{\text{core}}, \\ U_{\bar{K}}^{T_B=1} &= U_0^{\bar{K}} + U_1^{\bar{K}}/4A_{\text{core}}, \end{aligned} \quad (48)$$

whereas the (K^-, p) reaction gives information on only $U_{\bar{K}}^{T_B=1}$ for $T_B = 1$ states.

————— **FIG. 11** —————

In Fig. 11, we illustrate the real and imaginary parts of the \bar{K} -nucleus DD potentials for isospin $T = 0, 1$ states in $A = 11$ and 27 which are populated via nuclear (K^-, N) reactions on the ^{12}C and ^{28}Si targets, respectively. We find that $\text{Re}U_0^{\bar{K}}(0) \simeq -210-(-220)$ MeV and $\text{Re}U_1^{\bar{K}}(0) \simeq 120$ MeV at the nuclear center. It is also shown that the value of $\text{Re}U_1^{\bar{K}}(0) \sim 152-210$ MeV is obtained in a Breuckner calculation with $\bar{K}N$ interaction by fits to the low-energy $\bar{K}N$ scattering data [25]. However, the isospin dependence on the $U_1^{\bar{K}}$ Lane term has to be reduced by A_{core}^{-1} . Recently, Kishimoto et al. [21] have suggested $\text{Re}U_{\bar{K}}^{T_B=0} \sim -190$ MeV and $\text{Re}U_{\bar{K}}^{T_B=1} \sim -160$ MeV for ^{11}B by the DWIA analysis of the $^{12}\text{C}(\text{in-flight } K^-, N)$ data (PS-E548) at KEK. This means $\text{Re}U_1^{\bar{K}} \sim 660$ MeV. Consequently, this value seems to be too large in terms of the isospin dependence of the \bar{K} -nucleus potential.

The search for deeply-bound \bar{K} states is one of the most important subjects in \bar{K} nuclear physics. However, signals of the states lying above the $\pi\Sigma$ -threshold might be unclear in the (K^-, p) spectrum due to large decay widths of the main $\bar{K}N \rightarrow \pi\Sigma$ channels. If the deeply-bound \bar{K} state exists below the $\pi\Sigma$ -threshold, as discussed by Yamazaki and Akaishi [31] and by Mareš et al. [67], one expects that a clear signal of the bound state with the relative narrow width $\Gamma_{\bar{K}} \simeq 20-50$ MeV can be observed. In order to take account of these effects, we introduce the imaginary parts of the \bar{K} -nucleus potentials including a phase space factor $f(E)$;

$$\text{Im}U_{\bar{K}}(r) \rightarrow \text{Im}U_{\bar{K}}(r) \times f(E), \quad (49)$$

as attempted in Refs. [19, 23], Here we used the phase space factor $f(E)$ by Mareš et al. [67].

We calculate the \bar{K} nuclear *unstable* bound states by solving the Schrödinger equation instead of the Klein-Gordon equation for simplicity. Since the Hamiltonian $H = T + U_{\bar{K}}$ is not Hermitian, we have

$$\begin{aligned} H \varphi_{n\ell} &= E_{n\ell} \varphi_{n\ell}, \\ H^\dagger \tilde{\varphi}_{n\ell} &= E_{n\ell}^* \tilde{\varphi}_{n\ell}, \end{aligned} \quad (50)$$

where $E_{n\ell}$ is a complex eigenvalues for the \bar{K} unstable bound states. Thus, the \bar{K} nuclear binding energies and widths can be evaluated as

$$E_{n\ell} = (k_{n\ell}^{(pole)})^2/2\mu = -B_{n\ell} - i\Gamma_{n\ell}/2, \quad (51)$$

where $k_{n\ell}^{(pole)}$ denotes a pole position of the bound state in the complex momentum plane, and μ is the reduce mass of the \bar{K} -nucleus system. $\varphi_{n\ell}$ is a wave function for the eigenstate labeled by $E_{n\ell}$, and $\tilde{\varphi}_{n\ell}$ is the wave function given by a biorthogonal set; its conjugate state becomes $(\tilde{\varphi}_{n\ell})^* = \varphi_{n\ell}$. It is noticed that such radial wave functions must be normalized by so-called c -products [68],

$$\int_0^\infty r^2 dr (\tilde{\varphi}_{n\ell}(r))^* \varphi_{n\ell}(r) = \int_0^\infty r^2 dr (\varphi_{n\ell}(r))^2 = 1, \quad (52)$$

under the boundary condition for decaying states [69]. Therefore, we can obtain the completeness relation for Green's function as

$$G_\ell(\omega; r', r) = \sum_n \frac{\varphi_{n\ell}(r') (\tilde{\varphi}_{n\ell}(r))^*}{\omega - E_{n\ell} + i\epsilon} + \frac{2}{\pi} \int_0^\infty dk \frac{k^2 S_\ell(k) u_\ell(k, r') (\tilde{u}_\ell(k, r))^*}{\omega - E_k + i\epsilon}, \quad (53)$$

where the summation over n includes all the pole of the S -matrix in the complex k -plane.

In Table II, we show the numerical results of the K^- nuclear binding energies and widths for ${}^{11}_{\bar{K}}\text{-Be}=[K^- - {}^{11}\text{B}]$ and ${}^{27}_{\bar{K}}\text{-Mg}=[K^- - {}^{27}\text{Al}]$, considering the effects of the Coulomb potentials and of the imaginary parts of the DD potentials. Note that the relativistic effects for the \bar{K} binding energy and the core-polarization (shrinkage effects for the core-nucleus) are not taken into account. In order to see the effects of the widths, we listed up the calculated results without the imaginary parts of the DD potential (Real only). The wave function for this state resides in the nuclear inside, e.g., the rms radius $\sqrt{\langle r^2 \rangle} = 1.3$ fm for $(1s)_{\bar{K}-}$ in ${}^{11}_{\bar{K}}\text{-Be}$, in comparison to the rms radius of the ${}^{11}\text{B}$ core-nucleus, 2.28 fm. When the imaginary part multiplied by the phase space factor [67] is switched on (Full), we find that the $(1s)_{\bar{K}-}$

bound state in $^{11}_{K^-}\text{Be}$ have a relative narrow width of $\Gamma_{\bar{K}} \simeq 25$ MeV because its pole arises at $k_{1s}^{(pole)} = -0.09 + i1.82 \text{ fm}^{-1}$ below the $\pi\Sigma$ decay threshold. For $^{27}_{K^-}\text{Mg}$, we find that the $(1s)_{K^-}$ state has a narrow width of $\Gamma_{\bar{K}} \simeq 22$ MeV and a rms radius of $\sqrt{\langle r^2 \rangle} = 1.6$ fm, and $(1p)_{K^-}$ state also $\Gamma_{\bar{K}} \simeq 25$ MeV and $\sqrt{\langle r^2 \rangle} = 2.0$ fm. The K^- is located at the nuclear inside in terms of the rms radius of 2.93 fm for ^{27}Al . As several K^- nuclear bound states with broad widths of $\Gamma_{\bar{K}} \simeq 100$ MeV exist, the shape of the peaks in the spectrum do not necessarily correspond to that of a standard Breit-Wigner resonance located at $B_{n\ell}$ [20], as shown in Appendix B. The observed peaks in the energy spectrum might be often seen near the points of $B_{n\ell}$ calculated by the real parts of the optical (complex) potentials.

———— TABLE II ————

F. Integrated cross sections and (K^-, N) spectra

Using the inclusive spectrum in the forward $A(K^-, N)$ reaction in Eq. (18), we can evaluate the integrated cross section of the \bar{K} nuclear unstable bound state by the energy integration

$$\left(\frac{d\sigma}{d\Omega_N} \right) = \int dE_N \left(\frac{d^2\sigma}{dE_N d\Omega_N} \right), \quad (54)$$

even if such a bound state has a large width and also exists near the \bar{K} emitted threshold. Here we consider especially that the \bar{K} nuclear states have a relative narrow width, because the $\bar{K}N \rightarrow \pi\Sigma$ decay channel is closed if the deeply-bound \bar{K} states have $B_{\bar{K}} > \sim 100$ MeV. Since these states are located far from the K^- threshold, we will attempt to calculate the integrated cross sections, adapting the effective number technique into the DWIA [9, 18, 22, 46], as mentioned in Appendix B. Considering that the \bar{K} nuclear state with total spin J_B has a $n\ell_{\bar{K}}$ orbit for \bar{K} and a j_N^{-1} proton-hole state, we obtain the forward (K^-, N) cross section for the bound state with $(j_N^{-1}, n\ell_{\bar{K}})J_B$ in the DWIA;

$$\left(\frac{d\sigma}{d\Omega_N}(0^\circ) \right)_{\text{lab}}^{(j_N^{-1}, n\ell_{\bar{K}})J_B} = \alpha(0^\circ) \left\langle \frac{d\sigma}{d\Omega}(0^\circ) \right\rangle_{\text{lab}}^{K^-N \rightarrow N\bar{K}} \text{Re} N_{\text{eff}}^{(j_N^{-1}, n\ell_{\bar{K}})J_B}(0^\circ). \quad (55)$$

Here we introduced precisely the *complex* effective nucleon number $N_{\text{eff}}^{(j_N^{-1}, n\ell_{\bar{K}})J_B}(0^\circ)$, which is defined as

$$N_{\text{eff}}^{(j_N^{-1}, n\ell_{\bar{K}})J_B}(0^\circ) = (2J_B + 1)(2j_N + 1)(2\ell_{\bar{K}} + 1) \begin{pmatrix} \ell_{\bar{K}} & j_N & J_B \\ 0 & -\frac{1}{2} & \frac{1}{2} \end{pmatrix}^2 F(q)F^\dagger(q). \quad (56)$$

The form factor $F(q)$ denotes

$$F(q) = \int_0^\infty r^2 dr (\tilde{\varphi}_{n\ell_{\bar{K}}}(r))^* \tilde{j}_{L0}(p_N, p_{K^-}, 0^\circ; r) \varphi_{j_N}^{(N)}(r), \quad (57)$$

where $L = J_B \pm \frac{1}{2}$ and $\ell_{\bar{K}} + L + \ell_N$ must be even due to the non-spin-flip processes. $\varphi_{j_N}^{(N)}$ denotes a single-particle wave function for the nucleon, and $\tilde{\varphi}_{n\ell_{\bar{K}}}$ is a biorthogonal one for the \bar{K} , as given by Eq. (50). One should notice that $N_{\text{eff}}^{(j_N^{-1}n\ell_{\bar{K}})J_B}(0^\circ)$ must be a complex number due to the unstable bound states with the non-Hermite Hamiltonian. When the potential has no imaginary part, $N_{\text{eff}}^{(j_N^{-1}n\ell_{\bar{K}})J_B}(0^\circ)$ is reduced to a real number. The recoil effects are taken into account in the distorted waves of $\tilde{j}_{L0}(p_N, p_{K^-}, 0^\circ; r)$ by the factors of M_C/M_B and M_C/M_A , as seen in Eq. (22). The kinematical factor $\alpha(0^\circ)$ is often used in the effective number technique within the DWIA [9, 46, 56, 57, 58, 60]. The relation between the kinematical factors β and α is shown in Appendix B.

The production cross sections for the deeply-bound \bar{K} nuclear states by the (K^-, p) reaction were performed theoretically by several authors [9, 18, 22]. Moreover, Kishimoto and his collaborators [21] have analyzed the inclusive spectra in the (K^-, p) and (K^-, n) reactions on the nuclear ^{12}C and ^{16}O targets. Therefore, a comparison between our results and other ones would be warrant, in order to recognize the nature of the nuclear (K^-, N) reactions. Let us attempt to calculate the production cross sections by the (K^-, p) reaction on the ^{12}C and ^{28}Si targets. For the ^{12}C target, we use single-particle wave functions for a proton, which are calculated with a Woods-Saxon potential [70]:

$$U_N(r) = V_0^N f(r) + V_{ls}^N (\mathbf{l} \cdot \mathbf{s}) r_0^2 \frac{1}{r} \frac{d}{dr} f(r) \quad (58)$$

with $f(r) = [1 + \exp((r - R)/a)]^{-1}$, where $V_{ls}^N = -0.44V_0^N$, $a=0.67$ fm, $r_0=1.27$ fm and $R = r_0 A^{1/3} = 2.91$ fm. We choose the strength of $V_0^N = -64.8$ MeV, fitting to the charge radius of 2.46 fm [71]. A Coulomb potential with a uniform sphere of the radius R is included. We input the proton hole-energy of $\varepsilon_N = -16.0$ MeV for a $1p_{3/2}$ hole state, and the energy and width of $\varepsilon_N = -36.0$ MeV and $\Gamma = 10$ MeV for a $1s_{1/2}$ state. For the ^{28}Si target, we use also single-particle wave functions for a proton, which are calculated with the WS potential with $R = r_0 A^{1/3} = 3.86$ fm. We choose the strength of $V_0^N = -59.7$ MeV, fitting to the charge radius of 3.09 fm [71], and input $\varepsilon_N = -11.6$ MeV for a $1d_{5/2}$ proton-hole state, and $(\varepsilon_N, \Gamma) = (-16 \text{ MeV}, 4 \text{ MeV})$, $(-23 \text{ MeV}, 6 \text{ MeV})$ and $(-41 \text{ MeV}, 10 \text{ MeV})$ for $1p_{1/2}$, $1p_{3/2}$ and $1s_{1/2}$ proton-hole states, respectively [72].

1. $^{12}\text{C}(K^-, p)$ reactions

In Table III, we show the numerical results of the integrated lab cross sections of $(j_N^{-1}, n\ell_{K^-})J^\pi$ states, which are given in Eq. (55), for the forward $^{12}\text{C}(K^-, p)$ reactions at the incident K^- lab momentum $p_{K^-} = 1.0$ GeV/c. This (K^-, p) reactions can populate only the $T = 1$ states in $^{11}_K\text{-Be}$ which consists of the K^- and the ^{11}B nucleus. It is noticed that “spin-stretched” states are excited selectively due to a high momentum transfer $q(0^\circ) = -380(-210)$ MeV/c, where the negative momentum transfer means that the residual K^- recoils backward relative to the incident particle K^- . We list up the value of the real part of the effective nucleon numbers and its argument, $\text{Re}N_{\text{eff}}$ and $\text{Arg}N_{\text{eff}}$, in order to see the shape of the inclusive spectrum as a function of E_{K^-} . As seen in Table III, a negative value of the cross section in the transition $1s_{\frac{1}{2}} \rightarrow (2s)_{K^-}$ means that the shapes of the states are “upside-down peaks” rather than Breit-Wigner peaks because the arguments satisfy $\text{Arg}N_{\text{eff}} > 90^\circ$ with substantial inelasticity and background [73] (See Fig. 12). As discussed by Morimatsu and Yazaki [20], such peak structures are often predicted in the spectra of Σ^- atomic states, and also those of the K^- atomic states [74]. For $[K^- \otimes ^{11}\text{B}]$ atomic states, indeed, we found $\text{Arg}N_{\text{eff}} = -157.9^\circ$ at $B_{K^-} = 199$ keV and $\Gamma_{K^-} = 41.6$ keV for the transition $1p_{\frac{3}{2}} \rightarrow (1s)_{\text{atom}}$, $\Delta L = 1$, and $\text{Arg}N_{\text{eff}} = 90.4^\circ$ at $B_{K^-} = 81.0$ keV and $\Gamma_{K^-} = 0.76$ keV for the transition $1p_{\frac{3}{2}} \rightarrow (1p)_{\text{atom}}$, $\Delta L = 2$.

Yamagata et al. [74] have discussed in detail some interesting shapes of the inclusive (K^-, p) spectra for K^- atomic states. In Fig. 12, thus, we display the shape of the strength function $S^{(\text{pole})}(E)$ given by Eq. (B3) in the $K^- \otimes ^{11}\text{B}$ system, as a function of E_{K^-} ; (a) $\text{Arg}N_{\text{eff}} = 0.08^\circ$ at $B_{K^-} = -130$ MeV, $\Gamma_{K^-} = 25$ MeV for the nuclear transition $1p_{\frac{3}{2}} \rightarrow (1s)_{K^-}$, $\Delta L = 1$, (b) $\text{Arg}N_{\text{eff}} = 98.3^\circ$ at $B_{K^-} = +23$ MeV, $\Gamma_{K^-} = 87$ MeV for $1s_{\frac{1}{2}} \rightarrow (2s)_{K^-}$, $\Delta L = 0$, and (c) $\text{Arg}N_{\text{eff}} = -157.9^\circ$ at $B_{K^-} = -199$ keV, $\Gamma_{K^-} = 41.6$ keV for the atomic transition $1p_{\frac{3}{2}} \rightarrow (1s)_{\text{atom}}$, $\Delta L = 1$. These spectra are plotted by each suitable energy scale in order to compare their shapes. The spectrum (a) has a standard Breit-Wigner peak, whereas the spectra (b) and (c) are sizably modified by the background; the shape in (c) just indicates the upside-down peak. These shapes also depend strongly on the momentum transfer by choosing the incident momentum p_{K^-} . Thus we find that the calculated values of $\text{Re}N_{\text{eff}}$ and $\text{Arg}N_{\text{eff}}$ give valuable information concerning the structure of the \bar{K} unstable bound states formed by this reaction condition.

———— TABLE III ————

———— FIG. 12 ————

One of the most important subjects is to clarify the possibility of the detected signals of the deeply-bound K^- nuclear states; A deeply-bound K^- state with $(1p_{\frac{3}{2}}^{-1}, 1s_{K^-})_{\frac{3}{2}}^{3+}$ configuration is located below the $\pi\Sigma$ threshold, having the relative narrow widths ~ 25 MeV, for the K^- nuclear $1s$ bound state via the $(1p)_p \rightarrow (1s)_{K^-}$ transition in ^{12}C at the incident K^- lab momentum $p_{K^-} = 1.0$ GeV/c. Here we used the Fermi-averaged elementary cross section of $\langle d\sigma(0^\circ)/d\Omega \rangle_{\text{lab}}^{K^-p \rightarrow pK^-} = 3.5$ mb/sr in Eq. (17), which is slightly smaller than 5.2 mb/sr used in Ref. [9]. For distortion parameters in the DWIA, we choose $\bar{\sigma}_{NN}^{\text{tot}} = \bar{\sigma}_{K^-N}^{\text{tot}} = 40$ mb and $\alpha_{NN} = \alpha_{K^-N} = 0$, followed by precedent pioneering works [9, 18, 22, 23].

The calculated effective number for $(1p_{\frac{3}{2}}^{-1}, 1s_{K^-})_{\frac{3}{2}}^{3+}$ is $\text{Re}N_{\text{eff}}^{(1p_{\frac{3}{2}}^{-1}, 1s_{K^-})_{\frac{3}{2}}^{3+}} = 0.98 \times 10^{-2}$, which is in agreement with the result of 0.013 calculated in Ref. [9]. Thus, the integrated lab cross section for $(1p_{\frac{3}{2}})_p \rightarrow (1s)_{K^-}$ in Eq. (55) is obtained by

$$\left(\frac{d\sigma}{d\Omega_N}(0^\circ) \right)_{\text{lab}}^{(1p_{\frac{3}{2}}^{-1}, 1s_{K^-})_{\frac{3}{2}}^{3+}} = 1.78 \times 3.5 \text{ (mb/sr)} \times (0.98 \times 10^{-2}) = 61 \text{ } (\mu\text{b/sr}). \quad (59)$$

In Table IV, we compare this value of $(d\sigma(0^\circ)/d\Omega)_{\text{lab}}$ with those seen in other works on the ^{12}C target [9, 18, 22] under similar conditions of the momentum transfer q , together with the case of the ^{28}Si target: Our results seem to be in good agreement with those calculated by Yamagata et al. [22], who make a choice of $(d\sigma(0^\circ)/d\Omega)_{\text{lab}} = 8.8$ mb/sr for the input $K^- + p \rightarrow p + K^-$ cross section, whereas the kinematical factor $\alpha(0^\circ)$ and recoil effects were not included in their calculation. The difference from the results by Cieplý et al. [9] would come from $\alpha(0^\circ) = 0.69$ which was erroneously employed due to missing a negative momentum transfer, in addition to a use of harmonic-oscillator wave functions for proton-hole and K^- bound states, and the input $(d\sigma(0^\circ)/d\Omega)_{\text{lab}} = 5.2$ mb/sr.

———— TABLE IV ————

In Fig. 13, we show the inclusive spectrum from $^{12}\text{C}(K^-, p)$ reactions at $p_{K^-} = 1.0$ GeV/c, in the $^{11}_K\text{-Be}$ bound region obtained by our results listed up in Table II. Note that the contributions of the background of the K^- absorption processes and the continuum states for K^- are not included. In order to recognize the population by the (K^-, p) reaction, we also illustrate the integrated cross sections which are calculated by omitting the

imaginary parts of the DD potentials and the width of the $1s_{\frac{1}{2}}$ proton-hole state. The resultant spectra confirm that it is difficult to observe clear signals of the deeply-bound K^- states even if the relative narrow state such as $(1p_{\frac{3}{2}}^{-1}, 1s_{K^-})$ exists, as discussed in Refs. [23] and [21]; these cross sections are relatively reduced by the distortion of the incoming K^- and outgoing proton waves, i.e., the distortion factor becomes $D_{\text{dis}} \simeq \text{Re}N_{\text{eff}}^{\text{DW}}/\text{Re}N_{\text{eff}}^{\text{PW}} = 0.98 \times 10^{-2}/15.6 \times 10^{-2} = 0.063$ for the $(1p_{\frac{3}{2}})_p \rightarrow (1s)_{K^-}$ transition, where the superscripts DW and PW denote the distorted-wave and plane-wave approximations, respectively. In Figs. 14 and 15, we display the angular distributions of the formation of $\Delta L = 1, 3$ and $\Delta L = 0, 2$ in ${}^{12}_{K^-}\text{Be}$ via the (K^-, p) reaction at 1.0 GeV/c. The curves labeled by $(-)$ indicate the negative value for the cross section which means that the shape of these spectra for the corresponding bound states behaves such as upside-down peaks with substantial background, rather than Breit-Wigner peaks, as seen in Fig. 12.

———— **FIG. 13** ————

———— **FIG. 14** ————

———— **FIG. 15** ————

2. ${}^{12}\text{C}(K^-, n)$ reactions

In Fig. 16, we show the inclusive spectrum from ${}^{12}\text{C}(K^-, n)$ reactions at $p_{K^-} = 1.0$ GeV/c, which can be populate both $T = 1$ and $T = 0$ states of ${}^{11}_{K^-}\text{B}$, as shown in Eq. (32). Here we assumed that there appear the isospin good quantum number states in ${}^{11}_{K^-}\text{B}$, using the DD potentials and omitting the Coulomb potential. Then, we input the Fermi-averaged cross sections for $\Delta T = 0$ and $\Delta T = 1$, which are 19.6 mb/sr and 1.7 mb/sr, respectively, as shown in Fig. 9. We find that the shape and magnitude of the inclusive spectrum are almost determined by the contribution of the $T = 0$ configuration. The cross sections of the $T = 0$ states are almost 10 times larger than those of the $T = 1$ ones in the (K^-, n) reaction.

The analysis of the (K^-, N) reactions for the experimental data on light nuclear targets is expected to clarify the important information concerning the formation mechanism for K^- nuclear bound states and the nature of the \bar{K} -nucleus potentials. Particularly, we believe that the comparison between the (K^-, p) and (K^-, n) spectra provides the isospin properties

for the $K^- + N \rightarrow N + \bar{K}$ reactions and the \bar{K} -nucleus potentials, and the imaginary parts of the potentials, observing the spectrum of $\pi\Lambda$ decay processes,

$$[{}_{K^-}^{11}\text{B}] \rightarrow \pi + \Lambda + \text{nucleus}, \quad (60)$$

below the $\pi\Sigma$ threshold.

———— **FIG. 16** ————

3. ${}^{28}\text{Si}(K^-, p)$ reactions

For a heavier ${}^{28}\text{Si}$ target, we show the numerical results of the integrated lab cross sections for the forward (K^-, p) reactions at the incident K^- lab momentum $p_{K^-} = 1.0$ GeV/c, as listed up in Table V. In Fig. 17, we display the integrated cross sections and the inclusive spectrum, together with the contributions of $1d_{\frac{5}{2}}$, $1p_{\frac{1}{2}}$ and $1p_{\frac{3}{2}}$ proton-hole states. Note that the background and the continuum states for K^- which arise above the K^- threshold, are not taken into account. We find that the cross sections for the “spin-stretched” states coupled to the $1d_{\frac{5}{2}}$, $1p_{\frac{1}{2}}$, $1p_{\frac{3}{2}}$ and $1s_{\frac{1}{2}}$ hole states are populated selectively by the high momentum transfer, as seen clearly in Fig. 17 (top). However, we confirm also that it is difficult to observe a clear signal of the deeply-bound K^- nuclear state such as $(1s)_{K^-}$, because several states above the $\pi\Sigma$ threshold have a broad width of ~ 100 MeV, smudging out the narrow signal. Consequently, we believe that in order to avoid this difficulties at the present stage, one of the best ways might be to choose s -shell few-nucleons targets, ${}^3\text{H}$, ${}^3\text{He}$ and ${}^4\text{He}$, as proposed by the forthcoming E15 experiments at J-PARC.

———— **TABLE V** ————

———— **FIG. 17** ————

IV. DEEPLY-BOUND ANTIKAONIC STATES ON s -SHELL NUCLEI

We study the (K^-, N) reactions on the s -shell nuclear target, considering the transitions $(1s_{\frac{1}{2}})_N \rightarrow (1s)_{\bar{K}}$ to final \bar{K} nuclear states of total spin S and total isospin T where all the nucleons are in s -shell. These states give a testing ground for isospin properties of the

production and decay processes in \bar{K} nuclei, since the core-nucleus is often spin and isospin unsaturated.

The production amplitudes for the nuclear (K^-, N) reactions on the target A in Eq. (18), $F_{fi} = \langle \Psi_B | \hat{F} | \Psi_A \rangle$, are written in the LS -coupling scheme as

$$F_{fi}^{(K^-, n)} = \bar{f}_{K^-n \rightarrow nK^-} S_{S_B, K^-}^{1/2} \langle K^- \otimes (A-1) Z | \rho_{fi} | A \rangle + \bar{f}_{K^-p \rightarrow n\bar{K}^0} S_{S_B, \bar{K}^0}^{1/2} \langle \bar{K}^0 \otimes (A-1) (Z-1) | \rho_{fi} | A \rangle \quad (61)$$

for (K^-, n) reactions, and

$$F_{fi}^{(K^-, p)} = \bar{f}_{K^-p \rightarrow pK^-} S_{S_B, K^-}^{1/2} \langle K^- \otimes (A-1) (Z-2) | \rho_{fi} | A \rangle \quad (62)$$

for (K^-, p) reactions. Here the spectroscopic amplitude $S_{S_B, \bar{K}}^{1/2}$ for the spin S_B and charge \bar{K} channel is given by

$$S_{S_B, \bar{K}}^{1/2} = \left\langle [X_{S_{C'}, T_{C'}}^{(C')}, X_{0, \frac{1}{2}}^{(\bar{K})}]_{S_B} X_{\frac{1}{2}, \frac{1}{2}}^{(N)} \middle| \sum_{j=1}^A \hat{O}_{N_j} \middle| X_{0, \frac{1}{2}}^{(\bar{K})} \mathcal{A} [X_{S_C, T_C}^{(C)} X_{\frac{1}{2}, \frac{1}{2}}^{(N)}]_{S_A T_A} \right\rangle. \quad (63)$$

where $X_{0, \frac{1}{2}}^{(\bar{K})}$, $X_{\frac{1}{2}, \frac{1}{2}}^{(N)}$ and $X_{S_C, T_C}^{(C)}$ ($X_{S_{C'}, T_{C'}}^{(C')}$) denote the spin-isospin functions $X_{S, T}$ for \bar{K} , N and the core-nucleus in the target nucleus (the core-nucleus in the \bar{K} nuclear states), respectively, and \mathcal{A} is an antisymmetric operator for nucleons in the nucleus. The transition amplitude for $A \rightarrow B = [\bar{K} \otimes (A-1) Z]$ is given as

$$\langle \bar{K} \otimes (A-1) Z | \rho_{fi} | A \rangle = (-)^{J_B + L - \frac{1}{2}} i^L \sqrt{(2\ell_A + 1)(2\ell_B + 1)(2J_A + 1)(2L + 1)} \times \begin{pmatrix} \ell_B & L & \ell_A \\ 0 & 0 & 0 \end{pmatrix} \left\{ \begin{matrix} \ell_A & J_A & \frac{1}{2} \\ J_B & \ell_B & L \end{matrix} \right\} \langle \Phi_{C'} | \Phi_C \rangle F_{\ell_B \ell_A L}(q), \quad (64)$$

where the factor $\langle \Phi_{C'} | \Phi_C \rangle$ denotes an overlapping between the core-nucleus for the initial and final states, taken into account the effects of the nuclear shrinkage (core-polarization) which are expected to be found in the \bar{K} -nuclear states. The form factor $F_{\ell_B \ell_A L}(q)$ is given by

$$F_{\ell_B \ell_A L}(q) = \int_0^\infty r^2 dr (\tilde{\varphi}_{n\ell_B}(r))^* \tilde{j}_{L0}(p_N, p_{K^-}, 0^\circ; r) \varphi_{\ell_A}^{(N)}(r), \quad (65)$$

where $\varphi_{\ell_A}^{(N)}(r)$ is a relative wave function for the N -nucleus system, respectively, as a function of the relative coordinate between the nucleon and the core-nucleus, and $\tilde{\varphi}_{n\ell_B}(r)$ is a biorthogonal wave function for unstable \bar{K} -nucleus systems; $\tilde{j}_{L0}(p_N, p_{K^-}, 0^\circ; r)$ is a partial

distorted-wave with the angular momentum transfer L at $\theta_{\text{lab}} = 0^\circ$ from the incoming K^- to the outgoing nucleon. The factors of M_C/M_B and M_C/M_A in Eq.(22) are very important for the recoil effects in s -shell light nuclei. Therefore, the production lab cross section for the (K^-, n) or (K^-, p) reaction is given as

$$\left(\frac{d\sigma_{fi}}{d\Omega_N}(0^\circ)\right)_{\text{lab}} = \alpha(0^\circ) \frac{1}{2J_A + 1} \sum_{M_A} \sum_{M_B, m_s} \text{Re}(F_{fi}^{(K^-, N)} F_{fi}^{(K^-, N)\dagger}), \quad (66)$$

where m_s denotes a z -component of the outgoing nucleon.

A. ^4He target

Akaishi and Yamazaki [24, 25] suggested to look for a deeply-bound $\bar{K} \otimes [NNN]$ $T=0$, $S=1/2$ state having a binding energy of over 100 MeV and a relative narrow width of $\Gamma \simeq 20$ MeV, because the main decay channel $\bar{K}N \rightarrow \pi\Sigma$ is closed. Wycech also pointed out that the width of such states could be as small as 20 MeV [75]. Surprisingly, Suzuki et al. [26] reported the experimental evidence of the tribaryon $S^0(3115)$ by the $^4\text{He}(\text{stopped } K^-, p)$ reaction (KEK-PS E471). But recently it has been withdrawn (KEK-PS E549/570) [27]. From a viewpoint of microscopic few-body dynamics, we believe that the isospin nature of $[\bar{K} \otimes [NNN]_{T=1/2}]$ configuration fully reveals itself because the ^3He and ^3H core-nucleus are spin-isospin unsaturated. Therefore, we consider the $^4\text{He}(K^-, N)$ reaction in order to see isospin properties of (K^-, N) reactions and also $\bar{K}N$ interactions.

Reducing the spectroscopic factor $S_{S_B, \bar{K}}^{1/2}$ in Eq. (63), we obtain the production amplitudes of Eq. (61);

$$\begin{aligned} F_{fi}^{(K^-, n)} &= \bar{f}_{K^-n \rightarrow nK^-} \langle K^- \otimes ^3\text{He} | \rho_{fi} | ^4\text{He} \rangle - \bar{f}_{K^-p \rightarrow n\bar{K}^0} \langle \bar{K}^0 \otimes ^3\text{H} | \rho_{fi} | ^4\text{He} \rangle, \\ F_{fi}^{(K^-, p)} &= -\bar{f}_{K^-p \rightarrow pK^-} \langle K^- \otimes ^3\text{H} | \rho_{fi} | ^4\text{He} \rangle. \end{aligned} \quad (67)$$

Substituting the spin-isospin functions in Eq. (C2) into Eq. (67), thus, we can rewrite

$$\begin{aligned} F_{fi}^{(K^-, n)} &= \bar{f}_{\Delta T=0} \langle \bar{K}^3\text{H}; T_B = 0 | \rho_{fi} | ^4\text{He} \rangle + \bar{f}_{\Delta T=1} \langle \bar{K}^3\text{H}; T_B = 1 | \rho_{fi} | ^4\text{He} \rangle, \\ F_{fi}^{(K^-, p)} &= -\sqrt{2} \bar{f}_{\Delta T=1} \langle \bar{K}^3\text{n}; T_B = 1 | \rho_{fi} | ^4\text{He} \rangle, \end{aligned} \quad (68)$$

where $\bar{f}_{\Delta T=0}$ and $\bar{f}_{\Delta T=1}$ are the (normalized) Fermi-averaged isoscalar $\Delta T = 0$ and isovector $\Delta T = 1$ transition amplitudes for the ^4He target, respectively;

$$\begin{aligned} \bar{f}_{\Delta T=0} &= (\bar{f}_{K^-n \rightarrow nK^-} + \bar{f}_{K^-p \rightarrow n\bar{K}^0}) / \sqrt{2} = \bar{f}^{(0)} / \sqrt{2}, \\ \bar{f}_{\Delta T=1} &= (\bar{f}_{K^-n \rightarrow nK^-} - \bar{f}_{K^-p \rightarrow n\bar{K}^0}) / \sqrt{2} = \bar{f}^{(1)} / \sqrt{2} = \bar{f}_{K^-p \rightarrow pK^-} / \sqrt{2}. \end{aligned} \quad (69)$$

Here we can confirm the isospin relation of the cross sections in Eq.(41) and the dominance of the $T = 0$ excitation by the (K^-, n) reaction. In Table VI, we show the relative production cross sections by the forward (K^-, N) amplitude for $\bar{K} \otimes [NNN]$ states with $T_C = 1/2$ and $S_C = 1/2$.

———— TABLE VI ————

B. ${}^3\text{He}$ and ${}^3\text{H}$ targets

Now we focus on the three-body $\bar{K}NN$ system as a deeply-bound \bar{K} nuclear state. This state is expected to be the lightest and the most important system for the \bar{K} bound state [30, 42], and it is populated from the (K^-, N) reaction on the ${}^3\text{He}$ or ${}^3\text{H}$ target. For ${}^3\text{He}(K^-, N)$ reactions, the production amplitudes for the $\bar{K} \otimes [NN]$ $S = 0$ states on charge \bar{K} basis are written as

$$\begin{aligned} F_{fi}^{(K^-, n)} &= \frac{1}{\sqrt{2}} \bar{f}_{K^-p \rightarrow n\bar{K}^0} \langle \bar{K}^0 \{pn\} | \rho_{fi} \rangle | {}^3\text{He} \rangle - \bar{f}_{K^-n \rightarrow nK^-} \langle K^- \{pp\} | \rho_{fi} \rangle | {}^3\text{He} \rangle, \\ F_{fi}^{(K^-, p)} &= \sqrt{2} \bar{f}_{K^-p \rightarrow pK^-} \langle K^- \{pn\} | \rho_{fi} \rangle | {}^3\text{He} \rangle. \end{aligned} \quad (70)$$

Substituting the spin-isospin functions listed up in Eq. (C3) into Eq. (70), we rewrite these amplitudes as

$$\begin{aligned} F_{fi}^{(K^-, n)} &= \bar{f}_{\Delta T=0} \langle \bar{K}^2\text{H}; T_B = 1/2 | \rho_{fi} \rangle | {}^3\text{He} \rangle + \bar{f}_{\Delta T=1} \langle \bar{K}^2\text{H}; T_B = 3/2 | \rho_{fi} \rangle | {}^3\text{He} \rangle, \\ F_{fi}^{(K^-, p)} &= \frac{1}{\sqrt{6}} \bar{f}_{\Delta T=0} \langle \bar{K}^2\text{n}; T_B = 1/2 | \rho_{fi} \rangle | {}^3\text{He} \rangle + \frac{1}{\sqrt{3}} \bar{f}_{\Delta T=1} \langle \bar{K}^2\text{n}; T_B = 3/2 | \rho_{fi} \rangle | {}^3\text{He} \rangle, \end{aligned} \quad (71)$$

where $\bar{f}_{\Delta T=0}$ and $\bar{f}_{\Delta T=1}$ are the Fermi-averaged (normalized) isoscalar $\Delta T = 0$ and isovector $\Delta T = 1$ transition amplitudes for the ${}^3\text{He}$ target, respectively:

$$\begin{aligned} \bar{f}_{\Delta T=0} &= \sqrt{2/3} (\bar{f}_{K^-n \rightarrow nK^-} + \bar{f}_{K^-p \rightarrow n\bar{K}^0}/2), \\ \bar{f}_{\Delta T=1} &= -(\bar{f}_{K^-n \rightarrow nK^-} - \bar{f}_{K^-p \rightarrow n\bar{K}^0})/\sqrt{3} = -\bar{f}_{K^-p \rightarrow pK^-}/\sqrt{3}, \end{aligned} \quad (72)$$

involving the effects of the spectroscopic amplitude $S_{S_B, \bar{K}}^{1/2}$ due to spin-isospin nature on the unsaturated ${}^3\text{He}$ target. In Table VII, we show the relative formation cross sections of these states on ${}^3\text{He}$, where the core configuration is restricted by the Pauli principle to $\{S_C, T_C\} = \{0, 1\}$ or $\{1, 0\}$. For the ${}^3\text{H}$ target, we show the relative formation cross sections at the forward (K^-, N) reactions, as shown in Table VIII. It is noticed that the ${}^3\text{H}(K^-, p)$

reaction can populate only the isospin $T_B = 1$, $S = 1/2$ states, in comparison with the case of the ${}^3\text{He}(K^-, p)$ reaction.

————— **TABLE VII** —————

————— **TABLE VIII** —————

In a previous paper [41], we examined the ${}^3\text{He}(\text{in-flight } K^-, n)$ reaction at $p_{K^-} = 1.0$ GeV/c, $\theta_{\text{lab}} = 0^\circ$, with some simplified assumption. Only the $K^- + n \rightarrow n + K^-$ forward scattering has been considered, omitting the $K^- + p \rightarrow n + \bar{K}^0$ charge exchange process which can also contribute to the $[\bar{K} \otimes \{pp\}_{T=1}]_{T=1/2}$ formation through the coupling between $[K^- \otimes \{pp}]$ and $[\bar{K}^0 \otimes \{pn}]$ channels. Replacing the transition amplitude $\bar{f}_{K^-n \rightarrow nK^-}$ in Eq. (70) by $-\bar{f}_{\Delta T=0}$, we can roughly estimate this contribution [41]; the cross section of the K^-pp bound state is enhanced by about 18 % with the Fermi-averaged amplitudes. It is noticed that the $\bar{K}NN$ state with $T=1/2$ dominates the (K^-, n) reaction at $p_{K^-} = 1.0$ GeV/c because $|\bar{f}_{\Delta T=0}|^2/|\bar{f}_{\Delta T=1}|^2 \simeq 14$. This nature justifies the assumption that we treat a single channel of $[\bar{K} \otimes \{NN\}_{T=1}]_{T=1/2}$ as K^-pp restrictedly [41]. We believe that a full coupled-channel calculation is needed in order to get more quantitative results. Moreover, a choice of the parameters in the eikonal distorted waves also changes the absolute value of the cross section, but the distortion effect is not significant for ${}^3\text{He}$. For the in-flight (K^-, N) reaction, it would be not appropriate to use the decay rate measured by K^- absorption at rest [76], considering that its value depends on atomic orbits where K^- is absorbed through atomic cascade processes [77]. More theoretical and experimental considerations are needed.

V. SUMMARY AND CONCLUSION

We have investigated theoretically the formation of deeply-bound antikaonic K^-/\bar{K}^0 nuclear states by the (K^-, N) reaction, introducing the complex effective number in the DWIA. We have discussed the isospin properties of the (K^-, N) reaction on the basis of the Fermi-averaged elementary amplitudes of the $K^- + p \rightarrow p + K^-$, $K^- + n \rightarrow n + K^-$ and $K^- + p \rightarrow n + \bar{K}^0$ processes, and the integrated cross sections for the nuclear (K^-, N) reaction at the incident K^- lab momentum $p_{K^-} = 1.0$ GeV/c and $\theta_{\text{lab}} = 0^\circ$, concerning the kinematical condition. The results are summarized as follows:

- (1) The deeply-bound \bar{K} states with the isospin $T = 0$ can be populated dominantly by the (K^-, n) reaction on closed shell targets, e.g., ^{12}C and ^{28}Si , because of the isospin nature of the $K^- + N \rightarrow N + \bar{K}$ amplitudes.
- (2) The (K^-, N) reaction differs kinematically from hypernuclear production of (π^+, K^+) and (K^-, K^+) reactions, so that the kinematical factors of $\alpha(0^\circ)$ and $\beta(0^\circ)$ are larger than 1, thus, the cross sections are enhanced.
- (3) The integrated cross sections of deeply-bound \bar{K} nuclear states for the (K^-, N) reaction on nuclear ^{12}C and ^{28}Si targets, can be obtained fully by the complex effective nucleon number N_{eff} ; $\text{Re}N_{\text{eff}}$ and $\text{Arg}N_{\text{eff}}$ enable to see the structure of the \bar{K} unstable bound states.
- (4) The deeply-bound \bar{K} nuclear states for the (K^-, N) reaction on s -shell nuclear targets, ^3He , ^3H and ^4He , have a strong isospin dependence of the cross sections due to the spin-isospin unsaturated nuclear core-states.

In conclusion, the (K^-, n) reaction at $p_{K^-} = 1.0 \text{ GeV}/c$ excites preferentially $\Delta T = 0$ states in the deeply-bound \bar{K} region, and is complementary to the (K^-, p) reaction which excites only isovector $\Delta T = 1$ states. The complex effective number approach provides insight on the structure of the bound state spectrum. Although the inclusive nucleon spectra calculated at $p_{K^-} = 1.0 \text{ GeV}/c$ for ^{12}C and ^{28}Si targets do not show distinct peak structure in the \bar{K} bound region, they show substantial strength in this region, thus promising to shed light on the depth of the \bar{K} nuclear potential. We advocate measuring nucleon (K^-, N) spectra on s -shell targets, ^3H , ^3He and ^4He , attempting to resolve the isospin structure of deeply-bound \bar{K} nuclear states. This investigation is in progress.

Acknowledgments

We would like to thank Professor M. Iwasaki, Professor Y. Akaishi, Dr. Y. Hirabayashi and Dr. A. Umeya for many valuable discussions. We are pleased to acknowledge Professor A. Gal for useful comments. This work is supported by Grant-in-Aid for Scientific Research on Priority Areas (No. 17070002 and No. 17070007).

APPENDIX A: INCLUSIVE CROSS SECTION FOR THE $A(a, b)$ REACTION AND THE KINEMATICAL FACTOR β IN EQ.(18)

In order to see the formulation for the inclusive cross section of Eq.(21), we consider a nuclear two-body reaction

$$a + A \rightarrow b + B, \quad (\text{A1})$$

where a , b , A and B denote the incident (incoming), the detected (outgoing), the target and the residual particles, respectively. The differential cross section in the lab frame can be expressed [78] as

$$d^6\sigma_{fi} = \frac{(2\pi)^4}{v_a} \delta(E_b + E_B - E_a - E_A) \delta(\mathbf{p}_b + \mathbf{p}_B - \mathbf{p}_a - \mathbf{p}_A) |T_{fi}|^2 \frac{d\mathbf{p}_b}{(2\pi)^3} \frac{d\mathbf{p}_B}{(2\pi)^3}, \quad (\text{A2})$$

where $v_a = p_a/E_a$, and the nuclear T -matrix for the transition $a + A \rightarrow b + B$ within the impulse approximation is defined by

$$T_{fi} = \langle \Psi_B | \chi_b^{(-)*} \hat{\mathcal{O}} \chi_a^{(+)} | \Psi_A \rangle, \quad (\text{A3})$$

where $\chi_b^{(-)*}$ and $\chi_a^{(+)}$ are distorted waves of the outgoing b and the incoming a , respectively. $\hat{\mathcal{O}}$ denotes a transition operator. Integrating over $d\mathbf{p}_B$ in Eq.(A2), the differential cross section can be written as

$$d^3\sigma_{fi} = \frac{1}{(2\pi)^2 v_a} \delta(E_f(\mathbf{p}_b) - E_i) |T_{fi}|^2 p_b^2 dp_b d\Omega_b, \quad (\text{A4})$$

where $E_f(\mathbf{p}_b) = E_b(\mathbf{p}_b) + E_B(\mathbf{p}_a + \mathbf{p}_A - \mathbf{p}_b)$ and $E_i = E_a(\mathbf{p}_a) + E_A(\mathbf{p}_A)$. Summing over all the final states $f = \{b, B\}$, we obtain the differential cross section for the inclusive reaction within the DWIA factorized the two-body elementary T -matrix $a + N \rightarrow b + Y$ [20];

$$\begin{aligned} d^3\sigma &= \sum_f d^3\sigma_{fi} \\ &= \frac{p_b E_b}{(2\pi)^2 v_a} |\langle \mathbf{p}_Y^{(0)} \mathbf{p}_b^{(0)} | t | \mathbf{p}_N \mathbf{p}_a \rangle|^2 dE_b d\Omega_b \\ &\quad \times \frac{1}{2J_A + 1} \sum_{M_A} \sum_{b, B} \langle \Psi_A | \chi_a^{(+)*} \hat{\mathcal{O}}^\dagger \chi_b^{(-)} | \Psi_B \rangle \delta(E - E_B) \langle \Psi_B | \chi_b^{(-)*} \hat{\mathcal{O}} \chi_a^{(+)} | \Psi_A \rangle \end{aligned} \quad (\text{A5})$$

$$\begin{aligned} &= \frac{p_b E_b}{(2\pi)^2 v_a} |\langle \mathbf{p}_Y^{(0)} \mathbf{p}_b^{(0)} | t | \mathbf{p}_N \mathbf{p}_a \rangle|^2 dE_b d\Omega_b \\ &\quad \times (-) \frac{1}{\pi} \text{Im} \left\langle \Psi_A | \chi_a^{(+)*} \hat{\mathcal{O}}^\dagger \chi_b^{(-)} \frac{1}{E - H_B + i\epsilon} \chi_b^{(-)*} \hat{\mathcal{O}} \chi_a^{(+)} | \Psi_A \right\rangle, \end{aligned} \quad (\text{A6})$$

where $\langle \mathbf{p}_Y^{(0)} \mathbf{p}_b^{(0)} | t | \mathbf{p}_N \mathbf{p}_a \rangle$ denotes the T -matrix for the elementary $a + N \rightarrow b + Y$ reaction process in the lab frame, and $\mathbf{p}_Y^{(0)}$ and $\mathbf{p}_b^{(0)}$ denote the momenta of Y and b , respectively, and $E = E_a(\mathbf{p}_a) + E_A(\mathbf{p}_A) - E_b(\mathbf{p}_b)$. Here we used the relation

$$\sum_B |\Psi_B\rangle \delta(E - E_B) \langle \Psi_B| = (-) \frac{1}{\pi} \text{Im} \left[\frac{1}{E - H_B + i\epsilon} \right], \quad (\text{A7})$$

where $[E - H_B + i\epsilon]^{-1}$ is Green's function for many-body final states B including the Y +core-nucleus system. Note that $dE_b = p_b dp_b / E_b$ is obtained from the energy-momentum relation for the detected b , $E_b = \sqrt{\mathbf{p}_b^2 + m_b^2}$, because the δ -function in Eq. (A7) is held in Green's function.

In the case of the elementary process, $a + N \rightarrow b + Y$, the differential cross section at θ_{lab} in the lab frame is written as

$$\left(\frac{d\sigma}{d\Omega_b} \right)_{\text{lab}}^{aN \rightarrow bY} = \frac{p_b^{(0)} E_b^{(0)}}{(2\pi)^2 v_a p_b^{(0)} E_Y^{(0)} + E_b^{(0)} (p_b^{(0)} - p_a \cos \theta_{\text{lab}})} \frac{p_b^{(0)} E_Y^{(0)}}{p_b^{(0)} E_Y^{(0)} + E_b^{(0)} (p_b^{(0)} - p_a \cos \theta_{\text{lab}})} |\langle \mathbf{p}_Y^{(0)} \mathbf{p}_b^{(0)} | t | \mathbf{p}_N \mathbf{p}_a \rangle|^2, \quad (\text{A8})$$

where $E_b^{(0)}$ and $E_Y^{(0)}$ denote energies of the detected b and the residual Y , respectively, and the superscript (0) refers to the kinematics for the two-body reaction on a nucleon (N) target. Substituting Eq. (A8) into Eq. (A6), we obtain the double-differential cross section for the inclusive $A(a, b)$ reaction as

$$\left(\frac{d^2\sigma}{dE_b d\Omega_b} \right) = \beta \left(\frac{d\sigma}{d\Omega_b} \right)_{\text{lab}}^{aN \rightarrow bY} S(E), \quad (\text{A9})$$

where the strength function is defined as

$$\begin{aligned} S(E) &= \frac{1}{2J_A + 1} \sum_{M_A} \sum_{b,B} \left| \langle \Psi_B | \chi_b^{(-)*} \hat{O} \chi_a^{(+)} | \Psi_A \rangle \right|^2 \delta(E + E_b - E_i) \\ &= (-) \frac{1}{\pi} \text{Im} \left[\sum_{\alpha' \alpha} \int d\mathbf{r}' d\mathbf{r} F_{\alpha'}^\dagger(\mathbf{r}') G_{\alpha' \alpha}(E; \mathbf{r}', \mathbf{r}) F_\alpha(\mathbf{r}) \right] \end{aligned} \quad (\text{A10})$$

with the kinematical factor β which is defined by

$$\beta = \left(1 + \frac{E_b^{(0)} p_b^{(0)} - p_a \cos \theta_{\text{lab}}}{E_Y^{(0)} p_b^{(0)}} \right) \frac{p_b E_b}{p_b^{(0)} E_b^{(0)}}. \quad (\text{A11})$$

One can find the expression of Eq. (A9), in several articles applying Green's function to hypernuclear physics and the related subjects [20, 41, 60]. For the forward (K^- , N) reaction ($\theta_{\text{lab}} = 0^\circ$) in the lab frame, we replace p_a , p_b , E_b and E_Y by p_{K^-} , p_N , E_N and $E_{\bar{K}}$,

respectively, and we find that $q(0^\circ) = p_{K^-} - p_N^{(0)}$ is negative for the $K^- + N \rightarrow N + \bar{K}$ reaction. Thus, the kinematical factor is written by

$$\begin{aligned}\beta(0^\circ) &= \left(1 + \frac{E_N^{(0)} p_N^{(0)} - p_{K^-}}{E_{\bar{K}}^{(0)} p_N^{(0)}}\right) \frac{p_N E_N}{p_N^{(0)} E_N^{(0)}} \\ &= \left(1 - \frac{v_{\bar{K}}^{(0)}}{v_N^{(0)}}\right) \frac{p_N E_N}{p_N^{(0)} E_N^{(0)}},\end{aligned}\quad (\text{A12})$$

where $v_N^{(0)} = p_N^{(0)}/E_N^{(0)}$ is the velocity of the detected nucleon, and $v_{\bar{K}}^{(0)} = q(0^\circ)/E_{\bar{K}}^{(0)}$ for the residual \bar{K} . In the text, we represent the cross section of Eq.(21), as a function the energy-transfer ω instead of E .

APPENDIX B: INTEGRATED CROSS SECTION FOR THE FORMATION OF THE \bar{K} NUCLEAR BOUND STATES

In order to see the relation between the integrated cross section of Eq.(55) and the inclusive cross section of Eq.(21), we will perform explicitly the energy-integration of Eq.(54). Here we assume a Y -nuclear bound state in the nucleus B , using an optical potential which gives unstable bound states with complex eigenvalues $E_{n\ell} = \varepsilon_{n\ell} - i\Gamma_{n\ell}/2$ for simplicity. We can expand Green's function in the \bar{K} -nucleus bound region as

$$G_\ell(E; r', r) = \sum_n G_{n\ell}^{(pole)}(E; r', r) + G_\ell^{(bg)}(E; r', r), \quad (\text{B1})$$

where the summation over n includes all the pole of the S -matrix in the complex k -plane, and $G_\ell^{(bg)}(E; r', r)$ indicates the background contribution. The pole contribution for a $(n\ell)$ unstable bound state can be expressed as

$$G_{n\ell}^{(pole)}(E; r', r) = \frac{\varphi_{n\ell}(r')(\tilde{\varphi}_{n\ell}(r))^*}{E - E_{n\ell} + i\epsilon} \quad (\text{B2})$$

with $\varphi_{n\ell}(r)$ denoting a radial wave function of the bound state, and $\tilde{\varphi}_{n\ell}$ is a biorthogonal one for $\varphi_{n\ell}$, as normalized by Eq. (52). Thus, the contribution of the strength function can be written as

$$\begin{aligned}S^{(pole)}(E) &= (-)\frac{1}{\pi} \text{Im} \left[\int d\mathbf{r}' d\mathbf{r} F^\dagger(\mathbf{r}') Y_\ell(\hat{\mathbf{r}}') G_{n\ell}^{(pole)}(E; r', r) Y_\ell^*(\hat{\mathbf{r}}) F(\mathbf{r}) \right] \\ &= (-)\frac{1}{\pi} \text{Im} \left[\frac{N_{n\ell}^{(pole)}}{E - E_{n\ell} + i\epsilon} \right] \\ &= \frac{1}{\pi} \left\{ \frac{\Gamma_{n\ell}/2}{(E - \varepsilon_{n\ell})^2 + \Gamma_{n\ell}^2/4} \text{Re} N_{n\ell}^{(pole)} - \frac{E - \varepsilon_{n\ell}}{(E - \varepsilon_{n\ell})^2 + \Gamma_{n\ell}^2/4} \text{Im} N_{n\ell}^{(pole)} \right\},\end{aligned}\quad (\text{B3})$$

where the strength of a pole is given by

$$N_{n\ell}^{(pole)} = (2J_B + 1)(2j_N + 1)(2\ell_{\bar{K}} + 1) \begin{pmatrix} \ell_{\bar{K}} & j_N & J_B \\ 0 & -\frac{1}{2} & \frac{1}{2} \end{pmatrix}^2 F(q)F^\dagger(q), \quad (\text{B4})$$

where the form factor $F(q)$ is given as Eq.(57). Here we assumed that the final states have the $(j_N^{-1}, n\ell_{\bar{K}})J_B$ configurations. The integrated cross section can be evaluated by the energy integration;

$$\left(\frac{d\sigma}{d\Omega_b} \right) = \int dE_b \left(\frac{d^2\sigma}{dE_b d\Omega_b} \right) = \beta \left(\frac{d\sigma}{d\Omega_b} \right)_{\text{lab}}^{aN \rightarrow bY} \int dE_b S^{(pole)}(E). \quad (\text{B5})$$

Changing the dE_b -integration to dE_B -integration, $dE_b = |\partial E_b / \partial p_b| |\partial E_B / \partial p_b|^{-1} dE_B$, with the momentum conservation, where

$$\left| \frac{\partial E_b}{\partial p_b} \right| = \frac{p_b}{E_b}, \quad \left| \frac{\partial E_B}{\partial p_b} \right| = \frac{p_b E_B + E_b(p_b - p_a \cos \theta_{\text{lab}})}{E_b E_B}, \quad (\text{B6})$$

we can obtain

$$\begin{aligned} \int dE_b S^{(pole)}(E) &= (-) \frac{1}{\pi} \text{Im} \int dE_b \left[\frac{N_{n\ell}^{(pole)}}{E - E_{n\ell} + i\epsilon} \right] \\ &= \left(1 + \frac{E_b p_b - p_a \cos \theta_{\text{lab}}}{E_B p_b} \right)^{-1} (-) \frac{1}{\pi} \text{Im} \int dE_B \left[\frac{N_{n\ell}^{(pole)}}{E - E_{n\ell} + i\epsilon} \right] \\ &= \left(1 + \frac{E_b p_b - p_a \cos \theta_{\text{lab}}}{E_B p_b} \right)^{-1} \text{Re} N_{n\ell}^{(pole)}, \end{aligned} \quad (\text{B7})$$

where we substituted Eq. (B3) and used the relations

$$\int_{-\infty}^{\infty} d\bar{E} \frac{\Gamma/2}{(\bar{E} - E')^2 + \Gamma^2/4} = \pi, \quad \int_{-\infty}^{\infty} d\bar{E} \frac{\bar{E} - E'}{(\bar{E} - E')^2 + \Gamma^2/4} = 0. \quad (\text{B8})$$

Therefore, the integrated cross section can be expressed as

$$\begin{aligned} \left(\frac{d\sigma}{d\Omega_b} \right) &= \beta \left(1 + \frac{E_b p_b - p_a \cos \theta_{\text{lab}}}{E_B p_b} \right)^{-1} \left(\frac{d\sigma}{d\Omega_b} \right)_{\text{lab}}^{aN \rightarrow bY} \text{Re} N_{n\ell}^{(pole)} \\ &= \alpha \left(\frac{d\sigma}{d\Omega_b} \right)_{\text{lab}}^{aN \rightarrow bY} \text{Re} N_{n\ell}^{(pole)}, \end{aligned} \quad (\text{B9})$$

and the kinematical factor α [46] has a relation to β ,

$$\alpha = \beta \left(1 + \frac{E_b p_b - p_a \cos \theta_{\text{lab}}}{E_B p_b} \right)^{-1}, \quad (\text{B10})$$

where $(\dots)^{-1}$ is often called the recoil factor [79]. Especially, we confirm that for the forward reaction;

$$\begin{aligned}\alpha(0^\circ) &= \left(1 + \frac{(p_b^{(0)} - p_a)/E_Y^{(0)}}{p_b^{(0)}/E_b^{(0)}}\right) \frac{p_b E_b}{p_b^{(0)} E_b^{(0)}} \bigg/ \left(1 + \frac{(p_b - p_a)/E_B}{p_b/E_b}\right) \\ &= \left(\frac{1 - v_Y^{(0)}/v_b^{(0)}}{1 - v_B/v_b}\right) \frac{p_b E_b}{p_b^{(0)} E_b^{(0)}},\end{aligned}\tag{B11}$$

where $v_Y^{(0)}$ is a velocity of Y for the nucleon target, and v_B is a velocity of B for the nucleus target. The factor of Eq. (B11) is equivalent to that given in Eq.(2.10) by Dover et al. [46].

APPENDIX C: SPIN-ISOSPIN STATES FOR THE s -SHELL \bar{K} -NUCLEAR SYSTEMS

In the present paper, we use the isospin states for $\bar{K}N$ systems having the relation between the isospin and charge bases as the following:

$$\begin{aligned}|1, +1\rangle^{\bar{K}N} &= |\bar{K}^0 p\rangle, \\ |1, 0\rangle^{\bar{K}N} &= \sqrt{\frac{1}{2}}|\bar{K}^0 n\rangle + \sqrt{\frac{1}{2}}|K^- p\rangle, \\ |0, 0\rangle^{\bar{K}N} &= \sqrt{\frac{1}{2}}|\bar{K}^0 n\rangle - \sqrt{\frac{1}{2}}|K^- p\rangle, \\ |1, -1\rangle^{\bar{K}N} &= |K^- n\rangle,\end{aligned}\tag{C1}$$

where $|I, I_z\rangle^{\bar{K}N}$ denotes an isospin-function for the $\bar{K}N$ channel with isospin I and the z -projection I_z . Note that the phase definition of $|0, 0\rangle^{\bar{K}N}$ is an opposite sign of that given by Gopal et al. [44], i.e., $|0, 0\rangle^{\bar{K}N} = -|0, 0\rangle_{\text{Gopal}}^{\bar{K}N}$.

For $\bar{K}N$ systems, we assume a configuration with $S_C = 1/2$ and $T_C = 1/2$ in the $3N$ core-nucleus, ${}^3\text{He}$ or ${}^3\text{H}$. Thus we represent the spin-isospin states for the microscopic three-nucleon system, i.e., $|{}^3\text{He}\rangle^{3N}$ for isospin z -projection $\tau_C = +1/2$ and $|{}^3\text{H}\rangle^{3N}$ for $\tau_C = -1/2$. Thus, the spin-isospin states with total spin $S = 1/2$ in $[\bar{K} \otimes [NNN]_{T=1/2}]$ are written

as

$$\begin{aligned}
|\bar{K}^0 \text{He}\rangle_{T=1, \tau=+1} &= |\bar{K}^0\rangle |^3\text{He}\rangle^{3N}, \\
|\bar{K}^0 \text{H}\rangle_{T=1, \tau=0} &= \sqrt{\frac{1}{2}} |\bar{K}^0\rangle |^3\text{H}\rangle^{3N} + \sqrt{\frac{1}{2}} |K^-\rangle |^3\text{He}\rangle^{3N}, \\
|\bar{K}^0 \text{H}\rangle_{T=0, \tau=0} &= \sqrt{\frac{1}{2}} |\bar{K}^0\rangle |^3\text{H}\rangle^{3N} - \sqrt{\frac{1}{2}} |K^-\rangle |^3\text{He}\rangle^{3N}, \\
|\bar{K}^0 \text{n}\rangle_{T=1, \tau=-1} &= |K^-\rangle |^3\text{H}\rangle^{3N}.
\end{aligned} \tag{C2}$$

For $\bar{K}NN$ systems, the spin-isospin functions with total spin $S = 0$ and and isospin T are written as

$$\begin{aligned}
|\bar{K}^0 \text{He}\rangle_{T=3/2, \tau=+3/2} &= |\bar{K}^0\{pp\}\rangle, \\
|\bar{K}^0 \text{H}\rangle_{T=1/2, \tau=+1/2} &= \sqrt{\frac{1}{3}} |\bar{K}^0\{pn\}\rangle - \sqrt{\frac{2}{3}} |K^-\{pp\}\rangle, \\
|\bar{K}^0 \text{H}\rangle_{T=3/2, \tau=+1/2} &= \sqrt{\frac{2}{3}} |\bar{K}^0\{pn\}\rangle + \sqrt{\frac{1}{3}} |K^-\{pp\}\rangle, \\
|\bar{K}^0 \text{n}\rangle_{T=1/2, \tau=-1/2} &= \sqrt{\frac{2}{3}} |\bar{K}^0\{nn\}\rangle - \sqrt{\frac{1}{3}} |K^-\{pn\}\rangle, \\
|\bar{K}^0 \text{n}\rangle_{T=3/2, \tau=-1/2} &= \sqrt{\frac{1}{3}} |\bar{K}^0\{nn\}\rangle + \sqrt{\frac{2}{3}} |K^-\{pn\}\rangle, \\
|K^-\text{nn}\rangle_{T=3/2, \tau=-3/2} &= |K^-\{nn\}\rangle,
\end{aligned} \tag{C3}$$

and for total spin $S = 1$;

$$\begin{aligned}
|\bar{K}^0 \text{H}\rangle_{T=1/2, \tau=+1/2} &= |\bar{K}^0[pn]\rangle, \\
|\bar{K}^0 \text{n}\rangle_{T=1/2, \tau=-1/2} &= |K^-[pn]\rangle,
\end{aligned} \tag{C4}$$

Here we denoted the two-nucleon configuration of $\{N_1, N_2\} = N_1N_2 + N_2N_1$ with $^1\text{S}_0$, $T_{NN}=1$ and $[N_1, N_2] = N_1N_2 - N_2N_1$ with $^3\text{S}_1$, $T_{NN}=0$.

-
- [1] D. B. Kaplan and A. E. Nelson, Phys. Lett. **B175** (1986) 57.
 - [2] G. E. Brown and M. Rho, Phys. Rep. **269** (1996) 333.
 - [3] C. H. Lee, Phys. Rep. **275** (1996) 255.
 - [4] R.H. Dalitz, T.C. Wong and G. Rajasekaran, Phys. Rev. **153** (1967) 1617.
 - [5] A. Doté, H. Horiuchi, Y. Akaishi and T. Yamazaki, Phys. Rev. **C70** (2004) 044313.

- [6] E. Friedman, A. Gal and C.J. Batty, Phys. Lett. **B308** (1993) 6.
- [7] E. Friedman, A. Gal and C.J. Batty, Nucl. Phys. **A579** (1994) 518.
- [8] C.J. Batty, E. Friedman and A. Gal, Phys. Rep. **287** (1997) 385.
- [9] A. Cieplý, E. Friedman, A. Gal and J. Mareš, Nucl. Phys. **A696** (2001) 173.
- [10] E. Friedman and A. Gal, Phys. Rep. **452** (2007) 89, in particular Fig.23 and related text.
- [11] G.Q. Li, C.-H. Lee and G.E. Brown, Nucl. Phys. **A 625** (1997) 372, and references therein.
- [12] W. Scheinast et al., Phys. Rev. Lett. **96** (2006) 072301.
- [13] M. Prakash and J. M. Lattimer, Nucl. Phys. **A639** (1998) 433; P. J. Ellis, R. Knorren and M. Prakash, Phys. Lett. **B349** (1995) 11.
- [14] T. Waas, M. Rho and W. Weise, Nucl. Phys. **A617** (1997) 449, and references therein.
- [15] M. Lutz, Phys. Lett. **B426** (1998) 12.
- [16] J. Schaffner-Bielich, V. Koch and M. Effenberger, Nucl. Phys. **A669** (2000) 153.
- [17] A. Ramos and E. Oset, Nucl. Phys. **A671** (2000) 481.
- [18] T. Kishimoto, Phys. Rev. Lett. **83** (1999) 4701.
- [19] K. Ikuta, M. Arima and K. Masutani, Prog. Theor. Phys. **108** (2002) 917.
- [20] O. Morimatsu and K. Yazaki, Nucl. Phys. **A483** (1988) 493; Prog. Part. Nucl. Phys. **33** (1994) 679.
- [21] T. Kishimoto et al., Nucl. Phys. **A754** (2005) 383c; T. Kishimoto et al., Prog. Theor. Phys. **118** (2007) 181.
- [22] J. Yamagata, H. Nagahiro, Y. Okumura and S. Hirenzaki, Prog. Theor. Phys. **114** (2005) 301; **114** (2005) 905, Erratum.
- [23] J. Yamagata, H. Nagahiro and S. Hirenzaki, Phys. Rev. **C74** (2006) 014604.
- [24] Y. Akaishi and T. Yamazaki, in: S. Bianconi, et al. (Eds.), Proc. III Int. DAΦNE Workshop, Frascati Physics Series vol. XVI, LNF, Frascati, 1999, pp. 59-74.
- [25] Y. Akaishi and T. Yamazaki, Phys. Rev. **C65** (2002) 044005.
- [26] T. Suzuki, et al., Phys. Lett. **B597** (2004) 263.
- [27] M. Iwasaki, et al., in: J. Pochodzalla and Th. Walcher (Eds.), Proceedings of *IX International Conference on Hypernuclear and Strange Particle Physics (HYP2006)*, Springer-Verlag, Berlin, 2007, pp. 195-200; arXiv:0706.0297 [nucl-ex].
- [28] M. Sato, et al., Phys. Lett. **B659** (2008) 107; T. Suzuki, et al., Phys. Rev. **C76** (2007) 068202.
- [29] M. Agnello, et al., Phys. Rev. Lett. **94** (2005) 212303.

- [30] Y. Nogami, Phys. Lett. **7** (1963) 288.
- [31] T. Yamazaki and Y. Akaishi, Phys. Lett. **B515** (2002) 70.
- [32] N.V. Shevchenko, A. Gal and J. Mareš, Phys. Rev. Lett. **98** (2007) 082301.
- [33] N.V. Shevchenko, A. Gal, J. Mareš and J. Revai, Phys. Rev. **C76** (2007) 044004.
- [34] A.N. Ivanov, P. Kleine, J. Marton and E. Widmann, nucl-th/0512037.
- [35] Y. Ikeda and T. Sato, Phys. Rev. **C76** (2007) 035203.
- [36] A. Doté and W. Weise, in: J. Pochodzalla and Th. Walcher (Eds.), Proceedings of *IX International Conference on Hypernuclear and Strange Particle Physics (HYP2006)*, Springer-Verlag, Berlin, 2007, pp. 249-252; nucl-th/0701050.
- [37] T. Nishikawa and Y. Kondo, hep-ph/0703100; arXiv:0710.0948 [hep-ph].
- [38] A. Arai, M. Oka and S. Yasui, arXiv:0705.3936 [nucl-th].
- [39] For example, A. Hirtl, J. Marton, E. Widmann and J. Zmeskal (Eds.), Proceedings of the *International Conference on Exotic Atoms and Related Topics*, Austrian Academy of Science Press, Vienna, (2005).
- [40] M. Iwasaki, T. Nagae et al., J-PARC E15 experiment. The proposal for 1st PAC meeting is available from http://j-parc.jp/NuclPart/Proposal_0606_e.html.
- [41] T. Koike and T. Harada, Phys. Lett. **B652** (2007) 262.
- [42] T. Yamazaki and Y. Akaishi, Phys. Rev. **C76** (2007) 045201.
- [43] K. Suzuki, et al., Proceedings of the *International Conference on Exotic Atoms (EXA05)*, Austrian Academy of Science Press, Vienna, (2005) 83.
- [44] G.P. Gopal, et al., Nucl. Phys. **B119** (1977) 362.
- [45] B. Conforto, et al., Nucl. Phys. **B105** (1976) 189.
- [46] C.B. Dover and A. Gal, Ann. Phys. (N.Y.) **146** (1983) 309.
- [47] A.S. Rosenthal and F. Tabakin, Phys. Rev. **C22** (1980) 711.
- [48] B.W. Allardyce et al., Nucl. Phys. **A209** (1973) 1.
- [49] C.B. Dover and G.E. Walker, Phys. Rev. **C19** (1979) 1393; Phys. Rep. **89** (1982) 1.
- [50] C.B. Dover, D.J. Millener and A. Gal, Phys. Rep. **184** (1989) 1.
- [51] J. Hüfner, S.Y. Lee and H.A. Weidenmüller, Nucl. Phys. **A234** (1974) 429.
- [52] A. Bouyssy, Nucl. Phys. **A290** (1977) 324.
- [53] E.H. Auerbach, A.J. Baltz, C.B. Dover, A. Gal, S.H. Kahana, L. Ludeking and D.J. Millener, Ann. Phys. (N.Y.) **148** (1983) 381.

- [54] E. Marco and W. Weise, Phys. Lett. **B502** (2001) 59; S. Hirenzaki and E. Oset, Phys. Lett. **B527** (2002) 69; H. Nagahiro, D. Jido and S. Hirenzaki, Nucl. Phys. **A761** (2005) 92.
- [55] T. Harada, Phys. Rev. Lett. **81** (1998) 5287.
- [56] C.B. Dover, L. Ludeking and G.E. Walker, Phys. Rev. **C22** (1980) 2073.
- [57] R. Hausmann and W. Weise, Nucl. Phys. **A491** (1989) 598.
- [58] T. Motoba, H. Bandō, R. Wünsch and J. Žofka, Phys. Rev. **C38** (1988) 1322.
- [59] T. Harada and Y. Hirabayashi, Nucl. Phys. **A759** (2005) 143.
- [60] S. Tadokoro, H. Kobayashi and Y. Akaishi, Phys. Rev. **C51** (1995) 2656.
- [61] R.H. Dalitz and A. Gal, Ann. Phys. (N.Y.) **116** (1978) 167.
- [62] C.J. Batty, Nucl. Phys. **A372** (1981) 418.
- [63] N. Kaiser, P.B. Siegel and W. Weise, Nucl. Phys. **A594** (1995) 325.
- [64] E. Oset and A. Ramos, Nucl. Phys. **A635** (1998) 99; B. Krippa, Phys. Rev. **C58** (1998) 1333.
- [65] S. Hirenzaki, Y. Okumura, H. Toki, E. Oset and A. Ramos, Phys. Rev. **C61** (2000) 055205.
- [66] A. Baca, C. Gracia-Recio and J. Nieves, Nucl. Phys. **A673** (2000) 335.
- [67] J. Mareš, E. Friedman and A. Gal, Phys. Lett. **B606** (2005) 295; Nucl. Phys. **A770** (2006) 84; D. Gazda, E. Friedman, A. Gal and J. Mareš, Phys. Rev. **C76** (2007) 055204.
- [68] T. Berggren, Nucl. Phys. **A109** (1968) 265.
- [69] P.L. Kapur and R. Peierls, Proc. Roy. Soc. (London) **A166** (1938) 277.
- [70] A. Bohr and M. Mottelson, *Nuclear structure*, Vol. 1 (Benjamin, New York, 1969) p.238.
- [71] H. de Vries, C. W. de Jager and C. de Vries, At. Data Nucl. Tables **36** (1987) 459.
- [72] G. Jacob and T.A.J. Maris, Rev. Mod. Phys. **38** (1966) 121.
- [73] J.R. Taylor, *Scattering Theory: the quantum theory of nonrelativistic collisions*, (Dover Publication, Inc., New York, 1972).
- [74] J. Yamagata, H. Nagahiro, R. Kimura and S. Hirenzaki, Phys. Rev. **C76** (2007) 045204.
- [75] S. Wycech, Nucl. Phys. **A450** (1986) 399c.
- [76] P.A. Katz, K. Bunnell, M. Derrick, T. Fields, L.G. Hyman and G. Keys, Phys. Rev. **D1** (1970) 1267.
- [77] T. Onaga, H. Narumi and T. Kouhura, Prog. Theor. Phys. **82** (1989) 222.
- [78] For example, J.J. Sakurai, *Advanced Quantum Mechanics*, (Addison-Wesley, 1967).
- [79] S. Frullani and J. Mougey, in: J.W. Negele and E. Vogt (Eds.), *Advances in Nuclear Physics*, vol. 14, Plenum, New York, 1984, p. 1.

TABLE I: Summary of the isospin relation for $K^- + N \rightarrow N + \bar{K}$ lab amplitudes $f_{K^-N \rightarrow N\bar{K}}$ where \bar{K} denotes the \bar{K}^0 or K^- , to s -channel f_I and t -channel $f^{(t)}$ amplitudes which are labeled by I and t , respectively. ΔZ is a charge transfer defined by $\Delta Z = (i'_2)_z - (i_2)_z - 1$ for the reaction $i_1 + i_2 \rightarrow i'_1 + i'_2$ where $(i)_z$ is a z -component of the particle isospin i .

Reaction	$N \rightarrow \bar{K}$	ΔZ	$f_{K^-N \rightarrow N\bar{K}}$	
			t -channel	s -channel
$K^- + n \rightarrow n + K^-$	$n \rightarrow K^-$	-1	$(f^{(0)} + f^{(1)})/2$	f_1
$K^- + p \rightarrow n + \bar{K}^0$	$p \rightarrow \bar{K}^0$	-1	$(f^{(0)} - f^{(1)})/2$	$(f_1 + f_0)/2$
$K^- + p \rightarrow p + K^-$	$p \rightarrow K^-$	-2	$f^{(1)}$	$(f_1 - f_0)/2$

TABLE II: The K^- binding energies and widths of the K^- nuclear $(n\ell)_{K^-}$ bound states for ${}^{11}_{K^-}\text{Be} = [K^- - {}^{11}\text{B}]$ and ${}^{27}_{K^-}\text{Mg} = [K^- - {}^{27}\text{Al}]$ with the \bar{K}^- -nucleus DD potentials [67]. These values are estimated without (Real only) and with (Full) the imaginary parts which are multiplied by the phase space factor [67], of the potentials. The Coulomb potentials are taken into account. $k_{n\ell}^{(pole)}$ denotes a corresponding pole position of the bound state in the complex momentum plane.

States	Real only			Full		
	$-B_{n\ell}$ (MeV)	$k_{n\ell}^{(pole)}$ (fm $^{-1}$)	rms (fm)	$-B_{n\ell}$ (MeV)	$\Gamma_{n\ell}$ (MeV)	$k_{n\ell}^{(pole)}$ (fm $^{-1}$)
${}^{11}_{K^-}\text{Be}$						
$(1s)_{K^-}$	-130	$+i1.82$	1.3	-130	25	$-0.09+i1.82$
$(1p)_{K^-}$	-65	$+i1.28$	1.8	-63	91	$-0.43+i1.33$
$(2s)_{K^-}$	-11	$+i0.52$	3.1	+2.5	76	$-0.72+i0.67$
$(1d)_{K^-}$	-4.3	$+i0.33$	2.6	+6.6	97	$-0.84+i0.73$
${}^{27}_{K^-}\text{Mg}$						
$(1s)_{K^-}$	-169	$+i2.07$	1.6	-169	22	$-0.07+i2.07$
$(1p)_{K^-}$	-123	$+i1.77$	2.0	-123	25	$-0.09+i1.77$
$(1d)_{K^-}$	-74	$+i1.37$	2.3	-72	88	$-0.40+i1.41$
$(2s)_{K^-}$	-68	$+i1.32$	2.4	-66	91	$-0.42+i1.36$
$(1f)_{K^-}$	-23	$+i0.76$	2.7	-17	114	$-0.73+i0.99$
$(2p)_{K^-}$	-21	$+i0.74$	3.1	-12	100	$-0.70+i0.90$

TABLE III: The integrated lab cross sections of K^- nuclear bound states J^π for K^- - ^{11}B by transitions $(nl_j)_N \rightarrow (nl)_{K^-}$ in the forward (K^-, p) reaction on the ^{12}C target at the incident K^- lab momentum $p_{K^-} = 1.0$ GeV/c. The Fermi-averaged cross section of $\langle d\sigma(0^\circ)/d\Omega \rangle_{\text{lab}}^{K^-p \rightarrow pK^-} = 3.5$ mb/sr and distortion parameters $\bar{\sigma}_{NN}^{\text{tot}} = \bar{\sigma}_{K^-N}^{\text{tot}} = 40$ mb and $\alpha_{NN} = \alpha_{K^-N} = 0$ are used in the DWIA.

Transition	E_{K^-} (MeV)	Γ_{K^-} (MeV)	$q(0^\circ)$ (MeV/c)	$\alpha(0^\circ)$	J^π	$\text{Re}N_{\text{eff}}$ ($\times 10^{-2}$)	$\text{Arg}N_{\text{eff}}$ (deg.)	$d\sigma(0^\circ)/d\Omega$ ($\mu\text{b/sr}$)
$(1p_{\frac{3}{2}})_p \rightarrow (1s)_{K^-}$	-130	25	-375	1.78	$\frac{3}{2}^+$	0.98	0.08	61
$\rightarrow (1p)_{K^-}$	-63	91	-296	1.62	$\frac{1}{2}^-$	0.42	37.3	24
					$\frac{3}{2}^- \oplus \frac{5}{2}^-$	6.44	-12.1	365
$\rightarrow (2s)_{K^-}$	+2.5	77	-217	1.47	$\frac{3}{2}^+$	11.66	0.66	601
$\rightarrow (1d)_{K^-}$	+6.6	97	-212	1.46	$\frac{1}{2}^+ \oplus \frac{3}{2}^+$	24.39	-16.4	1249
					$\frac{5}{2}^+ \oplus \frac{7}{2}^+$	12.83	-37.3	657
$(1s_{\frac{1}{2}})_p \rightarrow (1s)_{K^-}$	-110	35	-375	1.77	$\frac{1}{2}^-$	0.29	4.15	18
$\rightarrow (1p)_{K^-}$	-43	101	-296	1.62	$\frac{1}{2}^+ \oplus \frac{3}{2}^+$	6.90	-0.75	391
$\rightarrow (2s)_{K^-}$	+23	87	-217	1.47	$\frac{1}{2}^-$	-0.08	98.3	-4.2
$\rightarrow (1d)_{K^-}$	+27	107	-212	1.46	$\frac{3}{2}^- \oplus \frac{5}{2}^-$	13.99	-14.0	717

TABLE IV: Comparison of the integrated cross sections $(d\sigma(0^\circ)/d\Omega)_{\text{lab}}$ for the formation of K^- nuclear $(1s)_{K^-}$ bound state, together with the momentum transfers $q(0^\circ)$, by the forward (K^-, p) reaction at the incident K^- lab momentum $p_{K^-} = 1.0$ GeV/c.

Target	Transition	Present		Ref. [9]		Ref. [18]		Ref. [22]	
		$d\sigma/d\Omega$ ($\mu\text{b/sr}$)	$q(0^\circ)$ (MeV/c)	$d\sigma/d\Omega$ ($\mu\text{b/sr}$)	$q(0^\circ)$ (MeV/c)	$d\sigma/d\Omega$ ($\mu\text{b/sr}$)	$q(0^\circ)$ (MeV/c)	$d\sigma/d\Omega$ ($\mu\text{b/sr}$)	$q(0^\circ)$ (MeV/c)
^{12}C	$1p_{3/2} \rightarrow (1s)_{K^-}$	61	-375	47 ^a	-369	100-490 ^a	-369	65 ^b	-379
^{28}Si	$1d_{5/2} \rightarrow (1s)_{K^-}$	2.1	-428	6.0 ^c	-404	35-180 ^c	-404	2.7 ^d	-458

^a $B_{K^-} = 122$ MeV and harmonic oscillator wave functions were used.

^b $B_{K^-} = 133$ MeV for a deep potential was used at $T_{K^-} = 600$ MeV ($p_{K^-} = 0.976$ GeV/c).

^c $B_{K^-} = 144$ MeV and harmonic oscillator wave functions were used.

^d $B_{K^-} = 191$ MeV for a deep potential was used at $T_{K^-} = 600$ MeV ($p_{K^-} = 0.976$ GeV/c).

TABLE V: The integrated lab cross sections of K^- nuclear bound states J^π for K^- - ^{27}Mg by transitions $(n\ell_j)_N \rightarrow (n\ell)_{\bar{K}}$ in the forward (K^-, p) reaction on the ^{28}Si target at $p_{K^-} = 1.0$ GeV/c. We listed up only the deeply bound states of $E_{\bar{K}} < -50$ MeV. The Fermi-averaged cross section of $\langle d\sigma(0^\circ)/d\Omega \rangle_{\text{lab}}^{K^-p \rightarrow pK^-} = 3.5$ mb/sr and distortion parameters $\bar{\sigma}_{NN}^{\text{tot}} = \bar{\sigma}_{K^-N}^{\text{tot}} = 40$ mb and $\alpha_{NN} = \alpha_{K^-N} = 0$ are used in the DWIA.

Transition	E_{K^-} (MeV)	Γ_{K^-} (MeV)	$q(0^\circ)$ (MeV/c)	$\alpha(0^\circ)$	J^π	$\text{Re}N_{\text{eff}}$ ($\times 10^{-2}$)	$\text{Arg}N_{\text{eff}}$ (deg.)	$d\sigma(0^\circ)/d\Omega$ ($\mu\text{b/sr}$)
$(1d_{\frac{5}{2}})_p \rightarrow (1s)_{K^-}$	-169	22	-428	1.93	$\frac{5}{2}^-$	0.0031	1.91	2.1
$\rightarrow (1p)_{K^-}$	-123	25	-373	1.81	$\frac{1}{2}^+ \oplus \frac{3}{2}^+$	-0.0004	-117.1	-0.01
					$\frac{5}{2}^+ \oplus \frac{7}{2}^+$	0.519	-0.7	32.9
$\rightarrow (1d)_{K^-}$	-72	88	-312	1.68	$\frac{1}{2}^-$	0.298	-18.5	17.5
					$\frac{3}{2}^- \oplus \frac{5}{2}^-$	0.637	4.4	37.6
					$\frac{7}{2}^- \oplus \frac{9}{2}^-$	3.079	-17.4	181.5
$\rightarrow (2s)_{K^-}$	-65	92	-304	1.67	$\frac{5}{2}^-$	0.316	17.6	18.4
$(1p_{\frac{1}{2}})_p \rightarrow (1s)_{K^-}$	-165	26	-428	1.93	$\frac{1}{2}^+$	0.0083	5.0	0.6
$\rightarrow (1p)_{K^-}$	-118	29	-373	1.81	$\frac{1}{2}^-$	0.029	-3.1	1.9
					$\frac{3}{2}^-$	0.193	1.5	12.3
$\rightarrow (1d)_{K^-}$	-68	92	-312	1.68	$\frac{1}{2}^+ \oplus \frac{3}{2}^+$	0.187	24.0	11.0
					$\frac{5}{2}^+ \oplus \frac{7}{2}^+$	1.207	-5.7	71.2
$\rightarrow (2s)_{K^-}$	-61	95	-304	1.67	$\frac{3}{2}^+$	-0.0115	140.0	-0.67
$(1p_{\frac{3}{2}})_p \rightarrow (1s)_{K^-}$	-158	28	-428	1.93	$\frac{3}{2}^+$	0.012	5.8	0.81
$\rightarrow (1p)_{K^-}$	-112	31	-373	1.81	$\frac{1}{2}^-$	0.061	-2.8	3.9
					$\frac{3}{2}^- \oplus \frac{5}{2}^-$	0.350	1.6	22.2
$\rightarrow (1d)_{K^-}$	-61	94	-312	1.68	$\frac{1}{2}^+ \oplus \frac{3}{2}^+$	0.320	26.1	18.9
					$\frac{5}{2}^+ \oplus \frac{7}{2}^+$	2.403	-6.1	141.7
$\rightarrow (2s)_{K^-}$	-54	97	-304	1.67	$\frac{3}{2}^+$	-0.025	147.1	-1.45
$(1s_{\frac{1}{2}})_p \rightarrow (1s)_{K^-}$	-140	32	-428	1.93	$\frac{1}{2}^-$	0.0004	16.4	0.03
$\rightarrow (1p)_{K^-}$	-94	35	-373	1.81	$\frac{1}{2}^+ \oplus \frac{3}{2}^+$	0.195	4.7	12.4

TABLE VI: Relative production cross sections of deeply-bound $\bar{K} \otimes [NNN]$ states on ${}^4\text{He}$. T and S denote the isospin and spin of the \bar{K} nuclear states, respectively.

T	S	$\sigma(K^-, n)$	$\sigma(K^-, p)$
0	$\frac{1}{2}$	$ f_{K^-n \rightarrow nK^-} + f_{K^-p \rightarrow n\bar{K}^0} ^2$	0
1	$\frac{1}{2}$	$ f_{K^-n \rightarrow nK^-} - f_{K^-p \rightarrow n\bar{K}^0} ^2$	$2 f_{K^-p \rightarrow pK^-} ^2$

TABLE VII: Relative production cross sections of deeply-bound $\bar{K} \otimes [NN]$ states on ${}^3\text{He}$. T and S denote the isospin and spin of the \bar{K} nuclear states, respectively. T_C and S_C are the isospin and spin of the NN core-nucleus states, respectively.

$T (T_C)$	$S (S_C)$	$\sigma(K^-, n)$	$\sigma(K^-, p)$
$\frac{1}{2} (0)$	1 (1)	$\frac{3}{2} f_{K^-p \rightarrow n\bar{K}^0} ^2$	$\frac{3}{2} f_{K^-p \rightarrow pK^-} ^2$
$\frac{1}{2} (1)$	0 (0)	$\frac{2}{3} f_{K^-n \rightarrow nK^-} + \frac{1}{2}f_{K^-p \rightarrow n\bar{K}^0} ^2$	$\frac{1}{6} f_{K^-p \rightarrow pK^-} ^2$
$\frac{3}{2} (1)$	0 (0)	$\frac{1}{3} f_{K^-n \rightarrow nK^-} - f_{K^-p \rightarrow n\bar{K}^0} ^2$	$\frac{1}{3} f_{K^-p \rightarrow pK^-} ^2$

TABLE VIII: Relative production cross sections of deeply-bound $\bar{K} \otimes [NN]$ states on ${}^3\text{H}$. T and S denote the isospin and spin of the \bar{K} nuclear states, respectively. T_C and S_C are the isospin and spin of the NN core-nucleus states, respectively.

$T (T_C)$	$S (S_C)$	$\sigma(K^-, n)$	$\sigma(K^-, p)$
$\frac{1}{2} (0)$	1 (1)	$\frac{3}{2} f_{K^-n \rightarrow nK^-} ^2$	0
$\frac{1}{2} (1)$	0 (0)	$\frac{2}{3} f_{K^-p \rightarrow n\bar{K}^0} + \frac{1}{2}f_{K^-n \rightarrow nK^-} ^2$	0
$\frac{3}{2} (1)$	0 (0)	$\frac{1}{3} f_{K^-p \rightarrow n\bar{K}^0} - f_{K^-n \rightarrow nK^-} ^2$	$ f_{K^-p \rightarrow pK^-} ^2$

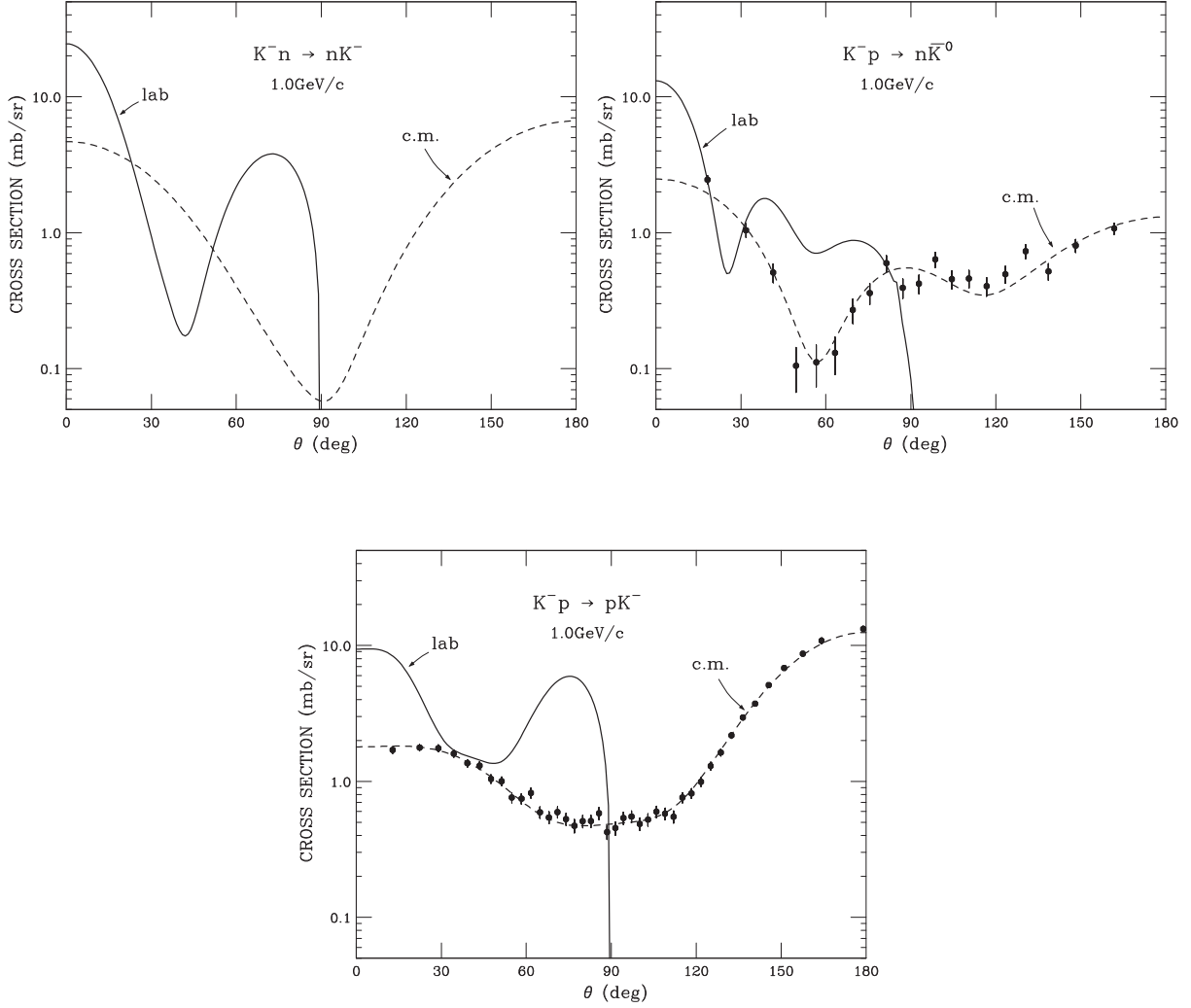


FIG. 1: The differential cross sections of $K^- + n \rightarrow n + K^-$, $K^- + p \rightarrow n + \bar{K}^0$ and $K^- + p \rightarrow p + K^-$ reactions in free space at the incident K^- lab momentum $p_{K^-} = 1.0 \text{ GeV}/c$, as a function of the scattering angle θ . The dashed and solid curves denote the c.m. and lab cross sections, respectively, which are obtained by Gopal et al. [44]. The experimental data are taken from Conforto et al. [45].

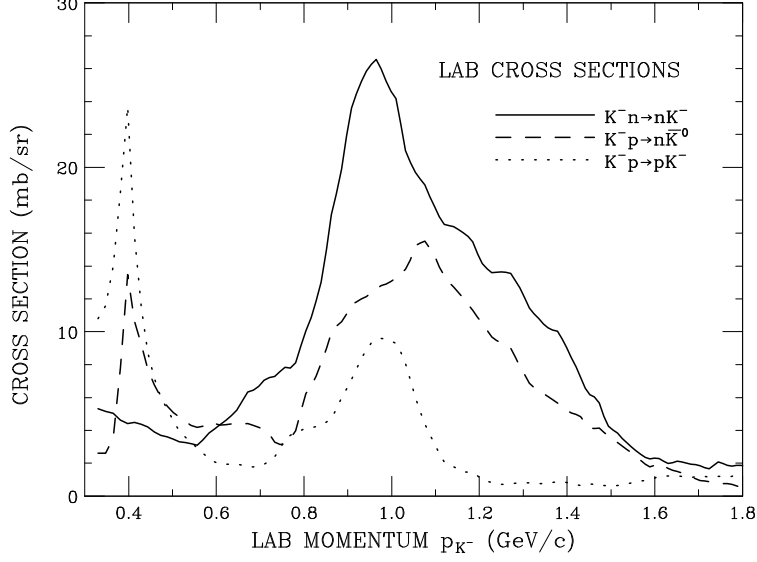


FIG. 2: The lab differential cross sections for the free space $K^- + n \rightarrow n + K^-$, $K^- + p \rightarrow n + \bar{K}^0$ and $K^- + p \rightarrow p + K^-$ reactions at the detected nucleon angle $\theta_{\text{lab}} = 0^\circ$, as a function of the K^- lab momentum p_{K^-} . The curves are constructed from the $K^- + N \rightarrow \bar{K} + N$ scattering amplitudes analyzed by Gopal et al. [44].

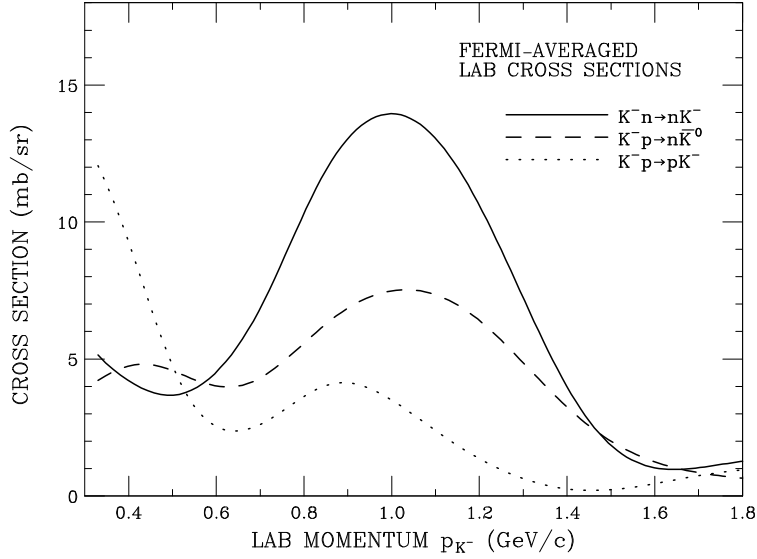


FIG. 3: The absolute values of the Fermi-averaged cross sections at $\theta_{\text{lab}} = 0^\circ$ for the $K^- + n \rightarrow n + K^-$, $K^- + p \rightarrow n + \bar{K}^0$ and $K^- + p \rightarrow p + K^-$ reactions, as a function of the K^- lab momentum p_{K^-} . The free space amplitudes of Gopal et al. [44] were used.

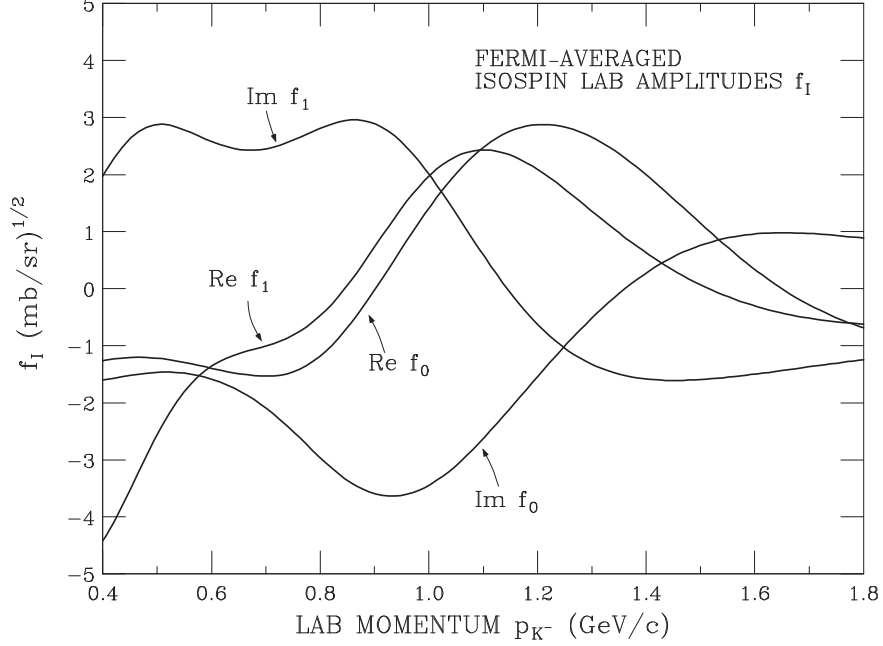


FIG. 4: Fermi-averaged $K^- + N \rightarrow N + \bar{K}$ amplitudes for f_I for s -channel isospin $I = 0, 1$, as a function of the incident K^- lab momentum at $\theta_{\text{lab}} = 0^\circ$. The amplitudes are calculated by averaging the T -matrices for ^{12}C with the harmonic oscillator momentum distribution. The free-space amplitudes of Gopal et al. [44] were used.

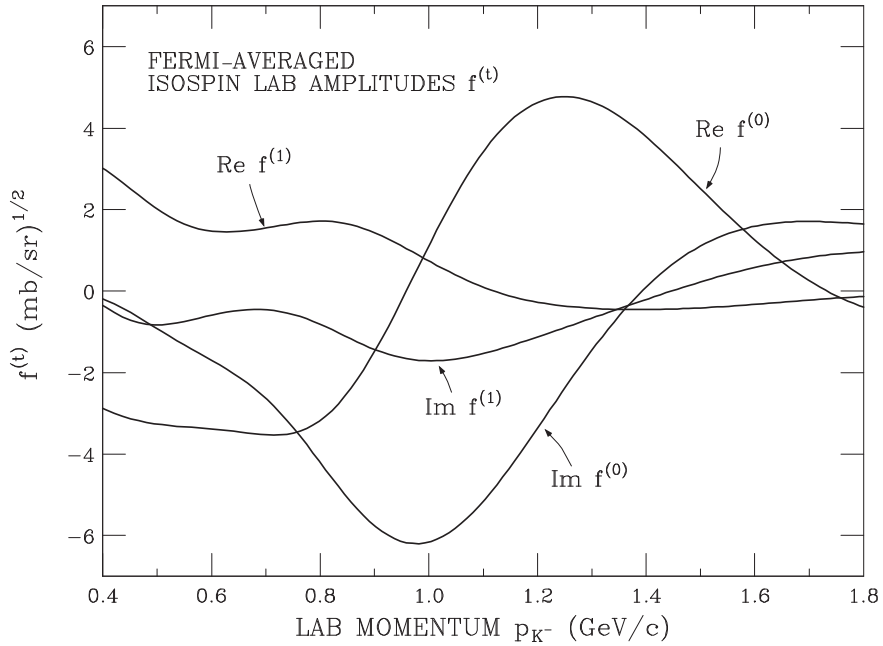


FIG. 5: Fermi-averaged $K^- + N \rightarrow N + \bar{K}$ amplitudes for $f^{(t)}$ for t -channel isospin $t = 0, 1$, as a function of K^- lab momentum at $\theta_{\text{lab}} = 0^\circ$. The free space amplitudes of Gopal et al. [44] were used.

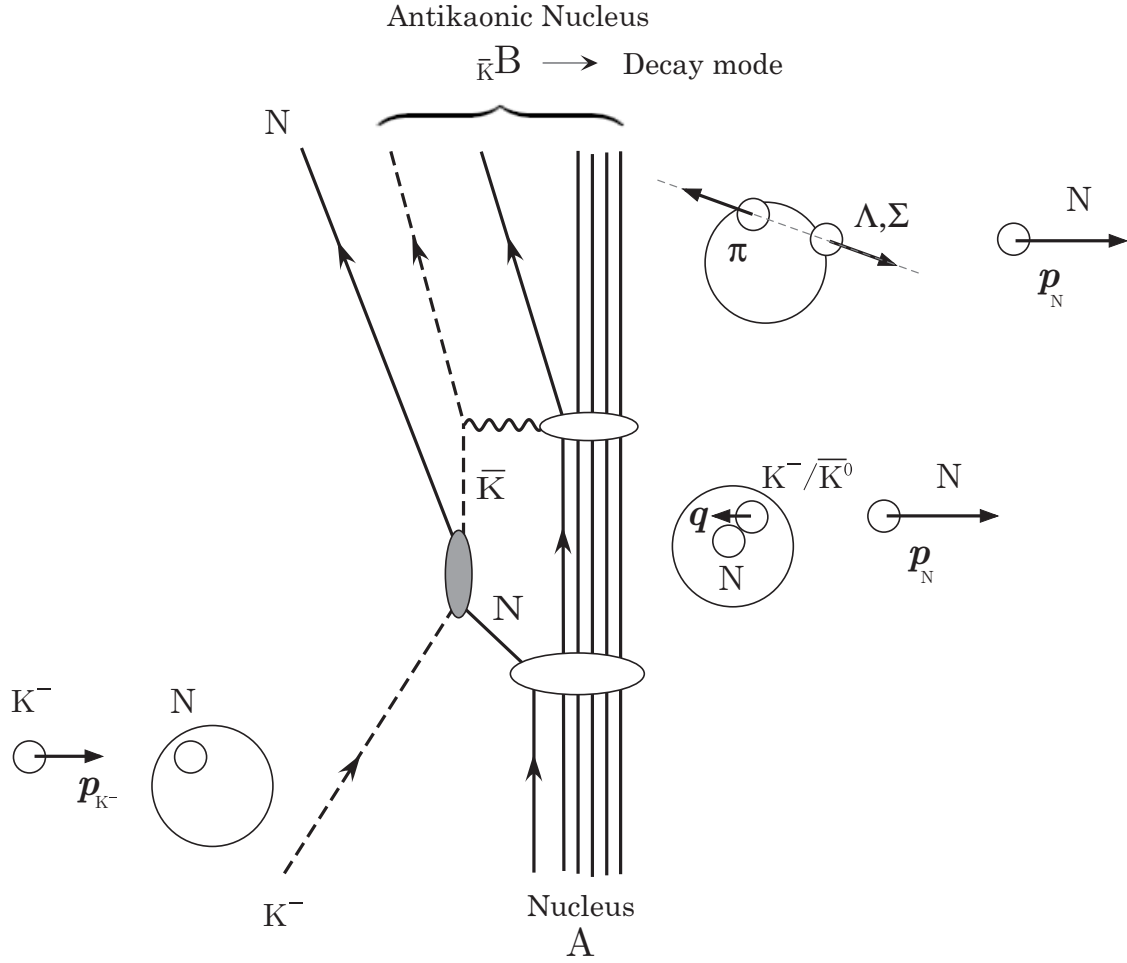


FIG. 6: Diagram of the impulse approximation for the (K^-, N) reaction on the nuclear target A.

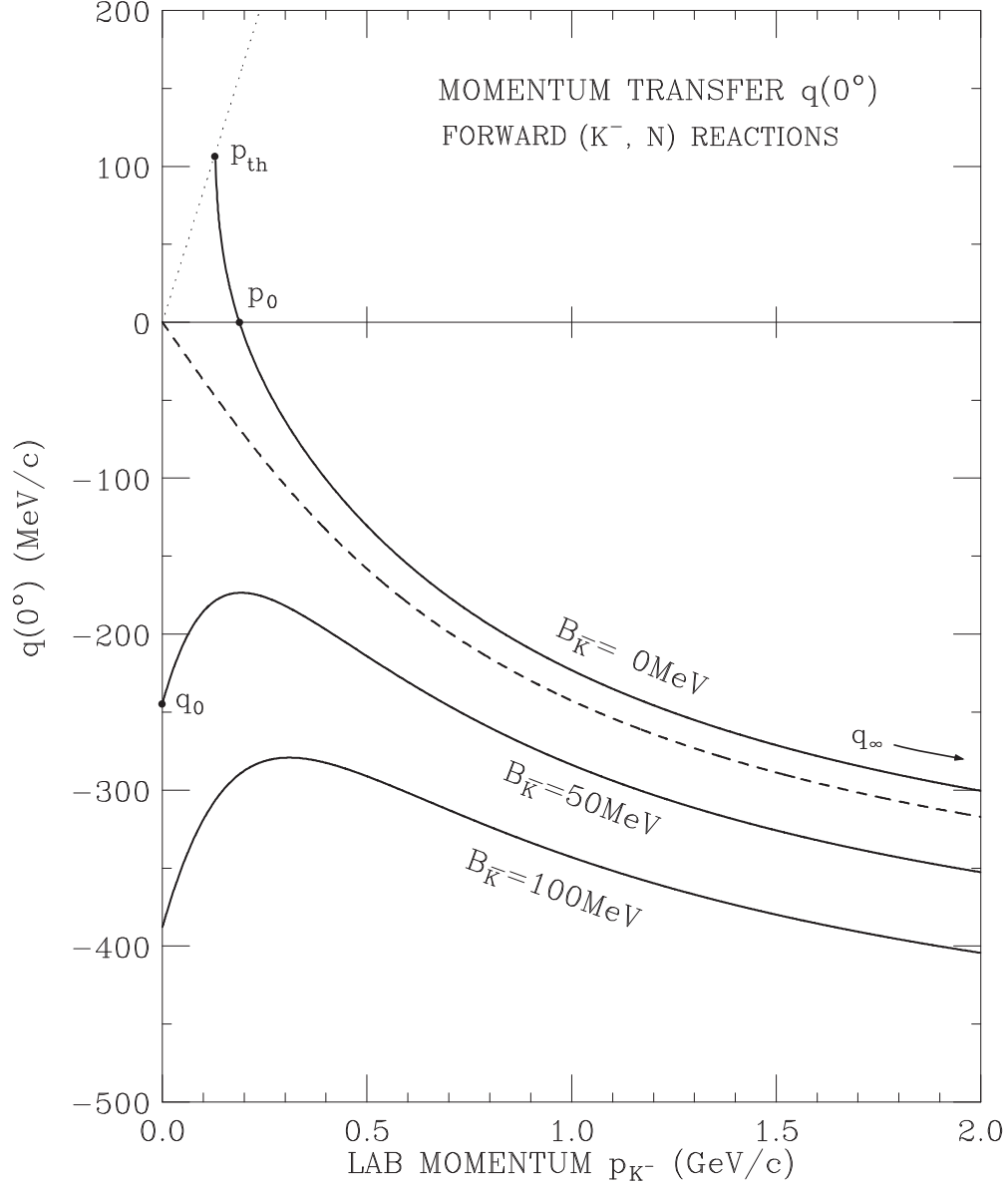


FIG. 7: Momentum transfer $q(0^\circ)$ to the \bar{K} nuclear states for the forward $K^- + N \rightarrow N + \bar{K}$ reaction on the target, as a function of the K^- lab momentum. Here the ^{12}C target is used. The \bar{K} binding energies are taken to be $B_{\bar{K}} = 0, 50, 100$ MeV. The negative value of $q(0^\circ)$ means that the residual \bar{K} recoils backward relative to the forward incident K^- . See also in the text.

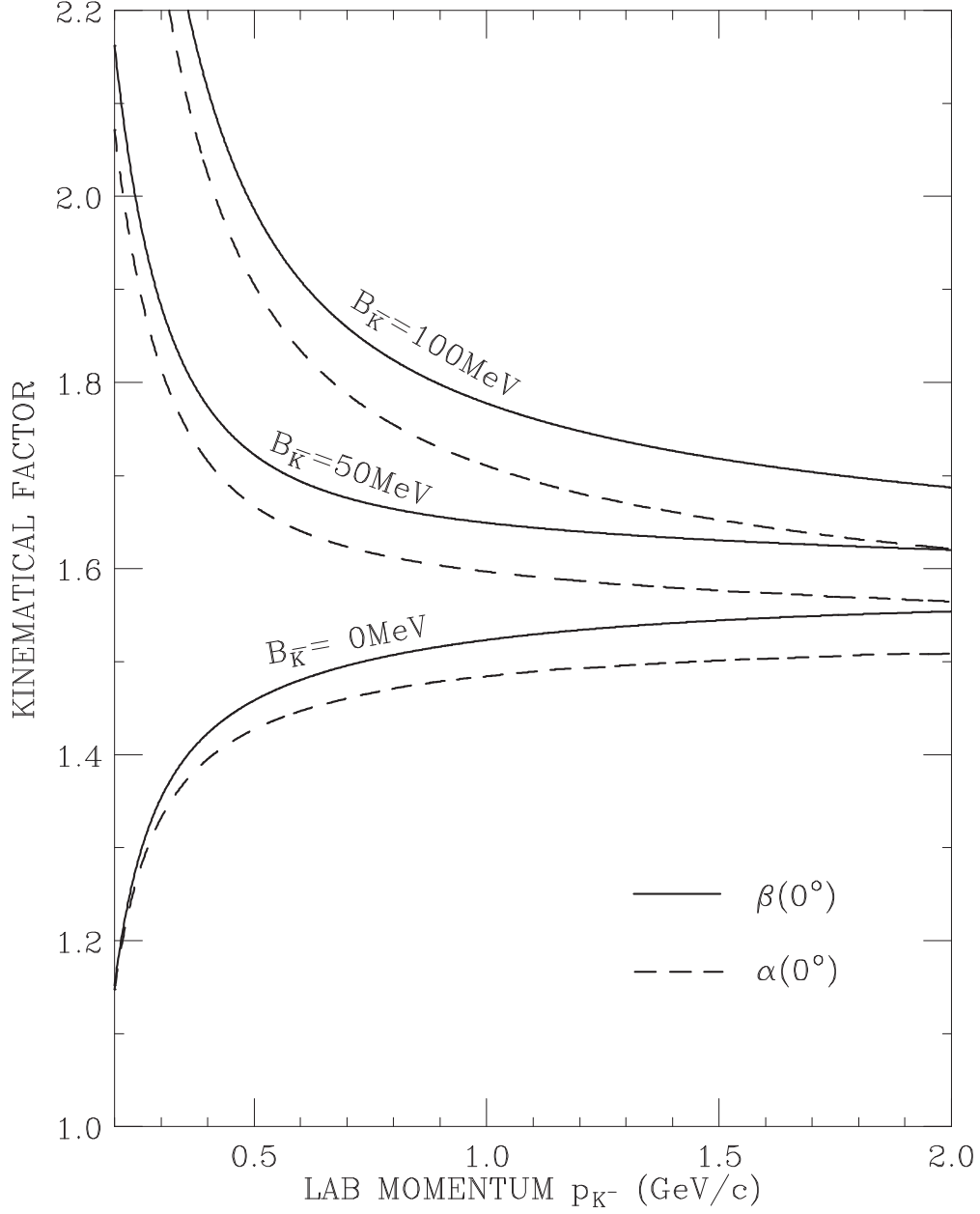


FIG. 8: The kinematical factor $\beta(0^\circ)$ and $\alpha(0^\circ)$, which are given by Eq. (29) and Eq. (B11), respectively, transforming from the two-body K^-+N system to the many-body K^- +nucleus system, as a function of the K^- lab momentum p_{K^-} . The \bar{K} binding energies are taken to be $B_{\bar{K}} = 0, 50, 100$ MeV. The ^{12}C target was used.

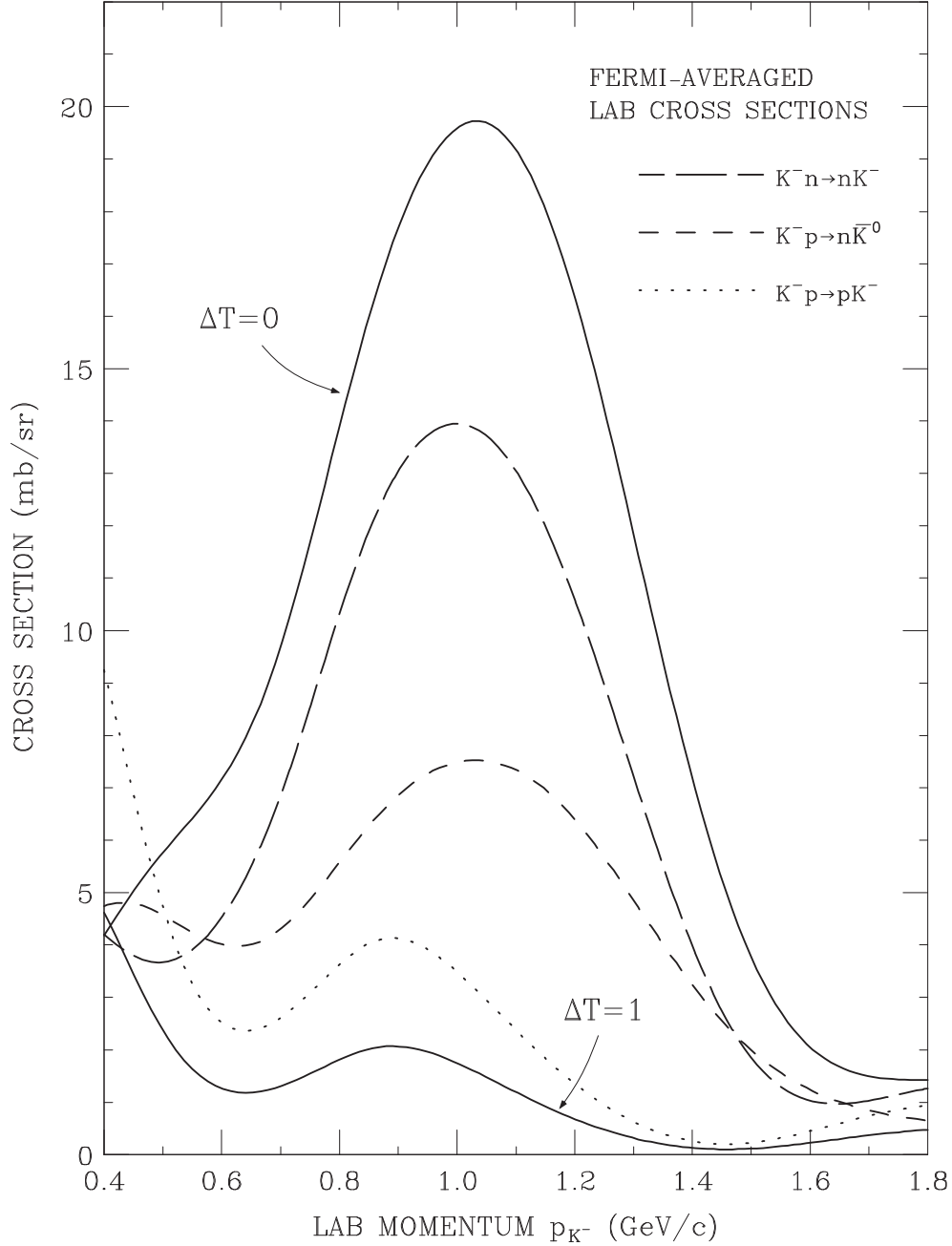


FIG. 9: The absolute values of the Fermi-averaged lab cross sections at $\theta_{\text{lab}} = 0^\circ$ for the isospin $\Delta T = 0, 1$ states for the (K^-, n) reaction on an isospin-0 target such as ^{12}C , as a function of the K^- lab momentum p_{K^-} . The Fermi-averaged lab cross sections for $K^- + n \rightarrow n + K^-$, and $K^- + p \rightarrow n + \bar{K}^0$, and $K^- + p \rightarrow p + K^-$ processes are also shown. The free space amplitudes of Gopal et al. [44] were used.

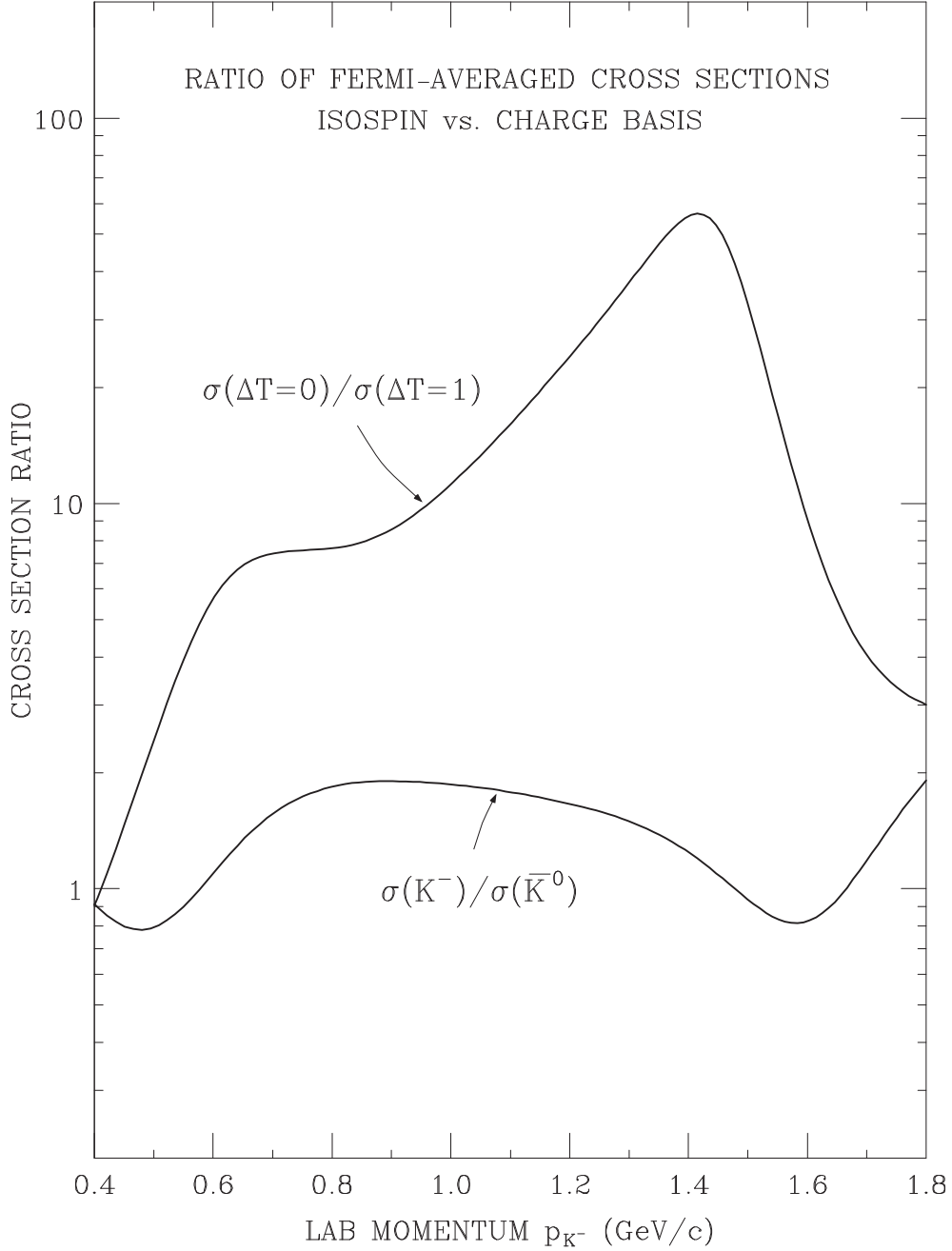


FIG. 10: Ratio of the Fermi-averaged cross section $\sigma(\Delta T=0)/\sigma(\Delta T=1)$ in isospin basis or $\sigma(K^-)/\sigma(\bar{K}^0)$ in the charge basis, as a function of K^- lab momentum p_{K^-} . The free space amplitudes of Gopal et al. [44] were used. These ratios refer to relative (K^-, n) cross sections for an isospin-0 target, leading to final \bar{K} nuclear configuration having a good isospin, or, a specific charge state.

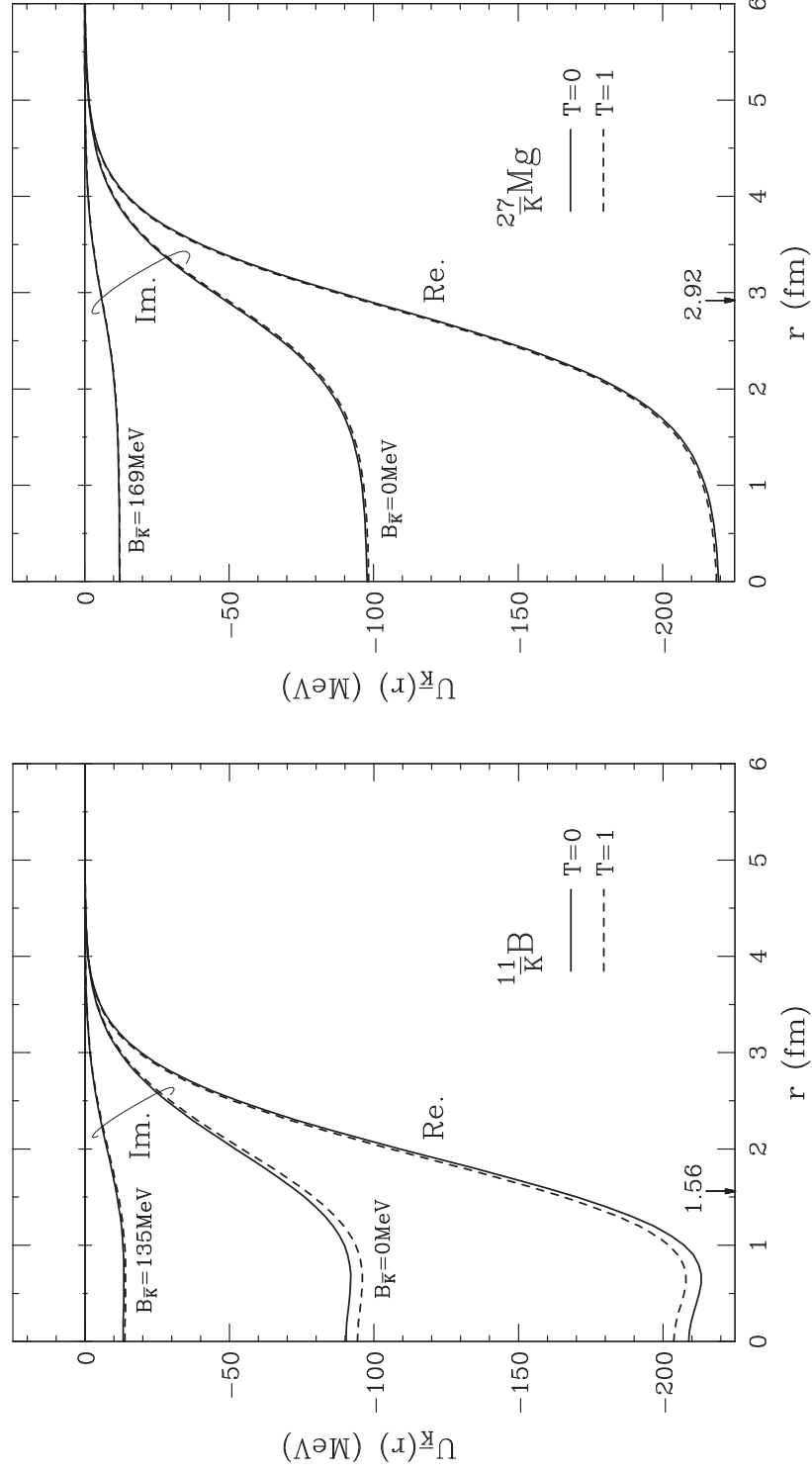


FIG. 11: Real and imaginary parts of the \bar{K} -nucleus DD potentials for (left) $^{11}\bar{K}$ B and (right) $^{27}\bar{K}$ Mg. The solid and dashed curves denote the potentials for total isospin of $T = 0$ and 1 , respectively. The imaginary parts of the potentials draw for $B_{\bar{K}} = 0$ MeV and 135 MeV to see the effects of the phase space factors given by Mareš [67].

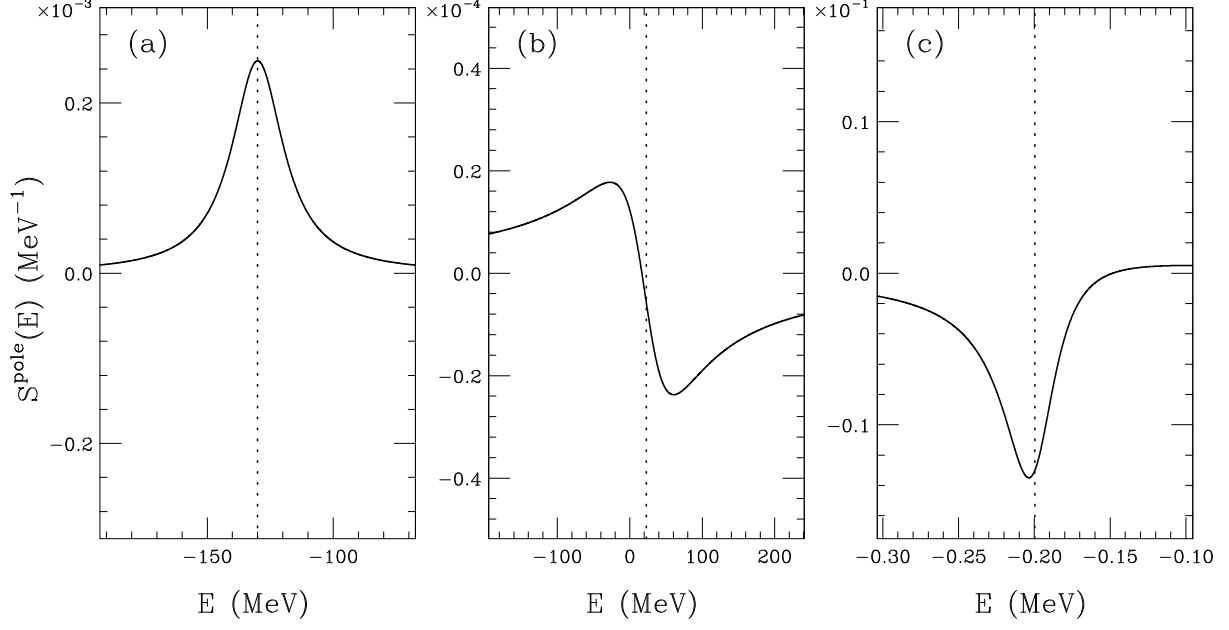


FIG. 12: Shape of the strength function $S^{\text{(pole)}}(E)$ for the unstable nuclear and atomic states in the $K^- \otimes {}^{11}\text{B}$ system as a function of E_{K^-} ; (a) $\text{Arg}N_{\text{eff}} = 0.08^\circ$ at $B_{K^-} = -130$ MeV and $\Gamma_{K^-} = 25$ MeV for the transition $1p_{\frac{3}{2}} \rightarrow (1s)_{K^-}$, $\Delta L = 1$, (b) $\text{Arg}N_{\text{eff}} = 98.3^\circ$ at $B_{K^-} = +23$ MeV and $\Gamma_{K^-} = 87$ MeV for the transition $1s_{\frac{1}{2}} \rightarrow (2s)_{K^-}$, $\Delta L = 0$, and (c) $\text{Arg}N_{\text{eff}} = -157.9^\circ$ at $B_{K^-} = -199$ keV and $\Gamma_{K^-} = 41.6$ keV for the transition $1p_{\frac{3}{2}} \rightarrow (1s)_{\text{atom}}$, $\Delta L = 1$. The dotted line denotes the position of B_{K^-} for each case.

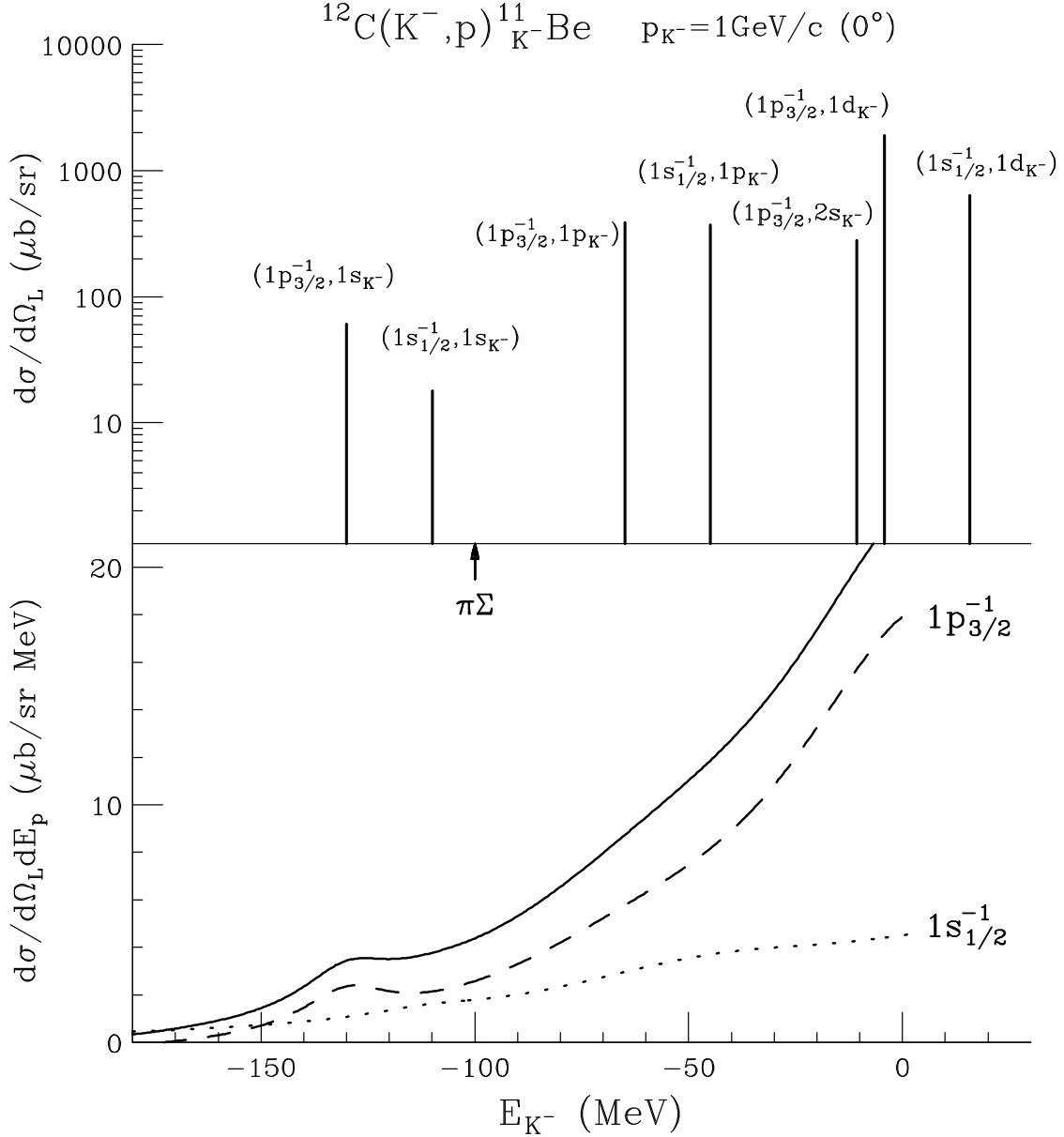


FIG. 13: The integrated cross sections (top) and the corresponding proton spectrum (bottom) for $^{11}_{K^-}\text{Be}$ from $^{12}\text{C}(K^-, p)$ reactions at $p_{K^-} = 1.0$ GeV/c and $\theta_{\text{lab}} = 0^\circ$. The values of the integrated cross section are estimated, omitting the imaginary part of the \bar{K} -nucleus DD potential [67], whereas the spectrum is obtained by using the \bar{K} -nucleus DD potential with the imaginary part multiplying the phase space factor [67]. The arrow denotes the $\pi\Sigma$ decay threshold of about $E_{K^-} \sim 100$ MeV. Note that the background and the continuum states for K^- are not included.

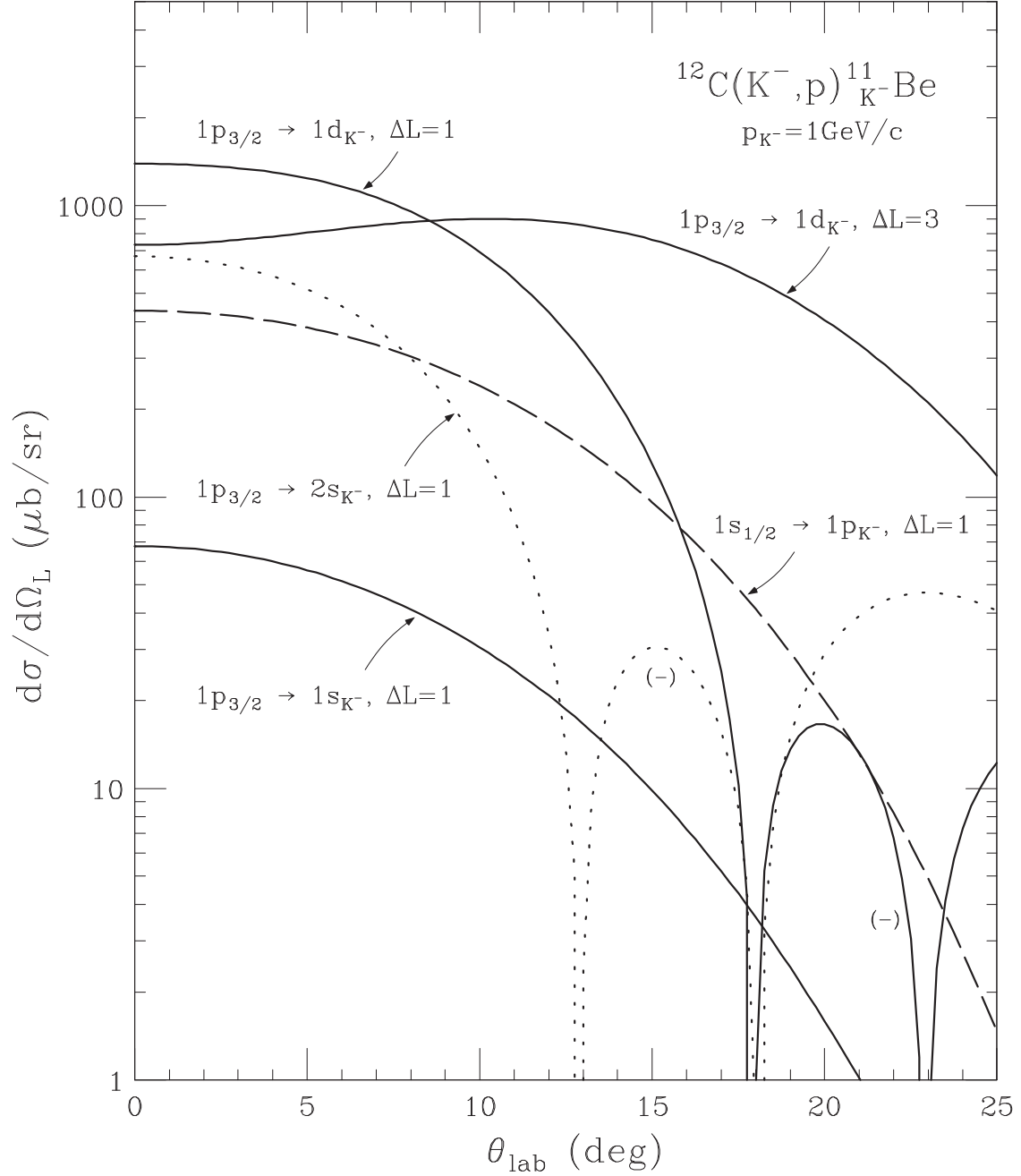


FIG. 14: Angular distribution of the lab cross sections for $^{11}_{K^-}\text{Be}$ by (K^-, p) reactions on a ^{12}C at $p_{K^-} = 1.0 \text{ GeV}/c$. The solid and dotted curves denote for the transitions $1p_{3/2} \rightarrow (1s)_{K^-}$, $(1d)_{K^-}$ with $\Delta L = 1$ or 3 , and $1p_{3/2} \rightarrow (2s)_{K^-}$ with $\Delta L = 1$, respectively. The dashed curve denotes for the transitions $1s_{1/2} \rightarrow (1p)_{K^-}$ with $\Delta L = 1$. The labeled (-) denotes the negative value for the cross section which means that the shape of the states grows into an upside-down peak with the background.

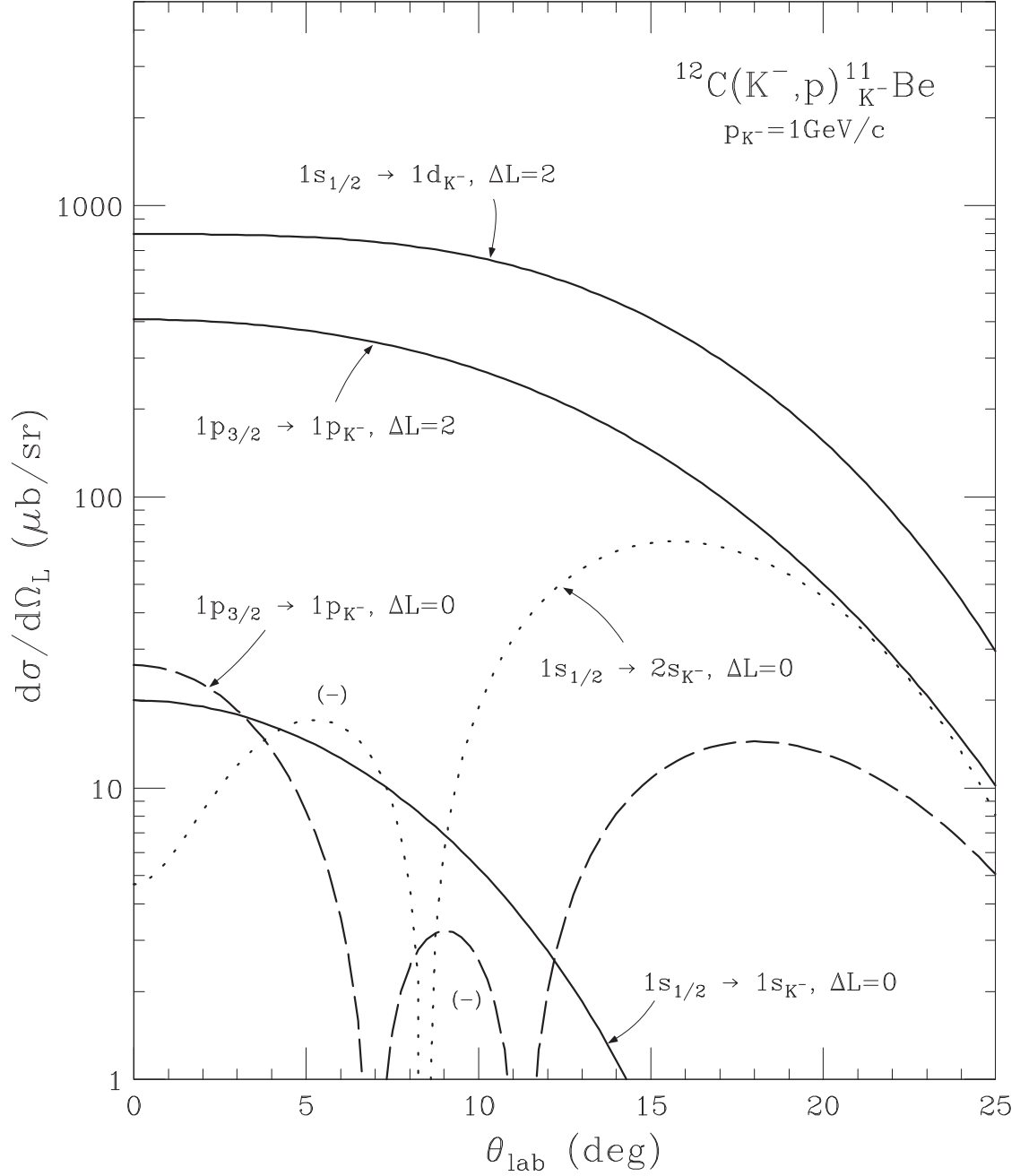


FIG. 15: Angular distribution of the lab cross sections for $^{11}_{K^-}\text{Be}$ by $^{12}\text{C}(K^-, p)$ reactions at $p_{K^-} = 1.0 \text{ GeV}/c$. The solid curves denote for the transitions $1s_{\frac{1}{2}} \rightarrow (1d)_{K^-}$ and $1p_{\frac{3}{2}} \rightarrow (1p)_{K^-}$ with $\Delta L = 2$, and the transition $1s_{\frac{1}{2}} \rightarrow 1s_{K^-}$ with $\Delta L = 0$. The dotted and dashed curves denote for the transitions $1s_{\frac{1}{2}} \rightarrow (2s)_{K^-}$ with $\Delta L = 0$ and $1p_{\frac{3}{2}} \rightarrow (1p)_{K^-}$ with $\Delta L = 0$, respectively. See the caption in Fig. 14.

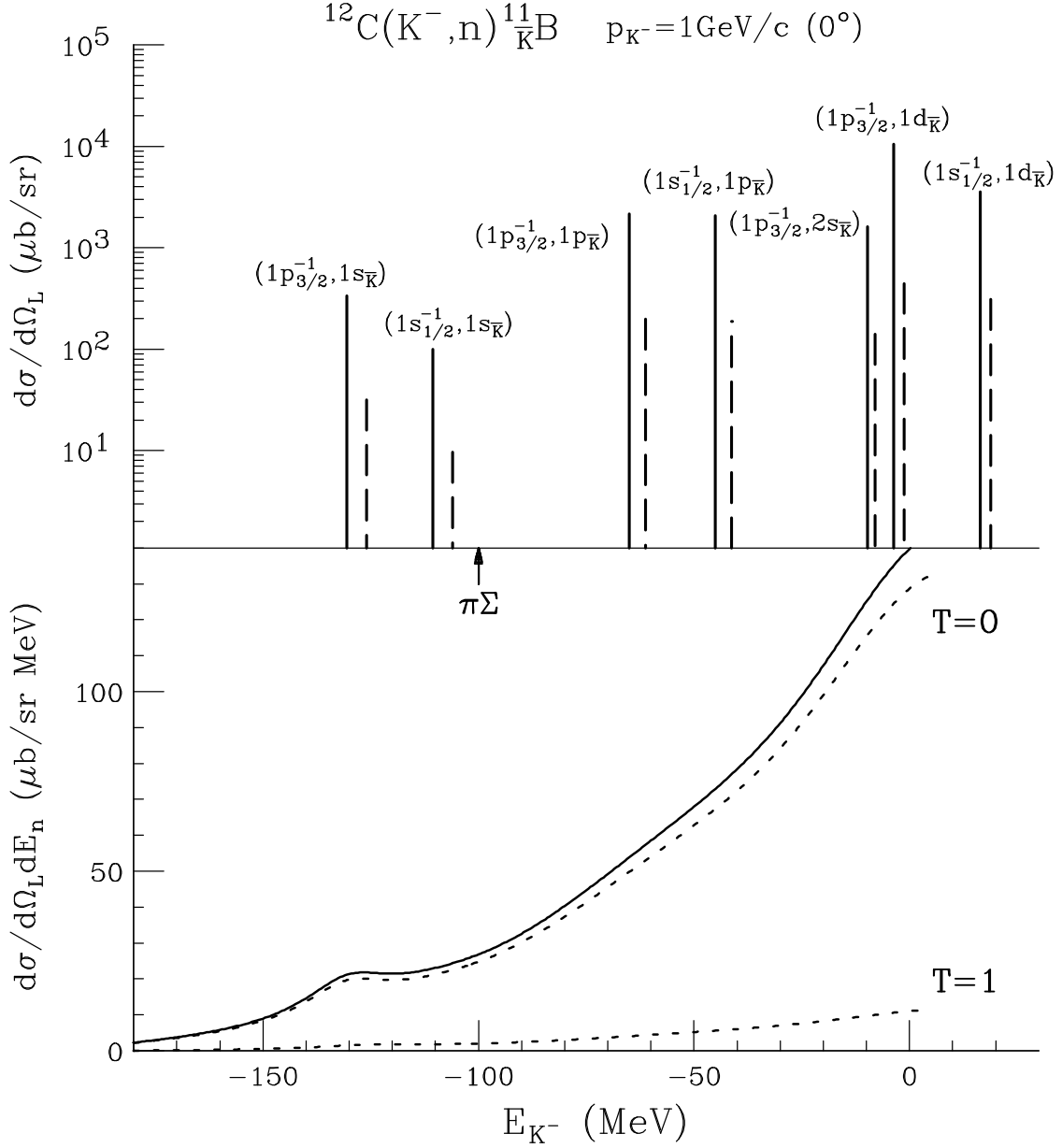


FIG. 16: The integrated cross sections for ^{11}B from $^{12}\text{C}(K^-, n)$ reactions at $p_{K^-} = 1.0 \text{ GeV}/c$ and $\theta_{\text{lab}} = 0^\circ$, using the DD potential (top). The solid and dashed lines denote the values of the cross sections for $T = 0$ and 1 states, respectively, omitting the imaginary parts of the potential. The inclusive (K^-, n) spectrum for ^{11}B from $^{12}\text{C}(K^-, n)$ reactions at $p_{K^-} = 1.0 \text{ GeV}$ (bottom). The dotted curves denote the contributions from isospin $T = 0$ and $T = 1$ states. See the caption of Fig. 13.

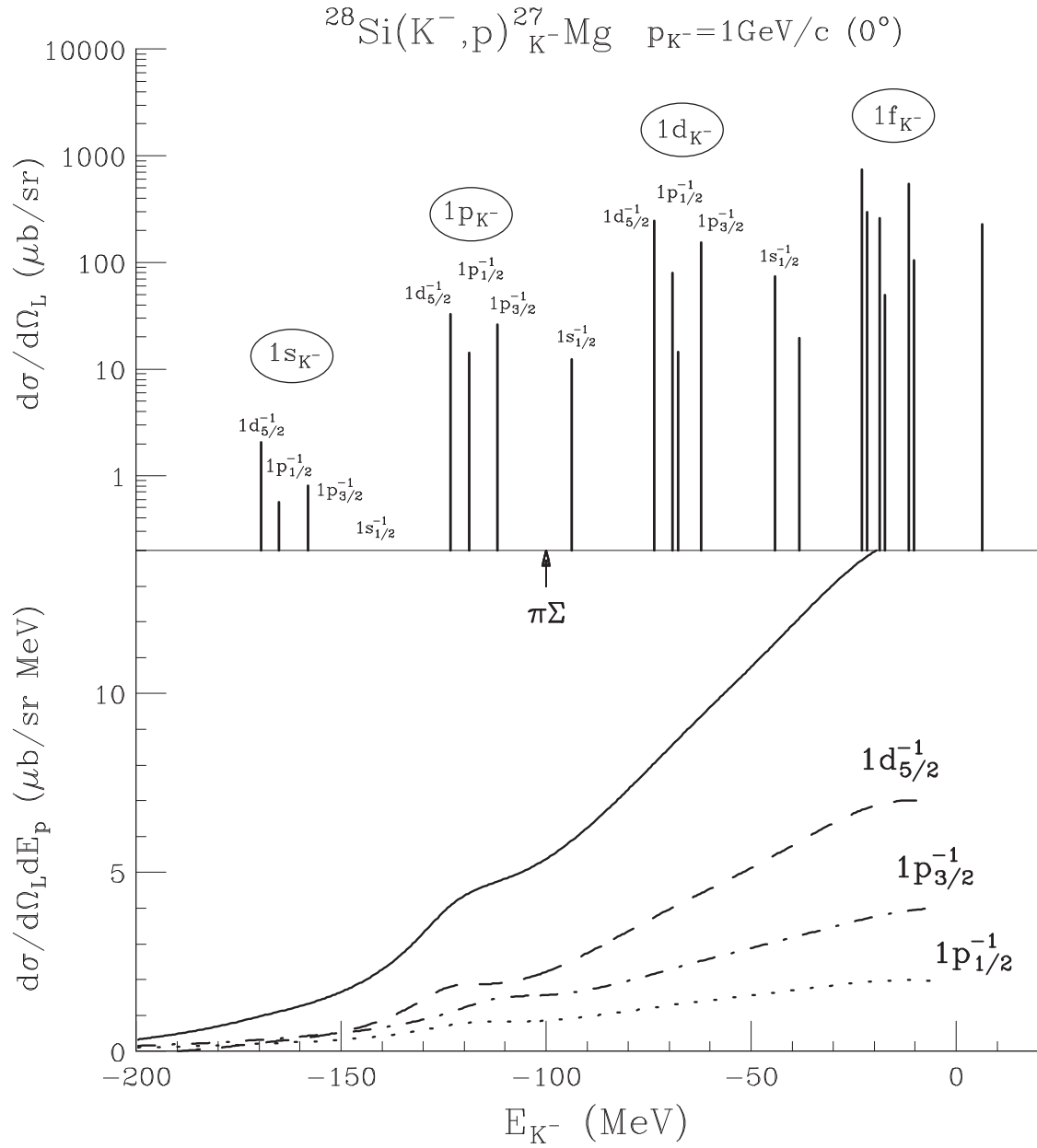


FIG. 17: The integrated cross sections (top) and the corresponding proton spectrum (bottom) for $^{27}_{K^-}\text{Mg}$ from $^{28}\text{Si}(K^-, p)$ reactions at $p_{K^-} = 1.0 \text{ GeV}/c$ and $\theta_{\text{lab}} = 0^\circ$. The dashed, dotted and dot-dashed curves denote the contributions from $1d_{5/2}^{-1}$, $1p_{1/2}^{-1}$, $1p_{3/2}^{-1}$ proton-hole states, respectively. See the caption of Fig. 13.